Capture and Activation of Carbon Dioxide Using Guanidine Superbases

by

Grace Furon Bomann

A thesis
submitted to Victoria University of Wellington
in fulfilment of the
requirements for the degree of
Master of Science
in Chemistry

Victoria University of Wellington

2017

Abstract

Due to its abundance and low-cost, carbon dioxide is a desirable C_1-building block within organic transformations. However, the thermodynamic and kinetic stability of CO_2 often necessitates preliminary activation before it can be inserted into organic molecules. This prompts the need for compounds that can effectively promote the activation of CO_2. This research investigates the capture and activation of carbon dioxide using a class of superbases that incorporate the bicyclic guanidine unit, 1,3,4,6,7,8-hexahydro-2*H*-pyrimido[1,2-*a*]-pyrimidine (hppH, **1**). A series of compounds containing multiple hpp-units assembled around a phenyl ring scaffold were synthesized and investigated in the functionalization of CO_2. The work presented in this study has demonstrated the ability of protonated superbasic hppH derivatives to efficiently and effectively capture and activate carbon dioxide from ambient air to form the corresponding guanidinium bicarbonate salts. A series of optimization reactions was carried out, and showed that addition of substoichiometric concentrations of a proton source activates these guanidine compounds to their fully protonated cationic forms, and results in CO_2 capture through bicarbonate formation.

A series of protonation studies were employed to fully characterize the cationic species. The tetraphenylborate and hydrochloride guanidinium salts were synthesized, isolated, and characterized by ^{1}H NMR and ^{13}C NMR spectroscopic analysis. Molecular structures of relevant crystals were obtained through single crystal X-ray diffraction. These structures revealed a complex hydrogen-bonding network within these ionic species, and showed efficient delocalization of the formal positive charge within the protonated guanidinium units.

The guanidine superbases were implemented in a series of reactions attempting the functionalization of CO_2 and an alcohol to form corresponding alkylcarbonate products. However, the synthesis of these carbonate products was not achieved under the reaction conditions employed. This lack of success has been attributed to the hygroscopic nature of this class of compounds, resulting in the preferential capture of ambient water.

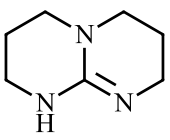

hppH (**1**)

Acknowledgements

First and foremost, I would like to extend a huge thank you to my supervisor Associate Professor Martyn Coles for all your help, feedback, and guidance over the last two years. Your passion for chemistry is inspiring, your innate intelligence intimidating, and excitement for *the* perfect crystal equal parts fascinating and perplexing. It has been a joy and honor to work with you throughout this project.

I'd like to also thank Ryan Schwamm for not only performing the previous work that allowed the precipitation to my entire thesis, but for the immense amount of help and advice you have given me throughout the duration of my studies. You taught me everything I know about air-sensitive chemistry, and have been my hppH spirit guide during this entire process.

Thank you to Dr. Robin Fulton for all the helpful feedback, and to the members in her group, in particular Dylan, Struan and Putri, for your assistance, guidance, and entertainment. You have all made my Masters such an enjoyable experience, even with the occasional lab fire.

A special thank you to the other organic chemists that I worked with, or at least in proximity to, in this lab. Your help, friendship, and generosity in constantly lending me methanol made the completion of my thesis possible.

Finally, thank you to my parents, my brother, and my sister for not only their continuous support, but for making Wellington feel like my home. To George, thank you for your endless encouragement and enthusiasm that always motivated me to work harder. Without you as my constant crutch, the completion of this thesis would not have been possible.

Table of Contents

List of Figures

List of Tables

List of Schemes

Glossary

δ	Chemical shift (ppm).
^{13}C NMR	Carbon nuclear magnetic resonance.
^{1}H NMR	Hydrogen nuclear magnetic resonance.
app	Apparent.
9-BBN	9-borabicyclo(3.3.1)nonane.
BIGs	Bis-iminoguanidine ligands.
br	Broad.
$CDCl_3$	Deuterated chloroform.
CD_3CN	Dueterated acetonitrile.
$[CO_3]^{2-}$	Carbonate anion.
D	Doublet.
DBN	1,5-diazabicyclo[3.4.0]non-5-ene.
DBU	1,8-diazabicycloundec-5-ene.
DFT	Density functional theory.
DMAN	*N*,*N*,*N*',*N*'-tetramethyl-1,8-napthalenediamine.
Et	Ethyl, CH_2CH_3.
equiv.	Equivalent(s).
$[HCO_3]^-$	Bicarbonate anion.
$[HNEt_3][BPh_4]$	Triethylammonium tetraphenylborate.
$[HNEt_3][Cl]$	Triethylamine hydrochloride.
Htbn	1,4,6-triazabicyclo[3.4.0]non-4-ene.
Htbo	1,4,6-triazabicyclo[3.4.0]oct-4-ene.
hppH	1,3,4,6,7,8-hexahydro-2*H*-pyrimido[1,2-*a*]-pyrimidine.
hppMe	1,3,4,6,7,8-hexahydro-1-methyl-2*H*-pyrimido[1,2-*a*]-pyrimidine.
Hz	Hertz.
ILs	Ionic liquids.
IR	Infrared.
$\mathcal{J}$	Scalar coupling constant (Hz).
K_{app}	Apparent equilibrium constant.
m	Multiplet.
m-	*meta*-
Me	Methyl, CH_3.
NMP	N-methyl-2-pyrrolidone.
o-	*ortho*-
p-	*para*-
Ph	Phenyl.
PMDBD	3,3,6,9,9-pentametil-2,10-diazabicyclo[4.4.0]dec-1-ene.
ppm	Parts per million.

PyBIG	2,6-pyridine-bis(iminoguanidine).
NMR	Nuclear magnetic resonance spectroscopy.
quint	Quintet.
q	Quartet.
s	Singlet.
(SB)	Superbasic guanidine species.
t	Triplet.
t-Bu	*tert*-Butyl, $C(CH_3)_3$
THF	Tetrahydrofuran.
TMG	*N,N,N'N'*-tetramethylguanidine.

Chapter 1

Introduction

1.1 Carbon Dioxide

As the principle greenhouse gas, carbon dioxide has largely contributed to the increase in global atmospheric temperatures. An urgent need to control the rising levels of atmospheric CO_2 has led many different industries and fields to investigate the development of efficient carbon capture systems. However, owing to the very low concentration of CO_2 within air (ca. 400 ppm), effective direct air capture requires a sorbent that optimally combines a number of attributes such as strong CO_2-binding affinity, fast sorption kinetics, stability and high capacity.[1]

Although it will not solve the global crisis alone, within organic synthesis there is an active goal to utilize CO_2 in the production of fuels or chemicals. The nontoxicity, availability, and recyclability of carbon dioxide make it a very desirable single carbon (C1) building block to use within organic transformations.[2] However, as CO_2 is the most oxidized form of carbon, it is very thermodynamically stable and often kinetically inert towards derivitization. As such, many current studies employ very harsh reaction conditions in order to activate carbon dioxide, limiting the applications of these methods. This precipitates a need for systems that are able to capture and activate CO_2 utilizing greener and more mild conditions.

1.2 Ionic Liquids in CO_2 Capture

A prominent industrial technology for CO_2 capture involves a chemisorption process by an aqueous alkanolamine solution, but requires significant energy to effectively sequester CO_2.[3] A

possible substitute to this methodology is the implementation of anion-functionalized ionic liquids (ILs).[4] ILs, or molten salts, in general are defined as liquid electrolytes composed entirely of ions, and have been found effective in biphasic catalysis reactions.[5] ILs offer an attractive carbon capture alternative to the processes used within industry as they have negligible vapor pressures, wide liquid ranges, high thermal stability, and large chemical tenability.[4] Many amino-functionalized ILs have been previously developed for CO_2 capture.[6,7] However, these ionic liquids generally chemisorb CO_2 through the single-site interaction between the electronegative nitrogen atom and CO_2, resulting in low equimolar stoichiometry.

To combat these low carbon capture capacities, Wang and co-workers instead developed pyridine-containing anion-functionalized ILs that were found to have an extremely high capacity for CO_2 capture, reaching levels of 1.60 mol CO_2 captured per mol IL.[8] The ILs were prepared through neutralization of various hydroxypyridine or 4-azabenzimidazole compounds (**2—6,** Figure **1.1**) with an ethanol solution of trihexyl(tetradecyl)phosphonium hydroxide, obtained by the anion-exchange method.

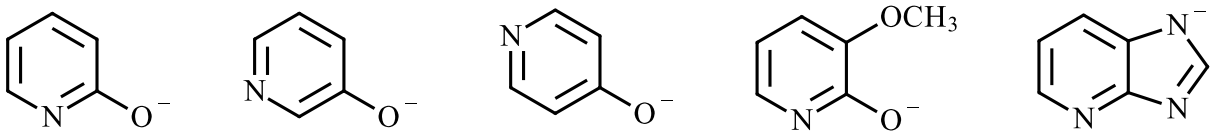

2 **3** **4** **5** **6**

Figure 1.1: Structures of the anions in pyridine-containing anion-functionalized ionic liquids[3]

The tested pyridine-derived ILs were found to have a significantly larger CO_2 capture capacity than neutral pyridine. The increased reactivity has been attributed to a positive cooperative interaction between multiple electronegative sites in the anion (both the nitrogen and oxygen atoms). The π-electron delocalization within the core pyridine ring allows for the nitrogen atom to share the negative charge of the oxygen atom. This increases the atomic charge of the nitrogen atom within the species, and results in enhanced interaction between this atom and CO_2.[8]

^{13}C NMR and IR spectroscopy revealed that CO_2 first binds to the oxygen atom within the anion, closely followed by a second molecule of CO_2 binds to the nitrogen atom (Scheme **1.1**).[8]

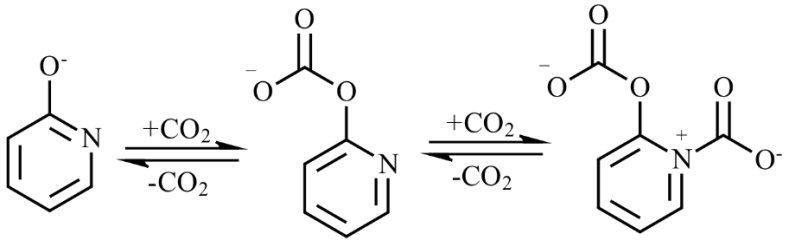

Scheme 1.1: Proposed mechanism of CO_2 absorption through multiple-site cooperative interactions[8]

It should be noted that water had a significant effect on the reactivity of these ILs. In the presence of adventitious water, the capture capacity of the ionic liquids was reduced to approximately 0.1 mol CO_2 captured per mol IL.[8] This was attributed to the preferential absorption of water over CO_2.

1.3 Nitrogenous Bases in CO_2 Capture

Hindered nitrogenous bases were found to be particularly efficient catalysts in the capture of CO_2.[9] These organic bases are able to promote activation and functionalization of CO_2 through the formation of either a zwitterionic carbamate adduct, or the corresponding bicarbonate salt by the formal addition of a hydroxyl unit to CO_2. In comparison to amines, sterically hindered amidines and guanidines have proven to be even more effective in CO_2 capture. These compounds contain conjugated π-systems that allow for the delocalization of charge over multiple nitrogen atoms, leading to increased stability of the resulting base-CO_2 adducts.[9]

1.3.1 Amidines

Many different hindered amidine bases have been investigated for carbon dioxide capture and activation. One example of such is the amidine 3,3,6,9,9-pentamethyl-2,10-diazobicyclo[4.4.0]dec-1-ene (PMDBD). González and co-workers were able to demonstrate that in the presence of adventitious water and under 1 atm CO_2, PMDBD successfully captures and activates CO_2, forming the corresponding crystalline bicarbonate salt (**7**, Figure **1.2**).[10] However, this reaction performed in previously dried solvent yielded no solid product.

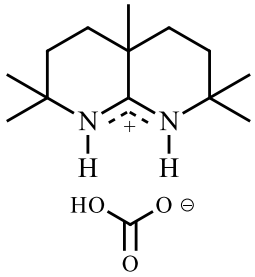

7

Figure 1.2: PMDBD bicarbonate salt (**7**) formed through CO_2 capture[10]

1,5-Diazabicyclo[3.4.0]non-5-ene (DBN) was also tested for CO_2 capture using the same experimental procedure.[10] However unlike the previous reaction with PMDBD, NMR analysis showed the formation of two different DBN-CO_2 adducts: a bicarbonate salt **8**, and a carbamate species **9** (Figure **1.3**).

The presence of adventitious water resulted in increased yields of the bicarbonate product **8**, whereas the reaction performed under anhydrous conditions favored the formation of the carbamate adduct **9**. This indicates that the carbamate product is unstable in the presence of moisture, most likely reacting with water, releasing CO_2 as a bicarbonate species, and reforming cationic DBN.[10]

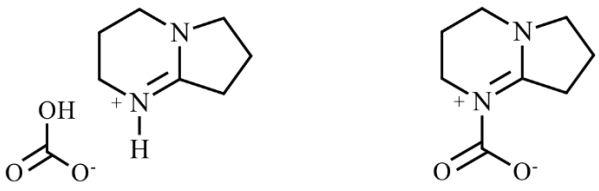

8 **9**

Figure 1.3: DBN-CO_2 bicarbonate (**8**) and carbamate (**9**) products formed via CO_2 capture[10]

Franco and co-workers implemented similar procedures with the amidine 1,8-diazobicycloundec-7-ene (DBU, **10**), and found that reacting this base under 1 atm CO_2 afforded both the corresponding carbamic zwitterion (**11**) and bicarbonate salt (**12**) products (Scheme **1.2**).[11] Thermogravimetric analysis of the carbamate adduct **11** showed a weight loss correlating to "CO_2 + H_2O". This suggests that these zwitterions are associated with one molecule of water through hydrogen bond interactions.[11]

Although spectral analysis confirmed the formation of both products, examination of the crystalline product through X-ray diffraction elucidated the structure to be solely the bicarbonate species **12**.[11] This suggests that structural changes occur to the carbamate adduct

throughout the crystallization process. It was proposed that the amidinium bicarbonate may be formed via proton transfer from a water molecule to the zwitterion, followed by the nucleophilic attack of the hydroxyl anion on the N–COOH moiety (Scheme **1.2**).[11]

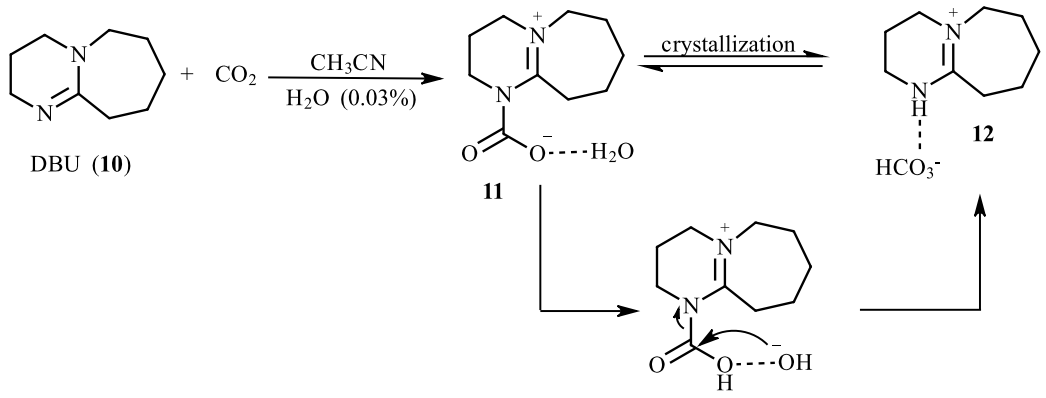

Scheme 1.2: Formation of DBU-CO_2 complexes[11]

1.3.2 Guanidines

Guanidines have also been extensively studied for the fixation of carbon dioxide. González and associates investigated the carbon capture capacity of TMG (*N,N,N',N'*-tetramethylguanidine).[12] It was found that reacting this compound under pressurized CO_2 in a solution containing trace amounts of water readily formed the corresponding bicarbonate salt (**14**). Similar to the determined reactivity of the amidine complexes, this study postulated that the bicarbonate adduct forms from a water-solvated carbamic intermediate (**13**) (Scheme **1.3**).[12]

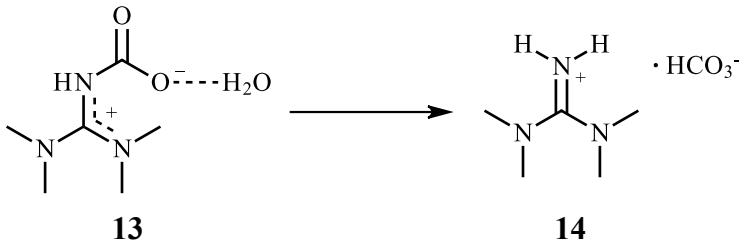

Scheme 1.3: TMG-CO_2 carbamate intermediate (**13**) and bicarbonate product (**14**) [12]

Due to their inherent electronic properties, cyclic guanidines offer an efficient alternative to CO_2 capture and bicarbonate formation. Their high basicity means they easily form the corresponding guanidinium cation upon protonation, which is stabilized by effective charge distribution throughout the molecule. These positively charged ions are then able to form

multiple, strong charge-assisted hydrogen bonds with various anionic groups.[13] Additionally, the high level of substitution about the central 'CN_3' guanidine core results in slight control over the direction of these projected hydrogen atoms.[13]

One bicyclic guanidine that has been implemented in CO_2 capture systems is 1,3,4,6,7,8-hexahydro-1-methyl-2*H*-pyrimido[1,2-a]pyrimidine (hppMe[1], **15**).[14,15] In a study investigating CO_2 capture with the use of room temperature ionic liquids in conjunction with a superbase, it was found that employing a system of 3-butyl-1-methylimidazolium bis(trifluoromethanesulfonyl)amide (**16**) and hppMe had a CO_2 absorption capacity of 1.08 mol per mol of superbase.[14] This value was found to be larger than both DBU and TMG, which had molar ratios of CO_2 to superbase of 0.99 and 0.49, respectively.[14] It should be noted that these absorption values were calculated with an accuracy of ±0.1 mg.[14] NMR and IR spectral data, showed that the product of this reaction is the corresponding amidinium carboxylate salt (**17**), as shown in Scheme **1.4**.[15]

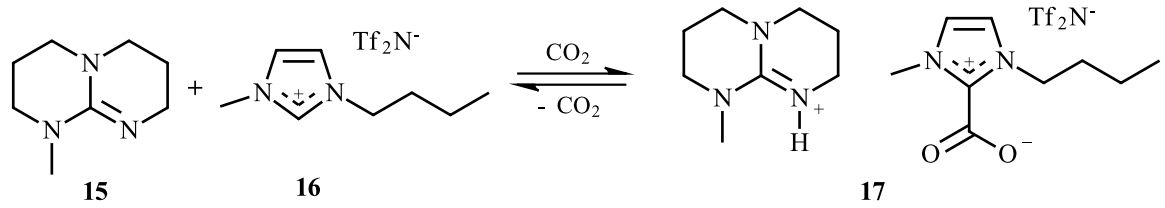

Scheme 1.4: Ionic liquid CO_2 capture using hppMe[15]

1.4 hppH

One of the most widely used bicyclic guanidines is the tetra substituted 1,3,4,6,7,8-hexahydro-2*H*-pyrimido[1,2-*a*]pyrimidine (hppH,[2] **1**, Figure **1.4**), whose framework is constrained such that, upon protonation, a favorable orbital alignment for delocalization of π-electron density is present.[16,17] This compound has been used extensively in coordination chemistry, where strong metal–ligand interactions occur through the imine nitrogen.[18]

[1] hppMe ≡ MTBD (7-methyl-1,5,7-triazabicyclo[4.4.0]dec-5-ene)
[2] hppH ≡ TBD (1,5,7-triazabicyclo[4.4.0]dec-5-ene)

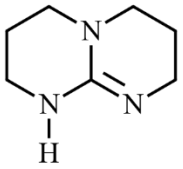

1

Figure 1.4: hppH (**1**)

1.4.1 hppH in CO_2 Capture

Similar to amidines, hppH (**1**) was studied for fixation and release of carbon dioxide.[9,12] It was initially proposed that the addition of pressurized CO_2 to this bicyclic guanidine would result in the formation of three complexes: a bicarbonate salt (**20**), and two tautomers containing carbamic functionalities (**18** and **19**, Scheme **1.5**).[12] Quantum mechanical calculations performed prior to the experimental reaction revealed that the carbamate complex **19** was less stable than **18**, suggesting that this species would not be formed in significant amounts.[12]

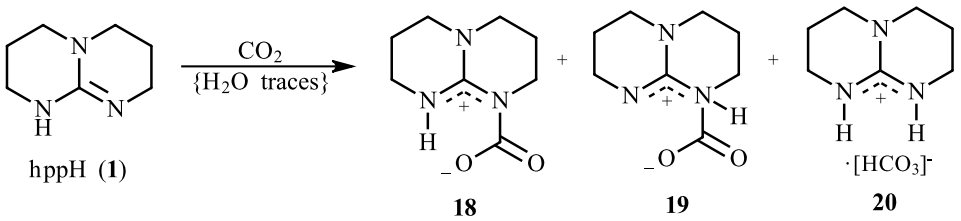

Scheme 1.5: Predicted products of hppH and CO_2 reaction[12]

Using acetonitrile as a solvent, hppH was reacted with a steady stream of CO_2 (10mL/min) in the presence of ambient moisture, and the resulting product characterized through ^{13}C and ^{1}H NMR analysis.[12] Resonances at δ_c 20.0, 38.0, and 46.0 ppm ($CDCl_3$) were attributed to three non-equivalent methylene carbons, which is not consistent with a fixed $C=N^+$ bond, but instead suggests that the $CDCl_3$ soluble portion of the product assumes a delocalized resonant structure symmetrical with respect to both rings, as pictured in Scheme **1.5**. Signals at δ_c 157.0 and 155.0 ppm are attributable to a guanidinic carbon and a carbamic carbonyl. Additionally, a signal resonating at δ_C 162.3 ppm was assigned to a water-free bicarbonate carbon. However, an unassigned signal that resonated at δ_C 165.4 ppm is not typical of either; instead, it is consistent with a bicarbonate carbonyl with a slightly different chemical environment than one found responsible for a resonance at δ_C 162.3 ppm.[12] This is then indicative of the presence of water, as found in previous reactions of nitrogenous bases with CO_2, where a deshielding of the carbonyl carbon would cause this difference in chemical shift. TGA-FTIR analyses of the

products show at least three CO_2 losses were identified, suggesting the presence of three CO_2 containing products as proposed in Scheme **1.5**.[12]

The hppH-CO_2 adducts were analyzed through X-ray crystallographic techniques.[9] It was found that in the bicarbonate salt [hppH$_2$][HCO$_3$] (**20**), the cation and anion are associated through two hydrogen bonds between the nitrogen and oxygen atoms. Additionally, the structure of these crystals present themselves with two cation-anion pairs forming a centrosymmetric dimer, arising from two hydrogen bonds between the oxygen atoms of two [HCO$_3$]$^-$ anions (Figure **1.5**).[9]

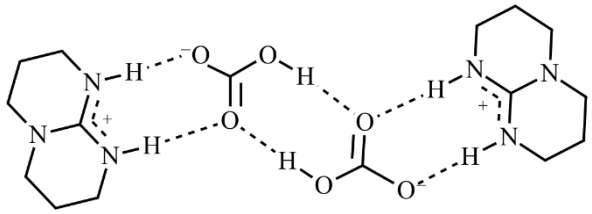

Figure 1.5: Dimeric structure of [hppH$_2$][HCO$_3$] (**20**)[9]

Diffusion of CO_2 into a solution of hppH under purely anhydrous conditions led to the precipitation of a carbamic hppH-CO_2 adduct (**18**).[9] Crystallographic analysis revealed that this compound is almost planar, in addition to being zwitterionic, as proven by the presence of both the guanidinium-type delocalized cationic system and the carboxylate-type anionic unit. Additionally, an induced stacking in the solid state occurs between hppH-CO_2 adducts. Crystallographic data showed three intermolecular C–H···O hydrogen bonds are formed between the CO_2 unit and three adjacent hppH-CO_2 adducts.[9] As there is also an intramolecular hydrogen bond (shown in Figure **1.6**), each oxygen atom then participates in two hydrogen bonds. It is important to note that this adduct was readily transformed into the corresponding bicarbonate salt [hppH$_2$][HCO$_3$] in the presence of water, both in the solid state under air and in solution with the use of wet solvents.[9]

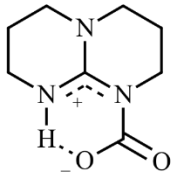

18

Figure 1.6: hppH-CO_2 adduct (**18**) intramolecular hydrogen bonding[9]

1.5 CO_2 Capture from Ambient Air

Although there have been many previous studies examining CO_2 capture utilizing hindered nitrogenous bases under high concentrations of carbon dioxide, there is little within the literature that explores their affinity for CO_2 from ambient air.

1.5.1 Htbn and Htbo in CO_2 Capture

Cotton and co-workers reported the ability of two bicyclic guanidinates derivatives, 1,4,6-triazabicyclo[3.3.0]oct-4-ene (Htbo, **21**) and 1,4,6-triazabicyclo[3.4.0]non-4-ene (Htbn, **22**) to sequester carbon dioxide from the minute levels of CO_2 found in air.[19] It was found that upon exposure to air, these compounds readily absorb atmospheric water and air to afford the corresponding bicarbonate salts. Crystals of these products ([H_2tbo][HCO_3], **23**, and [H_2tbn][HCO_3], **24**) were obtained in quantitative yield through slow evaporation in air of a solution of the neutral guanidine compounds in 90% (v/v) ethanol/water (Scheme **1.6**).

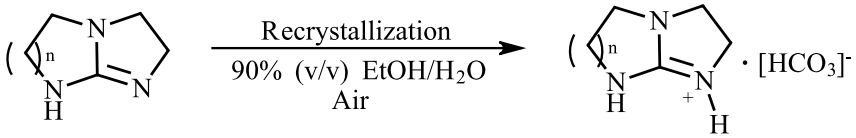

Htbo (**21**), n = 1
Htbn (**22**), n = 2

[H_2tbo][HCO_3] (**23**), n = 1
[H_2tbn][HCO_3] (**24**), n = 2

Scheme 1.6: CO_2 capture and bicarbonate formation using Htbo (**21**) and Htbn (**22**)[19]

Unlike the bicarbonate salt [hppH$_2$][HCO_3] (**20**), it was found that the extended solid-state structure of these bicarbonate products exist as infinite hydrogen-bonded chains in which the each cation alternates with two bicarbonate anions.[19]

1.5.2 PyBIG in CO_2 Capture

Custelcean and co-workers reported the successful capture of CO_2 from ambient air through use of an aqueous guanidine sorbent.[20] This guanidine, 2,6-pyridine-bis(iminoguanidine) (PyBIG, **25**) belongs to a class of bis-iminoguanidine ligands (BIGs) that have been found to form crystalline hydrogen-bonded salts with oxoanions. The resulting salts have low-aqueous

solubility, facilitating the separating of this class of anions through crystallization.[21,22] This approach also takes advantage of the electron-withdrawing properties of the pyridine ring in PyBIG, which imparts enhanced acidity to the guanidinium groups, leading to stronger binding and more effective separation of oxoanions. Thus, an aqueous solution of PyBIG was left open to ambient air over the course of days, resulting in the formation of large crystals, which was determined to be the tetrahydrated carbonate salt of PyBIG ($PyBIGH_2(CO_3)(H_2O)_4$, **26**) by single crystal X-ray diffraction (Scheme **1.7**).[20]

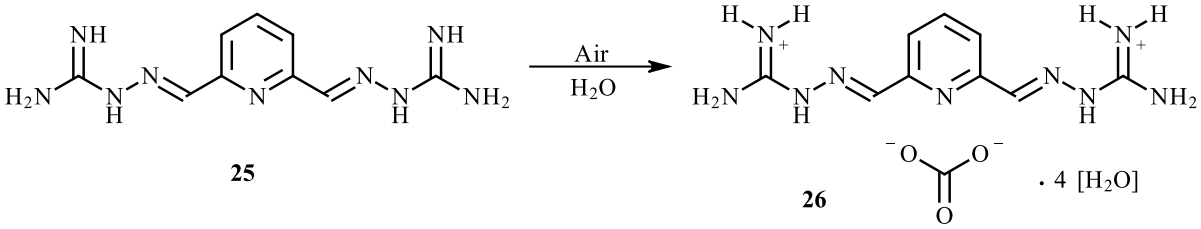

Scheme 1.7: CO_2 capture through use of aqueous PyBIG (**25**)[20]

Although this system is able to capture carbon dioxide forming the corresponding carbonate product **26** in only moderate yields (50.3 ± 0.4%) with relatively slow kinetics of crystallization, it employs completely passive conditions, and is able to capture CO_2 from only the low concentrations found in ambient air. It should be noted that the sorbent was effectively regenerated through heating the carbonate crystals at low temperature, releasing water and CO_2 and reforming PyBIG.[20]

1.6 Research Aims

Previous work in the Coles research group has involved the design of a series of compounds that incorporate more than one hpp-functionality. This enables the existence of multiple-site cooperative interactions, which have been found to improve CO_2 capture and functionalization.[8] Additionally, the incorporation of multiple guanidine units in a single molecular species allows for an increase in the number of sites at which cationic resonance can occur. These compounds are thus classified as superbases, defined as having a pK_a greater than that of the compound DMAN, the conjugated acid of which having a pK_a of 18.62 in acetonitrile.[16]

One of these superbasic compounds that had been investigated involves the addition of three methylene-supported hpp-units around a benzene ring scaffold (1,3,5-(hppCH$_2$)$_3$-C$_6$H$_3$, Scheme **1.8**). It was found that reaction of this compound with one equivalent of the proton source triethylamine hydrochloride, followed by subsequent recrystallization under air at room temperature yielded quantitative formation of the corresponding bicarbonate salt [1,3,5-(CH$_2$hppH)$_3$-C$_6$H$_3$][HCO$_3$]$_3$ (Scheme **1.8**).[23] This indicates that guanidine superbase is highly active for the capture and activation of CO_2 under atmospheric conditions.

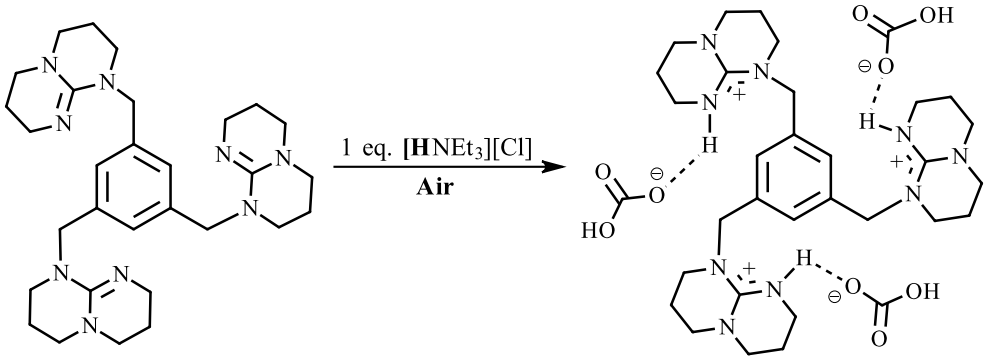

Scheme 1.8: Formation of [1,3,5-(CH$_2$hppH)$_3$-C$_6$H$_3$][HCO$_3$]$_3$[23]

The primary aim of this work was to develop this class of superbasic hpp-containing compounds and optimize their reactivity for CO_2 capture and activation. Characterization of the protonated guanidinium species under air was investigated through the formation of salts containing various counter-anions. Synthesis of organic carbonate products from alcohols through CO_2-functionalization was targeted to understand the scope of their reactivity within organic transformations.

Chapter 2

The Guanidinium Functionality and Analytical Approach

2.1 Cationic Guanidinium Species

Previous studies have explored the steric properties of various tetra-substituted guanidinate anions in detail, examining their bonding mode and directionality that develops at a metal center.[24] Larger substituents have been found to promote chelation by forcing nitrogen donor orbitals toward the center of a ligand, whereas smaller groups have been found to prefer a wider angle between the orbitals.[25] This idea can be extended to guanidinium cations, and how their nitrogen substituents control the direction of projected hydrogen bonds. Bicyclic guanidines, such as hppH, are of particular interest for these investigations as in their cationic form the geometry is fixed in an {*E,E*}-configuration, having the higher priority groups on the opposite side of the delocalized double bond, therefore promoting the projection of two hydrogen bonds in a parallel direction.[13] Another focus within the study of these highly basic species is their capability of effective charge delocalization upon protonation, and the difference in resonance stability of the neutral and ionic forms.[26] As shown in Figure **2.1**, the cationic $[hppH_2]^+$ species is structurally arranged in a manner that allows for full delocalization of the positive charge (**I**), or can stabilize the charge effectively through the rapid movement of electrons between the structures **II, III** and **IV**.[13]

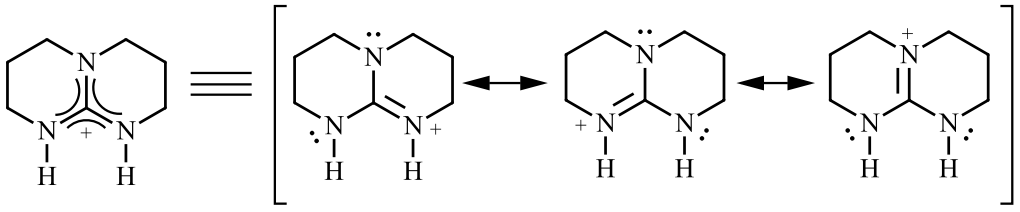

Figure 2.1: Resonance structures contributing to bonding in $[hppH_2]^+$ cation[13]

2.1.1 General Features of Guanidinium Crystal Structures

There has been significant work on the characterization of the molecular structures of protonated guanidine species. This work has identified various criteria to describe bonding properties within these species, and can be used to accurately represent the nature of the delocalization throughout the carbon-nitrogen framework.[13] The following parameters are described below, and will be utilized to describe crystal structures obtained for this project. The equations pertaining to the calculations for these values are summarized in Figure **2.2**.

Δ_{CN}: The Δ_{CN} value is the difference between the length of the C—N single and C=N double bonds.[27] This is a measure of the delocalization of π-electron density across the 'NCN' amidine component of the guanidine (**II** and **III,** Figure **2.1**). Although widely used to describe bonding properties of anionic guanidinates, it is equally applicable to cationic guanidinium species.

Δ'_{CN}: The Δ'_{CN} value is typically applied to bicyclic guanidine systems, and is defined as an approximation of the extent to which the lone-pair of the tertiary nitrogen contributes to the π-system at the CN_3-core of the guanidine.[28,29] Δ'_{CN} values corresponding to a protonated guanidinium cation typically fall between 0, reflecting a fully delocalized system (**I**, Figure **2.1**), to 0.10 Å. Negative Δ'_{CN} values may be observed if the contribution from resonance form **IV** predominates bonding within the guanidinium species (Figure **2.1**).[13]

DP: The degree of pyramidalization (DP) is expressed as a percentage, and serves as an estimation of the derivation of the bond angles within the three-coordinate center from the full angle, normalized to 90°.[30] Maximum pyramidalization (100%) is achieved if the sum of the three angles used within the calculation equates to 270°, correlating to three mutually perpendicular 2*p* atomic orbitals. Minimum pyramidalization (0%) corresponds a planar nitrogen atom.

ρ : The 'rho' value is a reflection of the elongation of the C=N double bond following protonation relative to the accompanying shortening of the average C—NR_2 distance.[31]

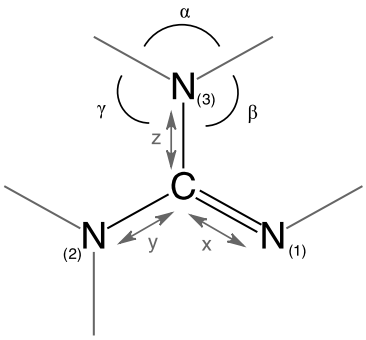

$\Delta_{CN}/Å = y - x$

$\Delta'_{CN}/Å = z - [\{x + y\}/2]$

DP % = $[360 - (\alpha + \beta + \gamma)]/ 0.9$

$\rho = 2x / (y + z)$

Figure 2.2: Summary of the geometric parameters used to describe the bonding within guanidinium cations

Although these calculated values are often statistically questionable when considering the inherent errors of X-ray diffraction data, they have been used qualitatively to understand trends in the bonding within these systems.

2.1.2 [hppH$_2$][BPh$_4$][13]

The bonding and structural properties of the cationic $[hppH_2]^+$ species was previously examined through the synthesis and characterization of different $[hppH_2]^+$ salts with varying counter-anions. One such compound was the tetraphenylborate salt, $[hppH_2][BPh_4]$, which was synthesized by stoichiometric reaction between the nitrogenous base and triethylammonium tetraphenylborate ($[HNEt_3][BPh_4]$) to form crystalline $[hppH_2][BPh_4]$.[13] The NMR spectral results suggest a symmetric structure for the bicyclic ring units of the protonated guanidinium salts, indicating a fully delocalized structure (**I**, Figure **2.1**), or the rapid movement of electrons between the tautomeric structures **II**, **III** and **IV** (Figure **2.1**).

^{1}H NMR analysis of the resulting tetraphenylborate salt $[hppH_2][BPh_4]$ showed a general downfield shift of the hpp-proton resonances (δ_H 3.22, 3.17, 1.89 ppm) in comparison to the neutral starting material hppH (δ_H 3.09, 3.03, 1.79 ppm).[13] It was proposed that this was due to deshielding of the resonating protons within the product that occurs upon protonation of the guanidine functionality. It was found that the central guanidinium carbon (CN_3) resonates further downfield (δ_C 165.3 ppm) than in the neutral starting material (δ_C 151.9 ppm). This large shift was attributed to the inability of the guanidinium ions to hydrogen-bond to the $[BPh_4]^-$ anion, causing deshielding of this carbon atom and a downfield shift within the spectral data.[13]

Single crystal X-ray diffraction was performed on this crystalline product. It was found that the packing of the $[hppH_2][BPh_4]$ ions in the solid-state showed an octahedral assembly of six borate anions that enclose the $[hppH_2]^+$ cation.[13] Eight phenyl substituents from these anions encapsulate the cation, shielding it from any strong electrostatic interactions. As postulated from the spectroscopic data, the molecular structure revealed that there was no hydrogen-bonding interaction between the cationic species and the tetraphenylborate anion.[13] Descriptions of the bonding within this compound were somewhat restricted due to the crystallographically induced symmetry, and thus the geometric parameters (Δ_{CN}, Δ'_{CN}, DP percentages, and ρ) described earlier were not calculated for this species.

2.1.3 $[hppH_2][Cl]$[13]

The corresponding $[hppH_2]^+$ cation was examined in the hydrochloride salt $[hppH_2][Cl]$ (**27**), synthesized through stoichiometric addition of triethylamine hydrochloride to hppH.[13] As in the tetraphenylborate example, NMR spectral data suggest a symmetric structure for the bicyclic ring units of the protonated guanidinium salt.

Although the molecular structures of the cationic species in both the tetraphenylborate and hydrochloride salts are identical, there were significant differences found in the ^1H and ^{13}C NMR spectra suggesting electronic differences in solution. One important discrepancy was the chemical shift of the central 'CN_3' carbon atom, which differed by 12.3 ppm, resonating at δ_C 165.3 ppm for the tetraphenylborate salt compared to the higher field resonance of δ_C 153.0 ppm for the hydrochloride salt.[13] Furthermore, there was a large difference between the N*H* chemical shifts in the ^1H NMR spectra, having a value of δ_H 8.38 ppm in the hydrochloride salt, and δ_H 5.76 ppm for the tetraphenylborate salt. These differences were attributed to ion-pairing in the hydrochloride salt, most likely consisting of hydrogen-bonds between the guanidinium protons and the chloride anion, where no such interaction is possible between the $[hppH_2]^+$ cation and $[BPh_4]^-$ anion.[13] This inference was supported by IR spectral data. The hydrochloride salt shows a series of absorptions for the N–H stretch in the region 3330-3139 cm^{-1} that are in a similar region to those found in the neutral compound, although the absorbencies in the cation spectrum were broader. Contrastingly, the tetraphenylborate salt has a single sharp absorbance at 3380 cm^{-1}, which was assigned to an N–H vibration. The multiple broad peaks at high frequency were attributed to the presence of hydrogen bonding

in the solid state, whereas the inability of the tetraphenylborate salt to form any hydrogen bonds leads to the observation of the N–H absorption as a single sharp peak.[13]

The molecular structure of the hydrohalide salt has also been investigated using single crystal X-ray diffraction. It was determined that the [hppH$_2$][Cl] solid-state structure consists of a monomeric guanidinium cation in which the protonated imine nitrogen and secondary amino nitrogen form two N–H···Cl hydrogen bonds with the halide counter-ion (Figure **2.3**).[13]

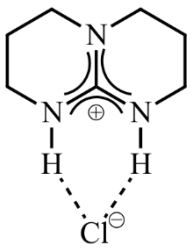

27

Figure 2.3: Structure of [hppH$_2$][Cl] salt[13]

The geometric parameters, as described in Section 2.11, calculated from the structural data show effective delocalization throughout the guanidinium moiety.[13] The low Δ_{CN} value of 0.012 Å shows a very small difference between the C—N and C=N bond lengths, as expected for delocalized systems. A negative Δ'_{CN} value of -0.005 Å indicates delocalization of the lone-pairs into the CN_3 core of the cation to offset the formal positive charge at the protonated nitrogen atom.[13] Additionally, the low DP percentage range (1.1—3.4%) supports efficient delocalization. Finally, the ρ value of 1.00 shows symmetrical bonding within the CN_3 core, indicating the effective distribution of the positive charge associated with the proton across all three carbon-nitrogen bonds.[13]

Examination of the extended molecular structure revealed an association of the [hppH$_2$][Cl] ion-pairs into dimers, in which the halide anions are located above the C_1–N_3 bond of the [hppH$_2$]$^+$ cation (Figure **2.4**).[13] This would correspond with a large contribution of resonance structure **IV** (Figure **2.1**), which allocates a large portion of the positive charge to this area, and is consistent with the negative Δ'_{CN} calculated from the structural data.

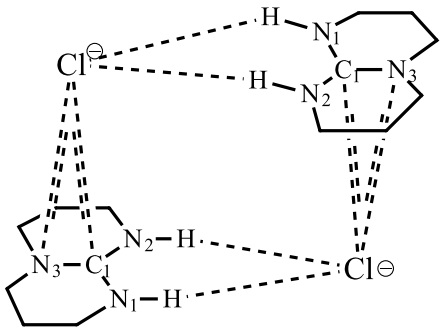

Figure 2.4: Association of [hppH$_2$][Cl] (**27**) ion pairs into dimeric units[13]

It should be noted that the species [hppH$_2$][Cl] is very hygroscopic, and the crystal structure has also been determined for the mono-hydrate hydrochloride salt.[32] This crystal structure showed hydrogen bonds between H$_1$ and the chloride anion, H$_2$ and the oxygen atom in H$_2$O, and a proton on the water molecule and the chlorine anion (Figure **2.5**).[32] In a crystalline ensemble, these molecules are form helical Cl·H$_2$O chains connected to each other by hydrogen bonding with the [hppH$_2$]$^+$ cations.[32]

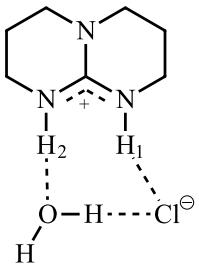

Figure 2.5: Structure of an individual molecule of [hppH$_2$]Cl·H$_2$O[32]

2.2 Synthetic and Analytical Strategies Adopted in this Project

2.2.1 Synthesis of Poly-hpp Compounds

To explore the reactivity and limitations of this system, a range of hpp-containing superbases were employed for CO_2 capture. These compounds were synthesized utilizing a similar one-pot, two-step reaction procedure, and is illustrated for the poly-hpp compound discussed in Chapter 1 (1,3,5-(CH$_2$hpp)$_3$-C$_6$H$_3$) in Scheme **2.1**.

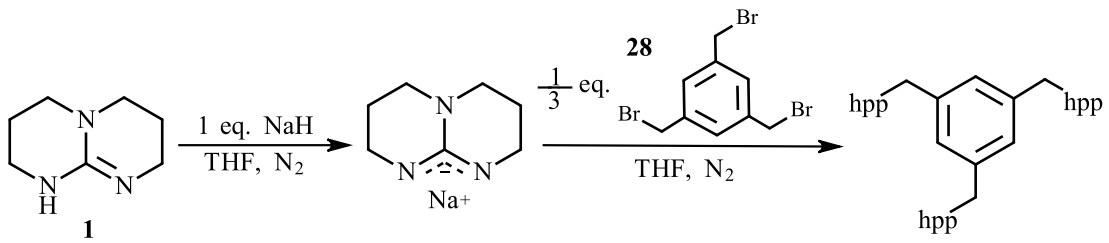

Scheme 2.1: Formation of poly-hpp compounds

An equimolar amount of sodium hydride was added to sublimed hppH (**1**) in THF and stirred for two hours at 60 °C, to afford a thick white solid of the corresponding sodium guanidinate species. The resulting mixture was then reacted with a bromobenzyl compound, in this example, one third equivalent of 1,3,5-tris(bromomethyl)benzene (**28**), for 24 hours at room temperature. Following the removal of the volatiles *in vacuo,* the product was extracted with toluene and filtered from the NaBr byproduct. Purification was performed by crystallization achieved through storage of the product in solution of toluene (2 mL) at -30 °C. The resulting crystallized poly-hpp products were achieved in moderate to good yield, ranging between 44—84%.

2.2.2 Compounds and structural considerations

As an active goal in this research is to understand how the structure of these bases either hinder or promote the activation of CO_2, a variety of hpp-derived compounds were synthesized.

Differing structural components within this class of compounds include the number of methylene supported hpp-units incorporated around a central benzene ring, and the substitution pattern of these moieties to explore the effect of their relative position. These considerations lead to the development of the compounds shown in Figure **2.6**: Ph(CH_2hpp) (**29**), 1,2-(CH_2hpp)$_2$-C_6H_4 (**30**), 1,3-(CH_2hpp)$_2$-C_6H_4 (**31**), 1,4-(CH_2hpp)$_2$-C_6H_4 (**32**), and the previously discussed 1,3,5-(CH_2hpp)$_3$-C_6H_3 (**33**, Scheme **1.8**).

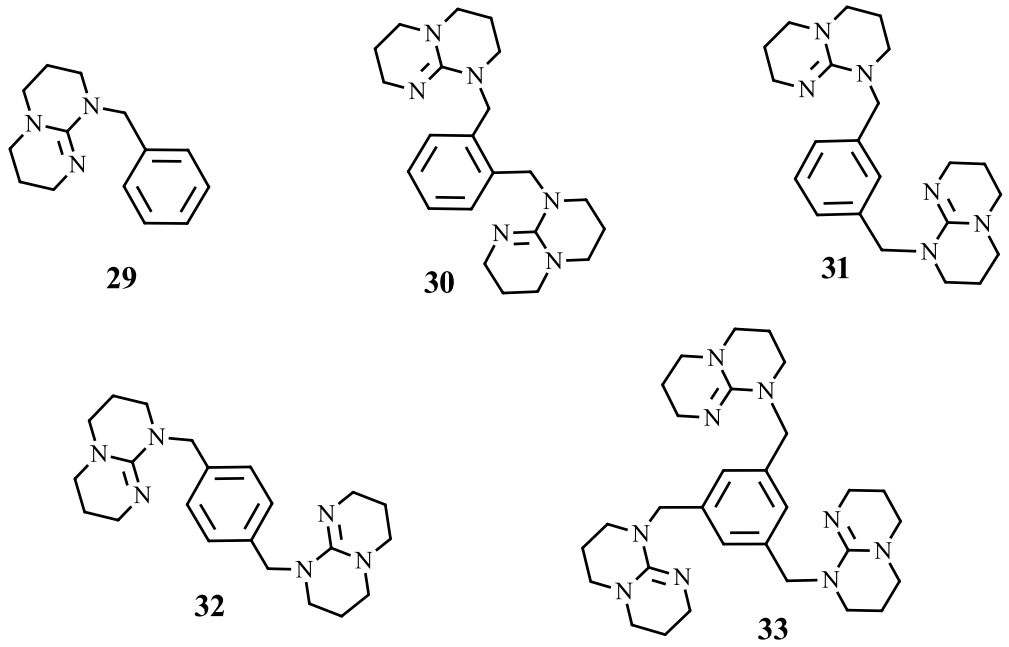

Figure 2.6: hpp-containing starting compounds

Another structural modification that has been taken into consideration throughout the investigation of this research is the incorporation of supplementary alkyl substituents about the C_6-ring. Two different hpp-containing compounds were developed and explored for this purpose: 2,4,6-$(CH_2hpp)_3$-mesitylene (**34**), and 1,3,5-$(CH_2hpp)_3$-2,4,6-$(Et)_3$-C_6 (**35**) (Figure **2.7**).

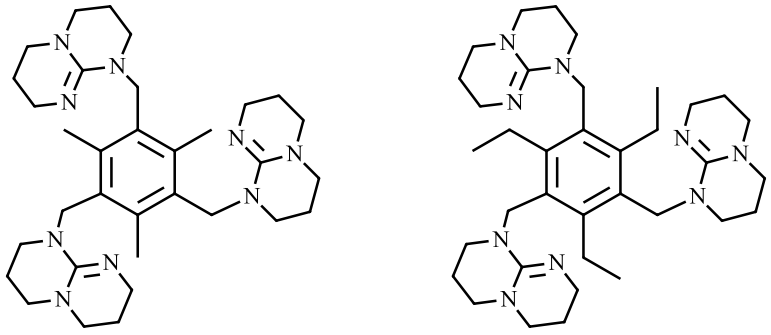

Figure 2.7: Poly-hpp starting compounds containing alkyl substituents

One interest in the implementation of compounds **34** and **35** is their structural conformation in the solid-state, and how these additional substituents effect the bonding properties of the protonated guanidinium functionalities. For example, within compound **35**, the solid-state molecular structure favors an arrangement where the three hpp-moieties are located on the same face of the plane defined by the C_6-ring. This is different from 1,3,5-$(CH_2hpp)_2$-C_6H_3

(**33**), in which the energetic preferential conformation in the solid-state has two hpp-units pointing towards one direction, and the third in the opposite direction. This spatial conformation of the guanidine functionalities could influence the reactivity of this compound towards CO_2 activation.

2.2.3 Analytical approach

The following chapters describe the synthesis and characterization of hppH-containing guanidinium salts incorporating a variety of counter-anions. The product labeling scheme found in the following chapters contain both a number denoting the identity of the hpp-containing superbase, and a letter that denotes the identity of the anionic species within the salt. The number labels of the guanidine correspond to those listed in section 2.2.2 (**29**—**35**), and neutral hppH (**1**). The anionic lettering is listed below, and should be used as a reference within the following discussion of the collected experimental results.

a = tetraphenylborate anion ($[BPh_4]^-$)
b = chloride anion ($[Cl]^-$)
c = bicarbonate anion ($[HCO_3]^-$)
d = carbonate anion ($[CO_3]^{2-}$)

Each reaction to synthesize the guanidinium salts was performed under air, and on a 0.10 g scale of neutral guanidine superbase. For clarity, Figure **2.8** illustrates the neutral and protonated hpp-units found in the starting material and products, respectively.

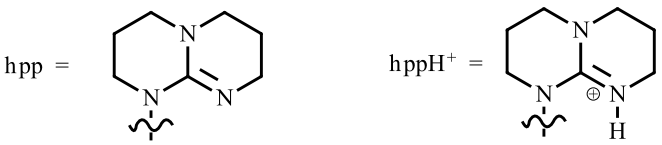

Figure 2.8: Neutral [hpp] fragment and protonated $[hppH]^+$ fragment

Volatiles were removed via slow evaporation at room temperature, unless stated otherwise. Crystallization of the product was performed through storage of the product in solution at -30 °C, or by slow evaporation of the solvent at room temperature. Crystalline products were not obtained for every species.

Each described guanidinium salt was characterized through ^1H NMR and ^{13}C NMR analysis. Elemental analysis and IR spectroscopy were also performed on select samples. Where good

quality crystals were obtained, the molecular solid-state structure was determined through single crystal X-ray diffraction. The geometric parameters describing the bonding within the guanidinium units were calculated from the data collected for every obtained molecular structure.

To aid in the interpretation of these values, geometric parameters were calculated from the crystal data of the neutral guanidine unit within 1,4-$(CH_2hpp)_2$-C_6H_4 (**32**, Figure **2.9**). These calculations will be used as a comparison within the discussion of the synthesized guanidinium salts within the following chapters (*vide infra*).

Crystals of compound **32** were obtained through storage of the product under air in a solution of acetonitrile (2 mL) at -30 °C. This molecule crystallizes in the $P\,2_1/n$ space group, and is located on a center of inversion which is located within the central aryl ring. Select bond lengths are listed in Table **2.1**, and the calculated geometric parameter values are listed in Table **2.2**.

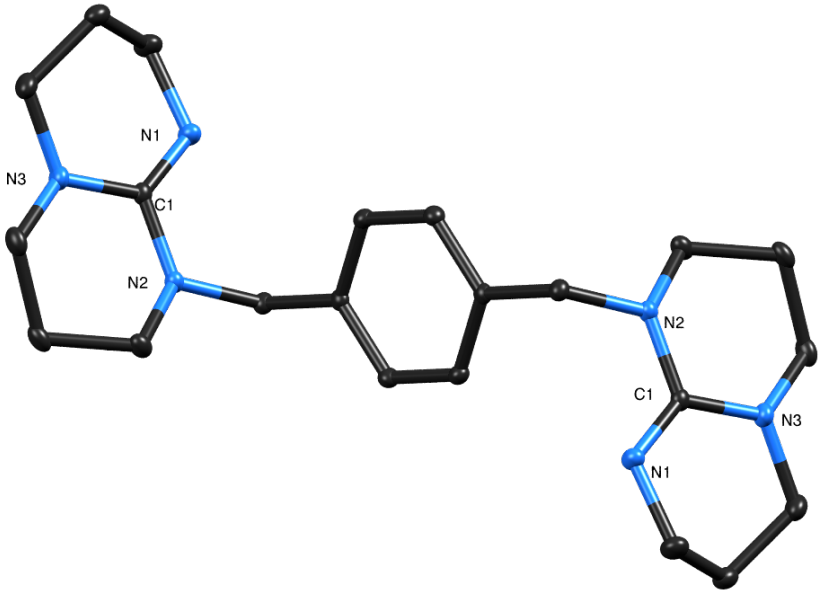

Figure 2.9: Thermal ellipsoid representation (20%) of 1,4-$(CH_2hpp)_2$-C_6H_4 (**32**). Hydrogens omitted for clarity. Selected bond lengths listed in Table **2.1**.

N**1**—C**1**	1.291(2) Å
N**2**—C**1**	1.387(2) Å
N**3**—C**1**	1.378(2) Å

Table 2.1: Select bond lengths in neutral **32**

Δ_{CN} / Å	0.096
Δ'_{CN} / Å	0.039
DP_{N2}	4.00%
DP_{N3}	5.55%
ρ **ratio**	0.93

Table 2.2: Summary of geometric data for the guanidine component of **32**

Chapter 3

Tetraphenylborate Salts

To understand the bonding parameters of the protonated guanidinium (cationic) units of this class of superbases, a series of reactions were employed utilizing various protonation sources containing differing counter-anions. [hppH$_2$][BPh$_4$][13] was used as a reference structure to allow comparison of the structures obtained in this study. As the tetraphenylborate anion is very bulky, unreactive, and incapable of hydrogen-bonding, it served as a benchmark reaction to characterize the cationic forms of these compounds and understand their distinct structural characteristics under air.

3.1 Synthesis and Characterization of [1,4-(CH$_2$hppH)$_2$-C$_6$H$_4$][BPh$_4$]$_2$ (32*a*)

3.1.1 Synthesis

To form tetraphenylborate salt **32*a***, two equivalents of triethylammonium tetraphenylborate were added to a solution of the neutral hpp-containing compound **32** in THF, and stirred under air for 20 minutes. Removal of the volatiles *in vacuo* afforded an off-white powder. Recrystallization from acetonitrile at -30 °C yielded white crystals of the desired tetraphenylborate salt (**32*a***) in 39% isolated yield (Scheme **3.1**).

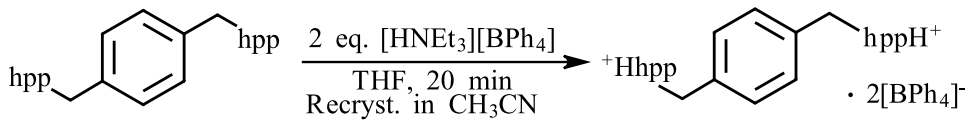

32 **32*a***

Scheme 3.1: Synthetic strategy for the formation of [1,4-(CH$_2$hppH)$_2$-C$_6$H$_4$][BPh$_4$]$_2$ (**32*a***)

3.1.2 Spectroscopic Properties

The ^{1}H NMR and ^{13}C NMR spectral data support the formation of the desired tetraphenylborate salt **32*a***. A downfield shift of the benzyl-methylene protons (δ_H 4.44 ppm) is observed when compared to the neutral starting material **32**. This is consistent with the delocalization of the resonating protons that occurs upon protonation of the guanidine functionality. This downfield shift is also seen in the NC*H*$_2$ hpp-proton resonances (δ_H 3.29 and 3.19 ppm). Signals found at δ_H 7.27, 6.99, and 6.84 ppm have an integration ratio of 2:2:1, and can be attributed to the *ortho*-, *meta*-, and *para*-phenyl protons of the $[BPh_4]^-$ anion, respectively. These data are consistent with literature values found for the analogous tetraphenylborate salt $[hppH_2][BPh_4]$.[13] Comparison of these integral values with those of the cationic species indicate the presence of two tetraphenylborate anions. It should be noted that there is a large water peak found at δ_H 2.20 ppm (HOD), which is to be expected as this class of superbasic compounds is highly hygroscopic. Additionally, the guanidinium N*H* resonance is absent from this spectrum, which can be attributed to rapid H/D exchange with either the deuterated acetonitrile.

The ^{13}C NMR data also supports the successful synthesis of tetraphenylborate salt **32*a***. A low field quartet signal observed at δ_C 163.8 ppm corresponds to the *ipso*-carbon of the anion showing coupling to ^{11}B ($I=\frac{3}{2}$, 80% abundant). A resonance at δ_C 151.0 ppm is assigned to the central carbon (CN_3) within the guanidinium functionality. Unlike the low field *C*N_3 signal observed in spectral data of $[hppH_2][BPh_4]$[13], this signal is found further upfield, believed to be due to the presence of hydrogen bonding between the guanidinium cations and water molecules in solution.

Elemental analysis was performed on the isolated crystals of this product. A large discrepancy between the calculated and experimentally found carbon weight content was found. It is possible that this is due to variable amounts of water or solvent found within the collected product. The distinct reason to this inconsistency is not fully understood, but is not uncommon with this analytical technique.

3.1.3 Solid-State Structure

Single crystal X-ray analysis confirmed the product as the monomeric tetraphenylborate salt, [1,4-(CH_2hppH)$_2$-C_6H_4][BPh_4]$_2$ (**32*a***, Figure **3.1**). Compound **32*a*** crystallizes in the $P\bar{1}$ space group, and lies on an inversion center. Select bond lengths of this compound are listed in Table **3.1**, and calculated geometric parameter data for the guanidinium cationic units is listed in Table **3.2**. As in [hppH$_2$][BPh_4],[13] the packing of the ions within this salt show that the phenyl substituents effectively encapsulate the cationic guanidinium functionalities, shielding these regions from any strong electrostatic interactions.

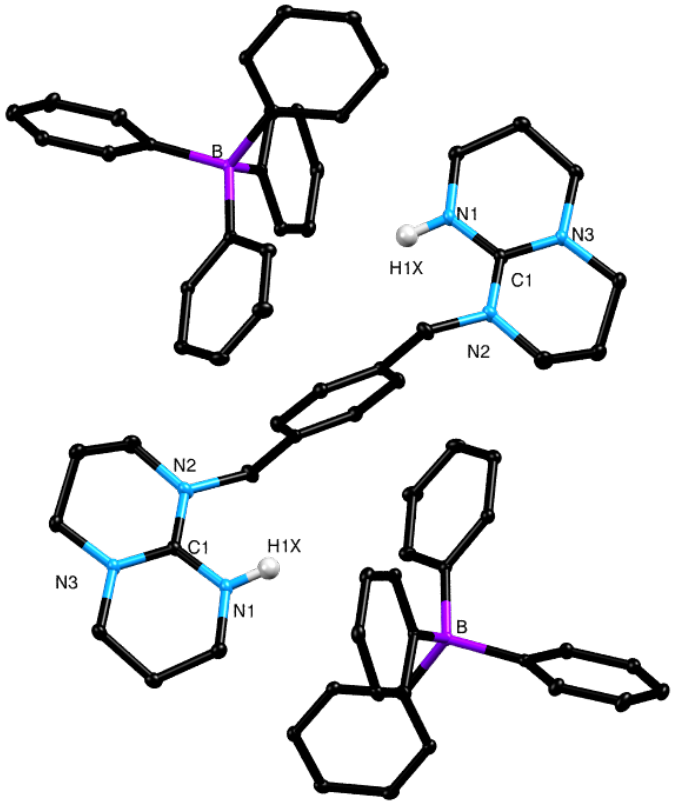

Figure 3.1: Thermal ellipsoid representation (30%) of tetraphenylborate salt **32*a***. Hydrogens (except N*H*) omitted for clarity. Selected bond lengths are reported in Table **3.1**.

Bond	**[1,4-(CH_2hppH)$_2$-C_6H_4][BPh_4]$_2$ (32*a*)**	**Neutral 1,4-(CH_2hpp)$_2$-C_6H_4 (32)**
N**1**—C**1**	1.3401(19) Å	1.291(2) Å
N**2**—C**1**	1.3428(19) Å	1.387(2) Å
N**3**—C**1**	1.3341(18) Å	1.378(2) Å

Table 3.1: Select bond lengths in tetraphenylborate salt **32*a*** and neutral **32**

Whereas there is a significant difference between the C—N single and C=N double bond lengths found within the neutral starting material **32** (Δ_{CN} = 0.096 Å) , this difference is less pronounced within the tetraphenylborate salt ***32a*** (Δ_{CN} = 0.008 Å), indicating a more delocalized structure. The low DP range (0.11—0.22%) serves as further evidence for delocalization of the guanidinium units, and is consistent with literature values found for previously characterized $[hppH_2]^+$ salts.[13] It should be noted that the DP percentage was not calculated for N**1** due to the inherent positional inaccuracies of the hydrogen atom. The negative Δ'_{CN} value of -0.007 Å calculated for compound ***32a*** indicates delocalization of the lone-pairs into the CN_3 core of the cation to offset the formal positive charge at the protonated nitrogen. The ρ ratio calculated from the crystal data of the starting material **32** is 0.93 (Table **2.2**), indicating that the length of the C=N double bond is 93% of the average C-NR_2 single bond. The ρ ratio calculated from the tetraphenylborate salt (***32a***) structure data is found to be 1.00. This change is expected upon protonation, as delocalization of the charge throughout the CN_3 core results in an increase in the C=N bond length and subsequent decrease of the C-NR_2 bonds. This ρ ratio of 1.00 also indicates effectively distributed positive charge across the carbon-nitrogen bonds, and complete symmetrical bonding within the central guanidinium core. This value is consistent with that calculated from the literature structural data of $[hppH_2][BPh_4]$.[13]

Δ_{CN} / Å	0.008
Δ'_{CN} / Å	-0.007
DP_{N2}	0.22%
DP_{N3}	0.11%
ρ ratio	1.00

Table 3.2: Summary of geometric data for the guanidinium components of tetraphenylborate salt ***32a***

3.2 Synthesis and Characterization of [1,2-(CH_2hppH)$_2$-C_6H_4][BPh_4]$_2$ (**30*a***)

3.2.1 Synthesis

Following the typical procedure of equimolar addition of $[BPh_4]^-$ anionic species per hpp-unit, two equivalents of triethylammonium tetraphenylborate were added to a solution of neutral 1,2-(CH_2hpp)$_2$-C_6H_4 (**30**) in THF, and stirred under air for 1 hour (Scheme **3.2**). The volatiles were removed *in vacuo.*, resulting in formation of a white powder. White crystals of the desired tetraphenylborate salt (**30*a***) were obtained in 94% yield through slow evaporation of acetonitrile.

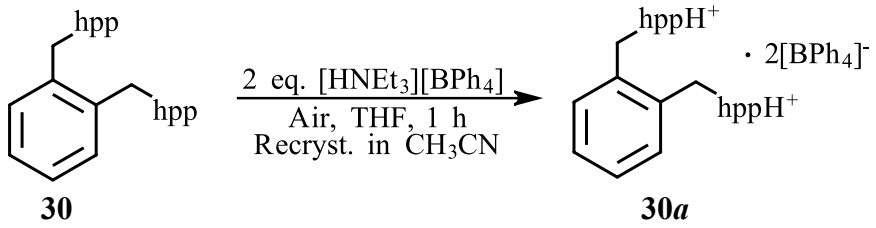

Scheme 3.2: Synthesis of [1,2-(CH_2hppH)$_2$-C_6H_4][BPh_4]$_2$ (**30*a***)

3.2.2 Spectroscopic Properties

The ^{1}H NMR and ^{13}C NMR spectral data support the formation of the desired tetraphenylborate salt **30*a***. Similarly to [1,4-(CH_2hppH)$_2$-C_6H_4][BPh_4]$_2$ (**32*a***), a downfield shift is observed for both the benzyl-methylene protons (δ_H 4.40 ppm) and the NC*H*$_2$ hpp-proton resonances (δ_H 3.37, 3.21, and 2.09 ppm) when compared to the neutral starting material **30**. Signals at δ_H 7.36, 7.08, and 6.93 ppm with an integration ratio of 2:2:1 can be assigned to the resonating *ortho-*, *meta-*, and *para-*phenyl protons within the anionic species, respectively. These data are consistent with the previously characterized salt **32*a*** and with literature values found for the analogous tetraphenylborate salt [hppH$_2$][BPh_4][13]. There is a broad water peak found at δ_H 2.92 ppm (HOD), which is to be expected as this class of superbasic compounds is highly hygroscopic. As in compound **32*a***, there is no signal corresponding to the guanidinium N*H* protons, which can be attributed to rapid exchange with the solvent or water present within the sample (*vide infra*). The ^{13}C NMR data is also consistent

with the successful synthesis of tetraphenylborate salt **30*a***. A low field quartet signal found at δ_C 163.8 ppm corresponds to the *ipso*-carbon within the anion. A resonance at δ_C 151.0 ppm can be assigned to the central carbon (CN_3) within the guanidinium functionality. As with compound **32*a***, this upfield signal can be attributed to the presence of hydrogen bonding between the protonated guanidinium cation and water molecules present in solution. This bonding causes a more shielded environment for the central CN_3 carbon, resulting in a high-field spectroscopic shift.

3.2.3 Solid-State Structure

Single crystal X-ray diffraction of the product confirmed the formation of the desired tetraphenylborate salt, 1,2-$(CH_2hppH)_2$-C_6H_4 (**30*a***, Figure **3.2**). This compound crystallizes in the $P2_1/c$ space group, and was found to contain one molecule of water solvate and one molecule of acetonitrile solvate (the latter is omitted from Figure **3.2** for clarity). There is hydrogen-bonding between both N*H* protons on the guanidinium units and the oxygen atom of the water molecule, which hydrogen bonds to the CH_3CN molecule (not pictured). Three of the annular methylene groups are disordered and were each modelled over two positions. Selected bond lengths are listed in Table **3.3**, and calculated geometric parameters of the guanidinium functionalities are listed in Table **3.4**.

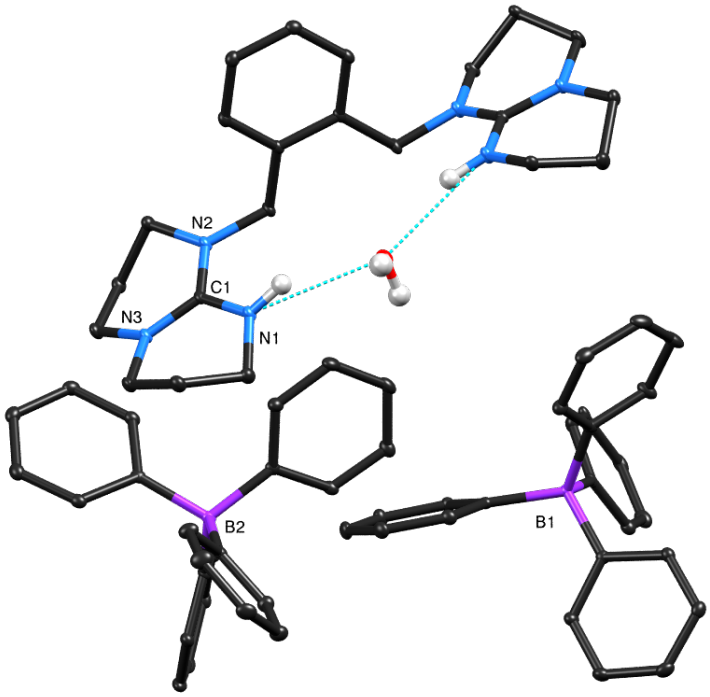

Figure 3.2: Thermal ellipsoid representation (20%) of **30*a***. Hydrogens (except N*H* and H_2O) omitted for clarity. Selected bond lengths are reported in Table **3.3**.

Bond	[1,2-(CH$_2$hppH)$_2$-C$_6$H$_4$][BPh$_4$]$_2$ (**30*a***)	Neutral 1,2-(CH$_2$hpp)$_2$-C$_6$H$_4$ (**30**)[23]
N**1**—C**1**	1.3355(15) Å	1.305(2) Å
N**2**—C**1**	1.3427(15) Å	1.374(2) Å
N**3**—C**1**	1.3387(15) Å	1.370(2) Å

Table 3.3: Select bond lengths in tetraphenylborate salt **30*a*** and neutral **30**

The geometric parameters calculated from the structural data of compound **30*a*** reflect efficient delocalization within guanidinium functionalities. The low Δ_{CN} value of 0.007 Å shows a very minimal difference between C—N single and C=N double bond lengths as would be expected in a delocalized system, whereas within the neutral starting material (**30**) this difference is much more pronounced (Δ_{CN} = 0.069 Å). The small negative Δ'_{CN} of -0.0004 Å and low DP percentage range (0.11—0.44%) also indicate delocalization throughout the hpp-unit. Finally, the ρ ratio of 1.00 reflects effectively distributed positive charge across the carbon-nitrogen bonds, and symmetrical bonding within the guanidinium cation.

Δ_{CN} / Å	0.007
Δ'_{CN} / Å	-0.0004
DP_{N2}	0.44%
DP_{N3}	0.11%
ρ ratio	1.00

Table 3.4: Summary of geometric data for the guanidinium components of tetraphenylborate salt **30*a***

3.3 Synthesis and Characterization of [1,3,5-$(CH_2hppH)_3$-C_6H_3][BPh_4]$_3$ (***33a***)

3.3.1 Synthesis

Under air, three equivalents of triethylammonium tetraphenylborate were added to a solution of neutral 1,3,5-$(CH_2hpp)_3$-C_6H_3 (***33***) in THF, resulting in the formation of a white precipitate. The suspension was stirred for 24 hours, and the volatiles removed *in vacuo.*, leaving a white powder (Scheme **3.3**). Although crystals were obtained through storage of the crude product in a solution of dichloromethane, they were unsuitable for crystallographic analysis. The solid product of [1,3,5-$(CH_2hppH)_3$-C_6H_3][BPh_4]$_3$ (***33a***) was collected in 89% yield, and characterized through ^{1}H NMR and ^{13}C NMR analysis.

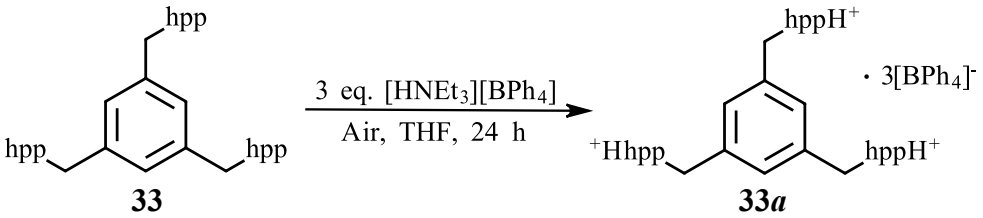

33 **33a**

Scheme 3.3: Synthesis of [1,3,5-$(CH_2hppH)_3$-C_6H_3][BPh_4]$_3$ (***33a***)

3.3.2 Spectroscopic Properties

^{1}H NMR and ^{13}C NMR spectral data support the successful formation of [1,3,5-$(CH_2hppH)_3$-C_6H_3][BPh_4]$_3$ (***33a***). As in the characterization of the previously discussed tetraphenylborate salts, the comparison of the ^{1}H NMR spectra of the product and starting material ***33*** show a downfield shift in the resonating proton signals. This shift shows greater deshielding of these protons in the product, indicating successfully protonated guanidine functionalities. This shift is seen most clearly in the singlet resonance of the benzyl-methylene protons (δ_H 4.44 ppm). Low-field signals at δ_H 7.26, 7.02 and 6.86 ppm can be assigned to the *ortho-*, *meta-*, and *para-*phenyl protons within the $[BPh_4]^-$ anion. The integrals within this spectrum show that there are three tetraphenylborate anionic groups per one tricationic species. It should be noted that there is a large water peak within this spectrum (δ_H 2.00 ppm, HOD). Additionally, there is no signal present that can be assigned to the guanidinium N*H* proton, most likely due to rapid proton exchange with the water present in the sample or H/D exchange with CD_3CN. The

^{13}C NMR spectral data also suggests formation of compound ***33a***. As in the previous hpp-containing tetraphenylborate salts, a low field quartet resonance is assigned to the *ipso*-carbon within the anion is found at δ_C 163.8 ppm. An upfield resonance at δ_C 151.0 ppm corresponding to the central guanidine carbon (CN_3) suggests hydrogen bonding of the cationic guanidinium units to water present within the solution.

3.3.3 Attempted Partial Protonation

Following the successful synthesis of $[1,3,5\text{-}(CH_2hppH)_3\text{-}C_6H_3][BPH_4]_3$ (***33a***), isolation of both the corresponding mono- and di-protonated guanidinium derivatives was attempted. Under the same reaction conditions outlined in Scheme **3.1**, in two separate reactions both one and two equivalents of triethylammonium tetraphenylborate were added to a solution of ***33,*** in the attempt to synthesize the mono- and di-protonated guanidinium derivatives, respectively. Crystalline products of these reactions were unable to be obtained, and thus characterization was performed on the crude products. ^1H NMR analysis of the crude products displayed a general downshift in the resonances, as found in the previous tetraphenylborate salts. However, the spectra also suggest that all three hpp-units are equivalent, fully protonated guanidinium ions despite the addition of a sub-stoichiometric amount of triethylammonium tetraphenylborate with respect to the hpp-groups. The presence of the three equivalent protonated guanidinium units is postulated to occur by one of two ways. One theory is that the partially protonated cationic species is successfully formed, but the guanidine units undergo rapid proton exchange in solution resulting in an average NMR spectroscopic signature. For example, in the attempted di-protonation of **33** through addition of two equivalents of $[HNEt_3][BPh_4]$, the resulting product would be $[1,3,5\text{-}(CH_2hpp)(CH_2hppH)_2\text{-}C_6H_3][BPh_4]_2$. A second possibility to explain this result is that the superbasic compound is sequestering protons from another source. As outlined in Scheme **1.8**, it has been observed previously that protonation of one guanidine functionality within this system activates the compound toward further protonation. This would suggest the successful formation of the tricationic species, however the composition of the anionic components is not fully known. Using the attempted di-protonation as an illustration, the synthesized product would be $[1,3,5\text{-}(CH_2hppH)_3\text{-}C_6H_3][BPh_4]_2[X]^-$, where $[X]^-$ is the unknown third counter-ion. It is possible that this anionic species is either a hydroxyl or bicarbonate anion, however the spectroscopic data gives no

evidence towards its identity. These inconclusive spectral results show the complexity of these superbasic systems, and has served as a limitation in their full characterization.

3.4 Synthesis and Characterization of [1,3,5-$(CH_2hppH)_3$-2,4,6-$(Et)_3$-C_6][BPh_4]$_2$ (**35*a***)

3.4.1 Synthesis

Under air, three equivalents of triethylammonium tetraphenylborate were added to a solution of neutral 1,3,5-$(CH_2hpp)_3$-2,4,6-$(Et)_3$-C_6 (**35**) in THF, resulting in the formation of a white precipitate. The suspension was stirred for 24 hours, and the volatiles removed *in vacuo.*, leaving a white powder (Scheme **3.4**). Although crystals were obtained through storage of the crude product in a solution of dichloromethane, they were unsuitable for crystallographic analysis. The solid product of [1,3,5-$(CH_2hppH)_3$-2,4,6-$(Et)_3$-C_6][BPh_4]$_3$ (**35*a***) was collected in 82% yield, and characterized through ^{1}H NMR and ^{13}C NMR analysis.

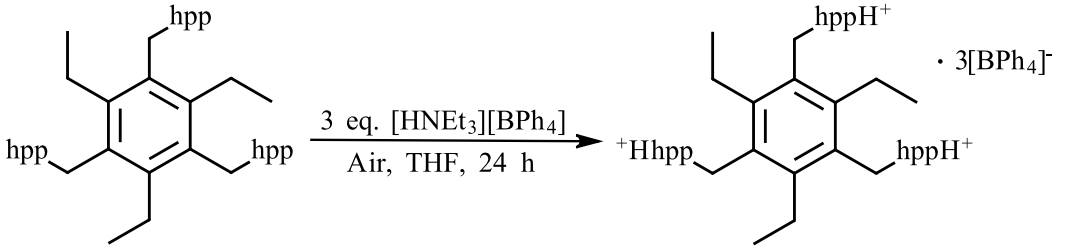

35 **35*a***

Scheme 3.4: Synthesis of [1,3,5-$(CH_2hppH)_3$-2,4,6-$(Et)_3$-C_6][BPh_4]$_3$ (**35*a***)

3.4.2 Spectroscopic Properties

^{1}H NMR and ^{13}C NMR spectral data indicate the successful formation of [1,3,5-$(CH_2hppH)_3$-2,4,6-$(Et)_3$-C_6][BPh_4]$_3$ (**35*a***). As characteristic of guanidinium salts, the comparison of the ^{1}H NMR spectra of the product and neutral starting material (**35**) show a downfield shift in the resonating proton signals. This is seen most clearly in the resonance of the benzyl-methylene protons (δ_H 4.39 ppm). Similar to the spectral evidence of the previous tetraphenylborate salts, low field signals at δ_H 7.31, 7.03 and 6.88 ppm having an integration ratio of 2:2:1 are assigned to the *ortho*-, *meta*-, and *para*-phenyl protons, respectively, within the [BPh_4]- anionic species.

Further comparison of the integration values show the presence of three tetraphenylborate anions. As expected for this hygroscopic class of compounds, there is a large water peak found at δ_H 2.00 ppm. There is no resonance corresponding to the guanidinium N*H* proton within the ^{1}H NMR spectrum, which can be attributed to rapid H/D exchange with the solvent. A low field quartet within the ^{13}C NMR spectrum at δ_C 163.2 ppm is assigned to the *ipso*-carbon within the tetraphenylborate anion. This is consistent with the literature values of the analogous species [hppH$_2$][BPh$_4$].[13] Also within the previous examples, an up field resonance found at δ_C 151.4 ppm corresponding to the central guanidine carbon (*C*N$_3$) suggests hydrogen bonding of the cationic guanidinium units to water present within the solution.

Chapter 4

Hydrochloride Salts

As discussed in Chapter one, the initial reaction that precipitated this research project involved the addition of one equivalent of triethylamine hydrochloride to 1,3,5-$(CH_2hpp)_3$-C_6H_3 (**33**) under air to form the corresponding bicarbonate salt (Scheme **1.8**), which formed in contrast to the anticipated hydrochloride salt. To optimize this class of compounds towards this reactivity and design a reliable synthetic strategy for CO_2 activation, this protonation source and reaction must be more fully understood. Thus, extensive experimentation was performed in the attempts to synthesize, isolate, and characterize the stable hydrochloride salts of the superbasic compounds under air.

Each of the following species is characterized by ^{1}H NMR and ^{13}C NMR analysis. Crystallographic data was additionally obtained for [1,4-$(CH_2hppH)_2$-C_6H_4][Cl]$_2$ (**32*b***) and [1,2-$(CH_2hppH)_2$-C_6H_4][Cl]$_2$ (**30*b***). As multiple synthetic strategies were employed to obtain these hydrochloride salts, the synthesis and reported spectroscopic properties discussed for these two compounds correspond to the reaction conditions under which crystals were obtained.

4.1 Synthesis and Characterization of [1,4-$(CH_2hppH)_2$-C_6H_4][Cl]$_2$ (32*b*)

4.1.1 Synthesis

Early investigation into the synthesis of these hydrohalide salts targeted the synthesis and isolation of the mono-protonated hydrochloride adduct. Thus, one equivalent of commercially available triethylamine hydrochloride was added to a solution of the neutral hpp-containing compound **32** in acetonitrile, and stirred under air for one hour. Slow evaporation of the volatiles over the course of 24 hours afforded a yellow oil. The oil product was redissolved in

acetonitrile, and subsequent removal of the solvent through slow evaporation yielded yellow crystals, that were determined by single crystal X-ray diffraction to be the diprotonated hydrochloride salt (**32*b***, Scheme **4.1**). This product was collected in 86% isolated crystallized yield (calculated for triethylamine hydrochloride as the limiting reagent), and further characterized through elemental analysis, FTIR analysis, and ^{1}H NMR and ^{13}C NMR spectroscopy.

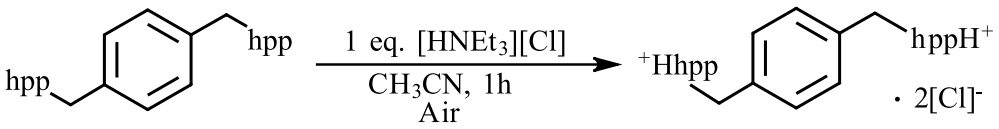

32 **32*b***

Scheme 4.1: Synthesis of [1,4-(CH_2hppH)$_2$-C_6H_4][Cl]$_2$ (**32*b***)

4.1.2 Spectroscopic Properties

The ^{1}H NMR spectral data for the resulting product is consistent with the successful formation of the desired hydrochloride salt **32*b***. When compared to spectral data of the neutral compound **32**, there is an observed downfield shift of all proton resonances. This is consistent with the presence of protonated hpp-imine functionalities, causing deshielding of the resonating protons. This downfield shift is also consistent with reported literature values for the isolated hydrochloride salt, [hppH$_2$][Cl].[13] This deviation in chemical shift is seen most clearly in the benzyl-methylene proton signal, which resonates at δ_H 4.55 ppm within the spectrum of the neutral starting material, and at δ_H 4.87 ppm in the hydrochloride product. There is significant overlap of the hydrochloride salt NC*H*$_2$ resonances (δ_H 3.29 ppm, m, 12H) that is not present in the spectrum of neutral starting material **32**. This overlap is indicative of a greater similarity of their chemical environments, and is consistent with a fully delocalized structure of cationic resonance between the central 'CN_3' carbon and the neighboring nitrogen atoms. It should be noted that there is a large water peak present within the spectrum (δ_H 2.00 ppm, HOD), which is to be expected as this class of superbasic compounds is predicted to be highly hygroscopic, as seen in the previously synthesized [hppH$_2$][Cl]·H_2O.[32] Additionally, there is no signal present that corresponds to the guanidinium N*H* proton, which can be attributed to possible H/D exchange with the solvent.

^{13}C NMR spectroscopic data also supports the successful formation of the desired hydrohalide salt **32*b***. There is an upfield shift of the central CN_3 carbon, found at δ_C 150.7 ppm within the

product and δ_C 151.5 ppm in the neutral compound **32**, indicating a more slightly more shielded environment in the hydrochloride product. Similarly to the previously synthesized [hppH$_2$][Cl], this suggests the presence of ion pairing in ***32b*** between the protonated imine nitrogen and chloride anion (and/or H_2O), causing a more shielded environment for the central carbon atom.[13] There is also a distinct downfield shift seen in the benzyl-methylene carbon signal (δ_C 53.5 ppm for ***32b***, δ_C 48.6 ppm for starting material **32**) that is consistent with deshielding expected in the protonated guanidinium species.

Infrared spectroscopy was employed to investigate this species. However, unlike previously characterized hppH-containing hydrohalide salts, the spectra collected of both the crude and crystallized product of ***32b*** did not differ from the spectrum corresponding to the neutral starting material. It is not clear why this should be the case. It is noted that in this study the IR samples were prepared in air, whereas previous studies were performed under anhydrous conditions. Possible contamination and protonation of the IR sample of neutral **32** under these conditions would give a false reference spectra. Additionally, elemental analysis was performed on this compound, but the results collected were inconsistent with the calculated values. This inconsistency is possibly due to variable amounts of solvent or water found within the tested sample.

4.1.3 Solid-State Structures

Single crystal X-ray analysis confirmed the crystalline product as the monomeric hydrochloride salt, [1,4-(CH$_2$hppH)$_2$-C$_6$H$_4$][Cl]$_2$ (***32b,*** Figure **4.1**). This hydrohalide salt contains two guanidinium cationic hppH-units in which the protonated imine nitrogen atoms each form one NH···Cl hydrogen-bond to the chloride counter-ion. This compound was found to be associated with two water molecules through hydrogen bond interactions between the hydrogen atom within H_2O and the chloride anion. Compound ***32b*** crystallizes in the $P2_1/n$ space group and lies on a two-fold rotation axis (C_2). Selected bond lengths are listed in Table **4.1**, and calculated geometric parameter data for the guanidinium cationic units is listed in Table **4.2**.

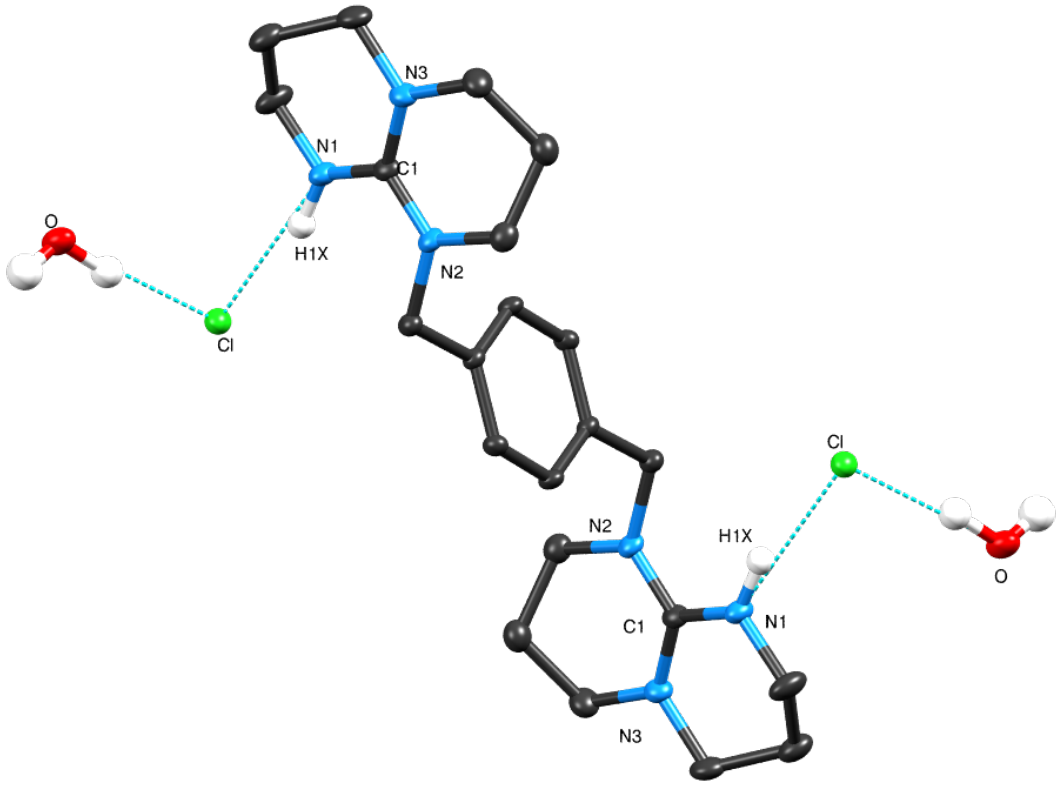

Figure 4.1: Thermal ellipsoid representation (30%) of hydrochloride salt **32*b***. Hydrogens in cation (except N*H*) omitted for clarity. Selected bond lengths are reported in Table **4.1**.

Bond	**[1,4-(CH$_2$hppH)$_2$-C$_6$H$_4$][Cl]$_2$ (32*b*)**	**Neutral 1,4-(CH$_2$hpp)$_2$-C$_6$H$_4$ (32)**
N**1**—C**1**	1.334(4) Å	1.291(2) Å
N**2**—C**1**	1.349(4) Å	1.387(2) Å
N**3**—C**1**	1.335(4) Å	1.378(2) Å

Table 4.1: Select bond lengths in hydrochloride salt **32*b*** and neutral **32**

Whereas there is a significant difference between the C—N single and C=N double bond lengths found within the neutral hpp-derivative **32** (Δ_{CN} = 0.096 Å), this difference is far smaller within the hydrochloride salt **32*b*** (Δ_{CN} = 0.014 Å), indicating delocalized guanidinium structures as anticipated. This value is consistent with the delocalization found in [hppH$_2$][Cl] (Δ_{CN} = 0.012 Å).[13] The low DP percentage range (0.11—0.33 %) and negative Δ'_{CN} value (-0.006 Å) for compound **32*b*** serve as further evidence of delocalization, the latter indicating delocalization of the lone-pairs into the CN$_3$ core of the cation to offset the formal positive

charge at the protonated nitrogen. The DP percentage for N**1** was not calculated due to the inherent positional inaccuracies of the hydrogen atom. The ρ ratio calculated from the crystal data of the neutral starting material **32** was found to be 0.93, indicating that the length of the C=N double bond is 93% of the average C-NR_2 single bond. The ρ ratio calculated from the hydrochloride salt structure data is found to be 0.99. This deviation is expected upon protonation, as delocalization of the charge throughout the CN_3 core results in an increase in the C=N bond length and subsequent decrease of the C-NR_2 bonds. A ρ ratio of 0.99 indicates effectively distributed positive charge across the carbon-nitrogen bonds, and nearly complete symmetrical bonding within the central guanidinium core.

Δ_{CN} / Å	0.014
Δ'_{CN} / Å	-0.006
DP_{N2}	0.33%
DP_{N3}	0.11%
ρ ratio	0.99

Table 4.2: Summary of geometric data for the guanidinium components of hydrochloride salt **32*b***

The extended molecular structure of this compound shows an infinite chain of centrosymmetric dimers, held together through hydrogen bonding interactions between two chlorine anions and two water molecules (Figure **4.2**).

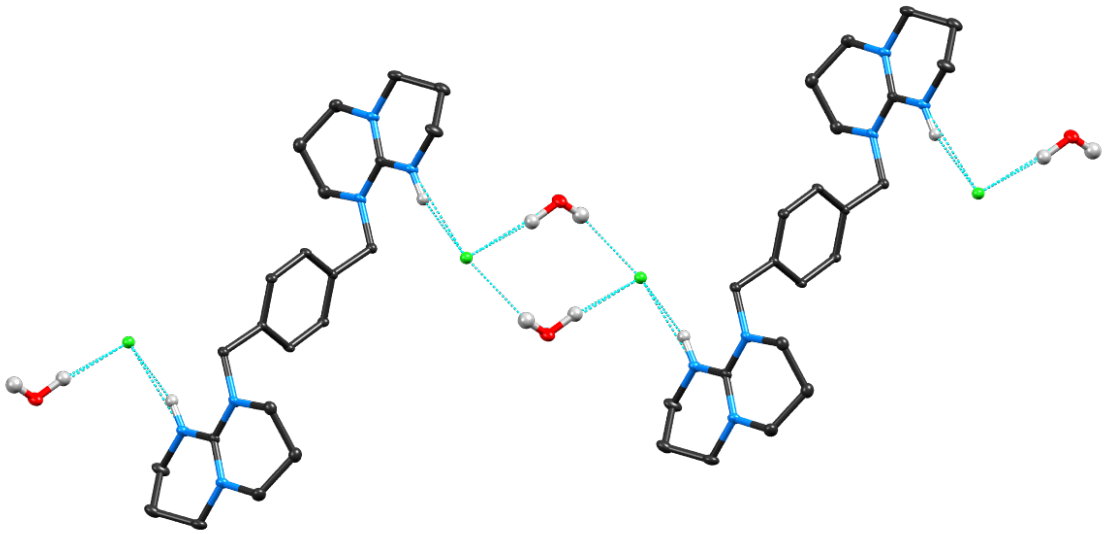

Figure 4.2: Thermal ellipsoid representation (20%) of extended chain structure of compound **32*b***. Hydrogens in cation (except N*H*) omitted for clarity.

4.2 Synthesis and Characterization of [1,2-(CH_2hppH)$_2$-C_6H_4][Cl]$_2$ (**30*b***)

4.2.1 Synthesis

Following the successful synthesis of the hydrochloride salt **32*b***, the same procedure was implemented for the synthesis of [1,2-(CH_2hppH)$_2$-C_6H_4][Cl]$_2$ (**30*b***). One equivalent of triethylamine hydrochloride was added to a solution of the neutral hpp-containing compound **30** in acetonitrile, and stirred under air for one hour. Slow evaporation of the volatiles over the course of 24 hours afforded a colorless oil. Following purification via recrystallization through solvation of the product in acetonitrile and subsequent storage of the solution at -30 °C, white crystals of the desired hydrochloride salt (**30*b***) were obtained in 82% isolated crystallized yield, calculated for triethylamine hydrochloride as limiting reagent (Scheme **4.2**).

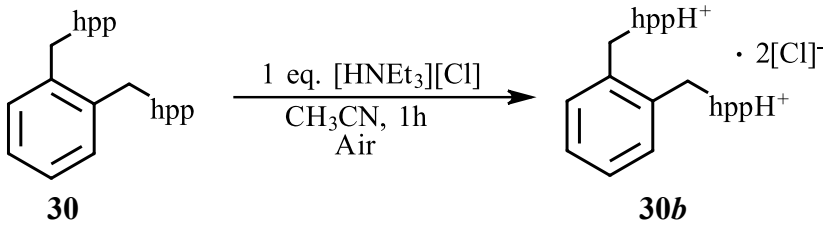

Scheme 4.2: Synthesis of [1,2-(CH_2hppH)$_2$-C_6H_4][Cl]$_2$ (**30*b***)

4.2.2 Spectroscopic Properties

^{1}H NMR analysis of the resulting product is consistent with the successful formation of the desired hydrochloride salt (**30*b***). Similar to the observed shifts within the spectra of the previously described hydrochloride salt, there is a consistent downfield shift of the proton resonances in the product, in comparison to the neutral guanidine **30**. This effect can be attributed to the presence of protonated hpp-imine functionalities, resulting in the deshielding of the resonating protons. The benzyl-methylene protons within the hydrochloride salt **30*b*** resonate at δ_H 4.93 ppm (s, 4H, $C_6H_4CH_2$), whereas this signal is found at δ_H 4.59 ppm in the starting material. There is also no N*H* resonance seen in the ^{1}H NMR spectrum, which can be attributed to H/D proton exchange between the product and NMR solvent. ^{13}C NMR spectral data was not obtained due to degradation of the product when heated to force into solution.

4.2.3 Solid-State Structure

Single crystal X-ray diffraction of the resultant crystalline product revealed the successful formation of the monomeric species, $[1,2\text{-}(CH_2hppH)_2\text{-}C_6H_4][Cl]_2$ (**30*b***, Figure **4.3**). Compound **30*b*** crystallizes in the $P\bar{1}$ space group, and was found to be associated with five water molecules in a complex framework through hydrogen-bonding interactions. One of the methylene groups within the hpp-fragment is disordered, and was modelled over two positions. Additionally, one water molecule is also disordered over two sites. Unlike the molecular structure of compound **32*b***, this structure does not contain a plane of symmetry. As the hppH-units are inequivalent in the solid-state, select bond lengths of each moiety within compound **30*b*** are listed in Table **4.3**, and geometric parameters calculated from the molecular structures of both guanidinium functionalities are listed in Table **4.4**.

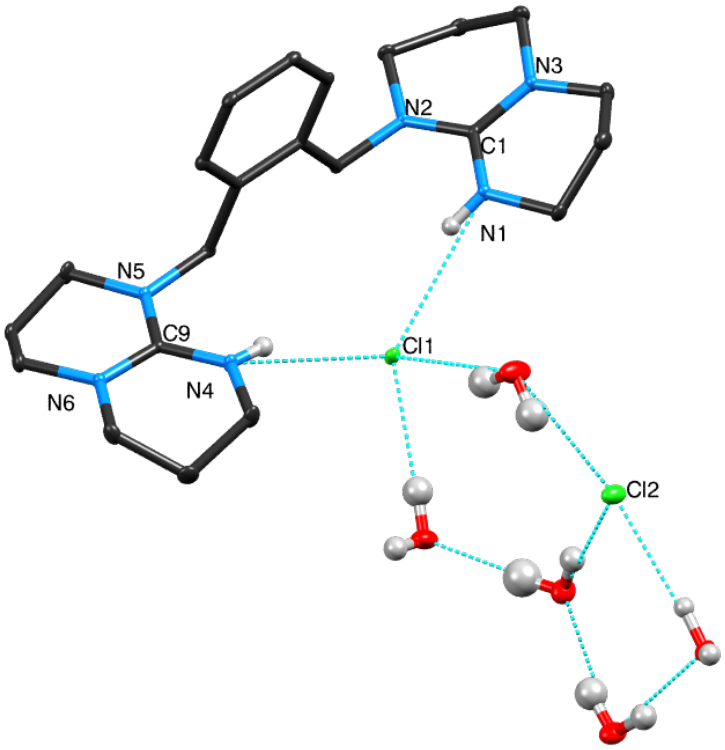

Figure 4.3: Thermal ellipsoid representation (30%) of hydrochloride salt **30*b***. Hydrogens in cation (except N*H*) omitted for clarity.

Table 4.3: Select bond lengths in hydrochloride salt **30*b*** and neutral **30**

Bond	**[1,2-(CH$_2$hppH)$_2$-C$_6$H$_4$][Cl]$_2$ (30*b*)**	**Neutral 1,2-(CH$_2$hpp)$_2$-C$_6$H$_4$ (30)**[23]
N**1**—C**1**	1.335(4) Å	1.305(2) Å
N**2**—C**1**	1.351(4) Å	1.374(2) Å
N**3**—C**1**	1.335(3) Å	1.370(2) Å
N**4**—C**9**	1.334(4) Å	1.305(2) Å*
N**5**—C**9**	1.347(4) Å	1.374(2) Å*
N**6**—C**9**	1.335(3) Å	1.370(2) Å*

* Guanidine units are equivalent in neutral compound **30**. Bond lengths of N**4**—C**9**, N**5**—C**9**, N**6**—C**9** are the same as N**1**—C**1**, N**2**—C**1**, N**3**—C**1**, respectively.

The geometric parameters calculated from the structural data of compound **30*b*** support successful protonation and efficient delocalization within the guanidinium moieties (Table **4.4**). The low Δ_{CN} values of 0.017 and 0.013 Å show little difference in the C—N single and C=N double bond lengths, as expected in a delocalized system. This difference is more pronounced in the neutral hpp-fragment (**30**, Δ_{CN} = 0.069 Å). The Δ'_{CN} values of -0.008 and -0.006 Å suggests successful protonation of both hpp-units, as a negative Δ'_{CN} value indicates delocalization of the lone-pairs into the CN_3 core of the cation to offset the formal positive charge at the protonated nitrogen. The relatively low calculated DP percentages (range = 0.29—1.04%) further support effective delocalization within the guanidinium species. The ρ ratios calculated from the structural data of each guanidinium units are 0.99, whereas the structure for the neutral hpp-unit gives ρ = 0.97. This increase within the product reflects the lengthening of the C=N double bond and shortening of the C—N single bond within the CN_3 core of the guanidine, indicating successful protonation and delocalization of the charge over each C—N bond.

$\Delta_{CN(1\text{-}3)}$ / Å	0.017	$\Delta_{CN(4\text{-}6)}$ / Å	0.013
$\Delta'_{CN(1\text{-}3)}$ / Å	-0.008	$\Delta'_{CN(4\text{-}6)}$ / Å	-0.006
DP$_{N2}$	1.04%	**DP$_{N5}$**	0.44%
DP$_{N3}$	0.29%	**DP$_{N6}$**	0.44%
ρ ratio (N**1**-N**3**)	0.99	**ρ ratio** (N**4**-N**6**)	0.99

Table 4.4: Summary of geometric data for each guanidinium unit of hydrochloride salt **30*b***

4.3 Synthesis and Characterization of [1,3-$(CH_2hppH)_2$-C_6H_4][Cl]$_2$ (**31*b***)

4.3.1 Synthesis

Utilizing the same synthetic strategy described in the previous examples, one equivalent of triethylamine hydrochloride was added to a solution of the neutral hpp-containing compound **31** in acetonitrile, and stirred under air for one hour. Slow evaporation of the volatiles over the course of 24 hours afforded a colorless oil. Purification was performed through recrystallization via storage of the product in a solution of acetonitrile at -30 °C, affording white crystals of the desired hydrochloride salt **31*b*** in 42% isolated yield, calculated using triethylamine hydrochloride as the limiting reagent (Scheme **4.3**). Although the resultant crystals were unsuitable for crystallographic analysis, the product was characterized through ^{1}H NMR and ^{13}C NMR spectroscopy.

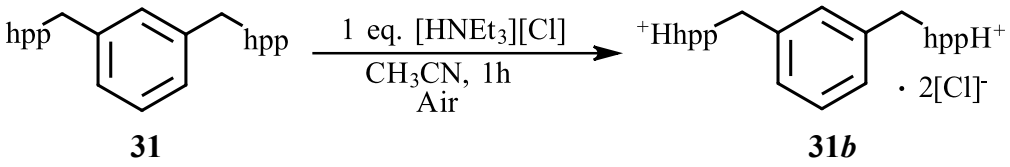

Scheme 4.3: Synthesis of [1,3-$(CH_2hppH)_2$-C_6H_4][Cl]$_2$ (**31*b***)

4.3.2 Spectroscopic Properties

The ^{1}H NMR spectral data for the resulting product is consistent with the formation of hydrochloride salt **31*b***. Similar to the shifts observed for the hydrochloride salts **32*b*** and **30*b***, there is a downfield shift of the proton resonances in the hydrochloride product, in comparison to the neutral guanidine. This quantitative difference in chemical shift is also comparable to the previously characterized hydrochloride salts. The benzyl-methylene protons within the hydrochloride salt **31*b*** resonate at δ_H 4.83 ppm, compared to δ_H 4.56 ppm in the neutral starting material (**31**). Significant shifts in the resonances of the protons within the NC*H*$_2$ hppH-units (δ_H 3.52, 3.34, and 3.24 ppm) are also consistent with successful formation of the desired hydrochloride salt (**31*b***). There is no signal attributable to the guanidinium N*H* resonance, due to possible H/D exchange with the deuterated solvent. It should be noted that, due to the

largely hygroscopic nature of these compounds, there is a large water peak present within the spectrum (δ_H 2.00 ppm, HOD). ^{13}C NMR analysis further supports the formation of **31*b*.** Up field shift of the 'CN_3' carbon resonance (δ_C 150.8 ppm) suggests a more shielded environment due to ion-pairing in **31*b*** between the protonated imine nitrogen and chloride anion. There is also an observed downfield shift of the benzyl-methylene carbon (δ_C 53.5 ppm) that is consistent with the signal found in hydrochloride salt **32*b*** discussed previously, further suggesting successful synthesis of compound **31*b*.**

4.4 Synthesis and Characterization of [Ph(CH_2hppH)][Cl] (29*b*)

4.4.1 Synthesis

One equivalent of triethylamine hydrochloride was added to a solution of neutral Ph(CH_2hpp) (**29**) in acetonitrile, and stirred under air for one hour. The volatiles were removed via slow evaporation at room temperature, and subsequent recrystallization through storage of the product in a solution of dichloromethane at -30 °C afforded white crystals of hydrochloride salt **29*b*** in 76% isolated yield (Scheme **4.4**). Although the resultant crystals were unsuitable for crystallographic analysis, the product was characterized through ^{1}H NMR and ^{13}C NMR spectroscopic techniques.

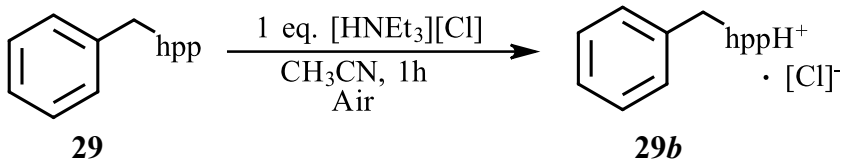

Scheme 4.4: Synthesis of [Ph(CH_2hppH)][Cl] (**29*b***)

4.4.2 Spectroscopic Properties

^{1}H NMR analysis of the product gives strong evidence of the successful formation of compound **29*b***. Comparison of the product ^{1}H NMR spectrum to that of the neutral starting material **29** shows a clear downfield shift of all proton signals, consistent with the induced deshielding of the resonating protons upon protonation of the guanidine functionality. This shift is most prominent in the benzyl-methylene proton singlet, which resonates at δ_H 4.83 ppm within the

product **29*b*** spectrum, and at δ_H 4.58 ppm in the neutral starting material **29**. The presence of a low field signal at δ 9.64 (br s, 1H, N*H*) offers further evidence of successful protonation of the guanidine functionalities. This low field value is consistent with that found in spectroscopic data of [hppH$_2$][Cl][13], and is indicative of ion-pairing within **29*b*** presumably between the N*H* protons and the chloride anion. It is interesting to note that this N*H* signal is present within spectral data of this compound and not of the previously discussed hydrochloride salts. The reason to this is unknown. There is also a large water peak found within the ^{1}H NMR spectrum (δ_H 2.00 ppm, HOD). The comparison between the ^{13}C NMR spectra of the product and neutral starting material also supports the formation of **29*b***. This is most clearly represented through the upfield shift in the resonance of the central guanidinium 'CN$_3$' carbon from δ_C 151.4 ppm in **29** to δ_C 150.9 ppm in **29*b***. This indicates a more shielded environment for this carbon in the product, and is consistent with a protonated guanidinium functionality. This is further evidenced by the upfield shift of the benzyl-methylene proton signal (δ_C 53.7 ppm).

4.5 Formation and Characterization of [1,3,5-(CH$_2$hppH)$_3$-2,4,6-(Et)$_3$-C$_6$][Cl]$_3$ (35*b*)

4.5.1 Synthesis

To maximize the chances of full protonation in the more sterically demanding superbasic systems, greater concentrations of protonation source were used. Thus, three equivalents of a solution of triethylamine hydrochloride were added to a solution of neutral 1,3,5-(CH$_2$hpp)$_3$-2,4,6-(Et)$_3$-C$_6$ (**35**) in acetonitrile, and stirred for one hour under air (Scheme **4.5**). The removal of the volatiles via slow evaporation at room temperature afforded a colorless oil. Crystallization was attempted multiple times through both slow evaporation at room temperature and storage of the product in a solution of acetonitrile at -30 °C. However, no crystalline product was obtained. The oil of **35*b*** was collected in 89% yield, and characterized through ^{1}H NMR and ^{13}C NMR spectroscopy.

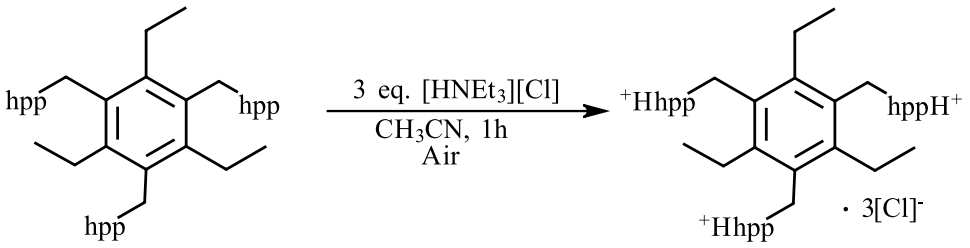

35 **35*b***

Scheme 4.5: Synthesis of [1,3,5-(CH_2hppH)$_3$-2,4,6-(Et)$_3$-C_6][Cl]$_3$ (**35*b***)

4.5.2 Spectroscopic Properties

^{1}H NMR and ^{13}C NMR analysis of the product support the successful formation of [1,3,5-(CH_2hppH)$_3$-2,4,6-(Et)$_3$-C_6][Cl]$_3$ (**35*b***). As in the guanidinium salts discussed previously, there is an observed downfield shift of the proton resonances within the ^{1}H NMR spectra when compared to that of the starting guanidine species. The benzyl-methylene protons resonate at δ_H 4.87 ppm within the product, and at δ_H 4.58 ppm in the neutral compound **35** consistent with the deshielding effect that occurs upon protonation of the guanidine functionality. Similar downfield shifts are observed in the NC*H*$_2$ hpp-proton resonances of compound **35*b*** (δ_H 3.55, 3.37, 3.27, 2.87 ppm). The spectrum shows a large water peak at δ_H 2.00 (HOD), and does not contain a signal corresponding to the guanidinium N*H* resonance, possibly due to rapid proton exchange with the solvent or sequestered water molecules.

The comparison of the ^{13}C NMR spectra of the product and neutral starting material shows discreet changes within the resonating carbon signals that would be expected in the synthesis of compound **35*b***. Curiously, there is not an observed downfield shift of the benzyl-methylene carbon resonance (δ_C 48.1 ppm) as seen in the previous hydrochloride salts. This could possibly be due the alkyl-substituents within this compound, shielding this carbon from electronic effects of the cationic guanidinium units.

4.6 Synthesis and Characterization of [2,4,6-$(CH_2hppH)_3$-mesitylene][Cl]$_3$ (**34*b***)

4.6.1 Synthesis

As described for [1,3,5-$(CH_2hppH)_3$-2,4,6-$(Et)_3$-C_6][Cl]$_3$ (**35*b***), three equivalents of a solution of triethylamine hydrochloride were added to a solution of neutral 2,4,6-$(CH_2hpp)_3$-mesitylene (**34**) in acetonitrile, and stirred for one hour (Scheme **4.6**). The removal of the volatiles via slow evaporation at room temperature affording a colorless oil. Crystallization was attempted multiple times through both slow evaporation at room temperature and storage of the product in a solution of acetonitrile at -30 °C, but no crystalline product was obtained. The oil of **34*b*** was collected in 93% yield, and characterized through ^{1}H NMR and ^{13}C NMR spectroscopy.

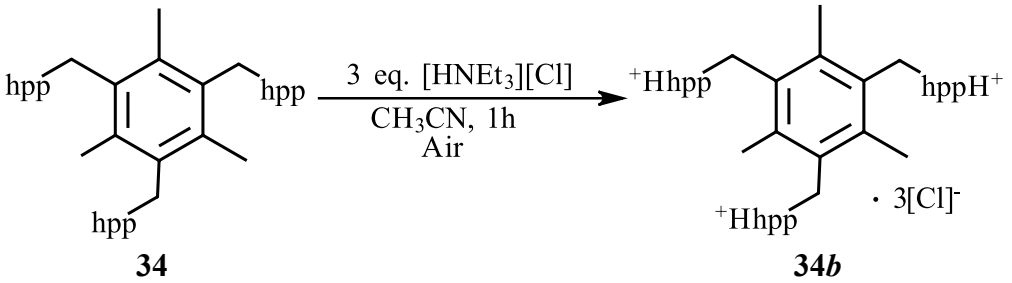

Scheme 4.6: Synthesis of [2,4,6-$(CH_2hppH)_3$-mesitylene][Cl]$_3$ (**34*b***)

4.6.2 Spectroscopic Properties

^{1}H NMR and ^{13}C NMR analysis of the product indicate the successful formation of [2,4,6-$(CH_2hppH)_3$-mesitylene][Cl]$_3$ (**34*b***). As characteristic in the previously discussed guanidinium salts, there is an observed downfield shift of the proton signals within the ^{1}H NMR spectra of product **34*b*** when compared to that of the neutral starting material **34**. The benzyl-methylene proton signal is found at δ_H 4.92 ppm within the product, and at δ_H 4.61 ppm in the hpp-containing starting material **34**. Similar downfield shifts are observed in the NC*H*$_2$ hpp-proton resonances of compound **34*b*** (δ_H 3.56, 3.39, 3.30, 2.84 ppm). There is also a low-field broad singlet signal at δ_H 9.48 ppm that can be attributed to the guanidinium N*H* proton. It is unclear why this signal is seen within this hydrochloride product and not within the previous salts, but may be due to the inherent structure of this compound, allowing for stronger hydrogen-bonding interactions. As expected for this hygroscopic class of compounds, the ^{1}H NMR

spectrum shows a water peak at δ_H 2.00 (HOD). ^{13}C NMR analysis is also consistent with the formation of hydrochloride salt **34*b***. In the comparison of the ^{13}C NMR spectra of the product and starting material, there is an observed slight downfield shift of the benzyl-methylene carbon (δ_C 45.8 ppm), as found in many of the previously characterized hydrochloride salts. This shift is less dramatic than the previous examples due to shielding of this carbon by the benzyl-methyl substituents. Upfield shifts in the hpp-carbon N*C*H$_2$ resonances (δ_C 48.3, 47.5, 41.5, 38.7 ppm) and central guanidinium *C*N$_3$ carbon (δ_C 151.3 ppm) of **34*b*** are consistent with the induced shielding within the guanidinium unit, and are in agreement with the spectral results collected for the previously discussed analogous hydrochloride salts.

Chapter *5*

Bicarbonate Salts

5.1 Synthesis and Characterization of [1,4-(CH_2hppH)$_2$-C_6H_4][HCO_3]$_2$ (**32*c***)

5.1.1 Introduction

Based on the reaction forming [1,3,5-(CH_2hppH)$_3$-C_6H_3][HCO_3]$_3$ (Scheme **1.8**), initial strategies for synthesizing [1,4-(CH_2hppH)$_2$-C_6H_4][HCO_3]$_2$ (**32*c***) were derived from recreating similar conditions to reproduce this novel result. As shown in Scheme **1.8**, the addition of one equivalent of triethylamine hydrochloride to a superbasic compound containing three hpp-functionalities, and subsequent recrystallization under air afforded the corresponding bicarbonate product. It was hypothesized that this sub-stoichiometric amount of proton source per guanidine unit was necessary for this reaction to proceed.

5.1.2 Synthesis

The stoichiometric approach to achieve the bicarbonate salt is described below, and optimization of this reaction is discussed later.

Under air, 0.5 equivalents of triethylamine hydrochloride were added to a solution of neutral 1,4-(CH_2hpp)$_2$-C_6H_4 (**32**) in acetonitrile, and stirred for 0.5 hours. Crystallization of the product via slow evaporation at room temperature yielded yellow crystals of the desired bicarbonate salt (**32*c***) in 77% isolated yield (Scheme **5.1**). This procedure differed to that described for the synthesis of the hydrochloride salt **32*b***, in which one equivalent of triethylamine hydrochloride was added to **32**.

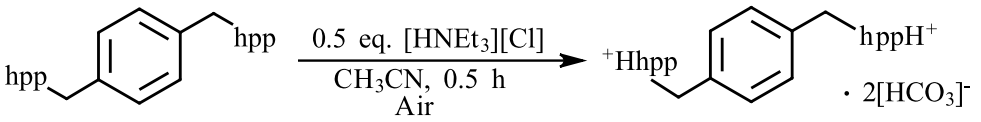

32 **32*c***

Scheme 5.1: Synthesis of bicarbonate salt [1,4-$(CH_2hppH)_2$-C_6H_4][HCO_3]$_2$ (**32*c***)

The resulting crystals were characterized through ^{1}H NMR and ^{13}C NMR spectroscopy, elemental analysis, FTIR analysis, and single crystal X-ray diffraction techniques.

5.1.3 Spectroscopic Properties

^{1}H NMR analysis of the crystallized product (Appendix **C2a**) supports the successful formation of the bicarbonate product **32*c***. There is a general downfield shift of the proton signals in comparison to the neutral compound, as seen within the hydrochloride and tetraphenylborate salts. This shift is seen most clearly through the benzyl-methylene proton signal, which resonates at δ_H 4.74 ppm within the bicarbonate product **32*c***, and at δ_H 4.56 ppm in the neutral starting material (**32**). Once again we note a water peak present within the spectrum (δ 2.00 ppm, HOD), which is to be expected due to the largely hygroscopic nature of this class of superbasic compounds. There is also no resonance corresponding to the proton within the bicarbonate anion or the guanidinium N*H* proton. These absences can be attributed to rapid proton exchange occurring between the bicarbonate anionic species and [HCO_3]$^-$, the gunainidinium proton, and water molecules present in solution. The ^{13}C NMR spectral data (Appendix **C2b**) supports the formation of the desired product. There is a downfield shift in the benzyl-methylene carbon (δ_C 52.0 ppm) in comparison to the neutral starting material (δ_C 50.9 ppm) suggests successful protonation of both guanidine units. It should be noted that the resonance of the bicarbonate anion carbon is not seen. As the samples were highly concentrated and run for extended lengths of time, the reason for this absence is unknown.

5.1.4 Solid-State Structure

Single crystal X-ray analysis confirmed the product as the monomeric bicarbonate salt, [1,4-$(CH_2hppH)_2$-C_6H_4][HCO_3]$_2$ (**32*c***, Figure **5.1**). This compound contains two guanidinium cationic hppH-units in which the protonated imine nitrogen units each form one NH···O

hydrogen-bonds to the bicarbonate counter-ion (1.878 Å). The molecule is located on a center of inversion which is located within the central aryl ring. Compound **32*c*** crystallizes in the $P2_1/c$ space group, and was found to contain acetonitrile solvate. This molecule of acetonitrile has been omitted from Figure **5.1** for clarity, as it is not involved in the hydrogen bonded network of the molecular structure. Selected bond lengths are listed in Table **5.1**, and geometric parameter data for the guanidinium cationic units is listed in Table **5.2**.

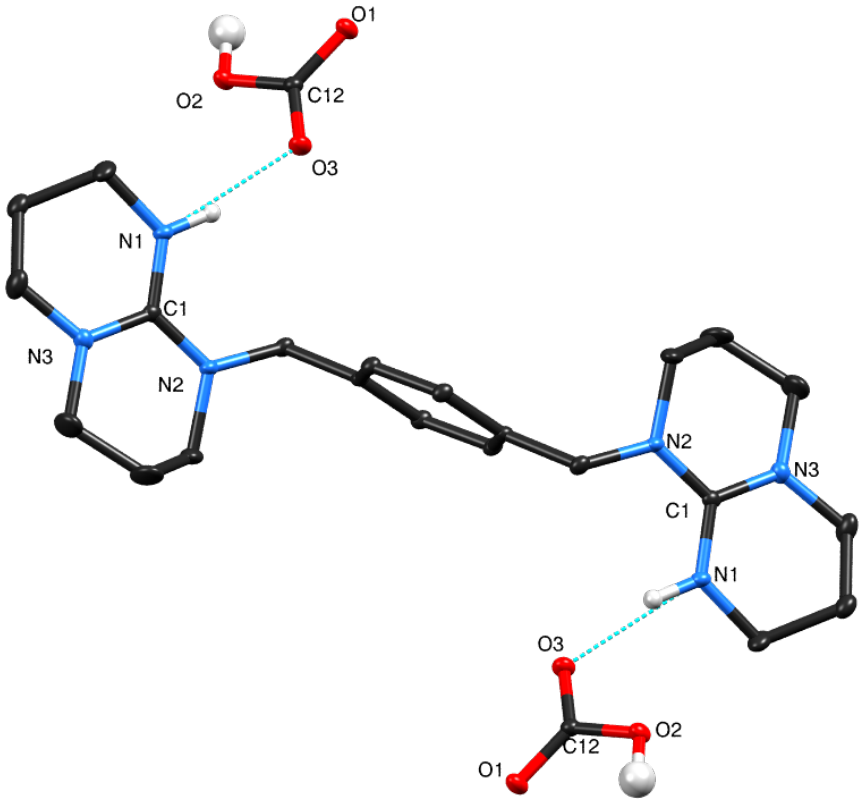

Figure 5.1: Thermal ellipsoid representation (20%) of bicarbonate salt **32*c*** (Structure **I**). Both acetonitrile solvate and hydrogens within the cation (except N*H*) omitted for clarity. Selected bond lengths are reported in Table **5.1**.

Bond	**[1,4-(CH$_2$hppH)$_2$-C$_6$H$_4$][HCO$_3$]$_2$ (32*c*)**	**Neutral 1,4-(CH$_2$hpp)$_2$-C$_6$H$_4$ (32)**
N**1**—C**1**	1.331(2) Å	1.291(2) Å
N**2**—C**1**	1.343(2) Å	1.387(2) Å
N**3**—C**1**	1.340(2) Å	1.378(2) Å

Table 5.1: Select bond lengths in bicarbonate salt **32*c*** and neutral **32**

The geometric parameters calculated from the structural data of compound **32*c*** (structure **I**) support successful protonation and efficient delocalization within the guanidinium moieties. The Δ_{CN} value of 0.012 Å shows a small differential between the C—N single and C=N double bond lengths, as expected with a delocalized system. This value is consistent with that found from the structural data of the corresponding hydrochloride product **32*b*** (Δ_{CN} = 0.014 Å)[13], as discussed in chapter 4. The low DP percentage range (0.01—0.77 %) and Δ'_{CN} value (0.003 Å) for compound **32*c*** serve as further evidence of protonation and delocalization. As found for hydrochloride salt **32*b***, the ρ ratio of the bicarbonate salt **32*c*** is 0.99. This increase in ρ value from that calculated for the neutral starting material **32** (ρ = 0.93) is in agreement with the formation of the guanidinium cation, and indicates effectively distributed positive charge and symmetrical bonding within the central guanidinium core.

Δ_{CN} / Å	0.012
Δ'_{CN} / Å	0.003
DP_{N2}	0.94%
DP_{N3}	0.01%
ρ ratio	0.99

Table 5.2: Summary of geometric data for the guanidinium components of bicarbonate **32*c*** (Structure **I**)

The extended crystallographic structure of compound **32*c*** (structure **I**) shows formation of a centrosymmetric dimer bound by hydrogen bond interactions between two bicarbonate species (Figure **5.2**). Each pair of bicarbonate anions bond through a pair of two OH···O hydrogen-bonds having bond lengths of approximately 1.646 Å. This chain formation is the same structural motif as that seen in the bicarbonate species [$hppH_2$][HCO_3] (Figure **1.5**).[9]

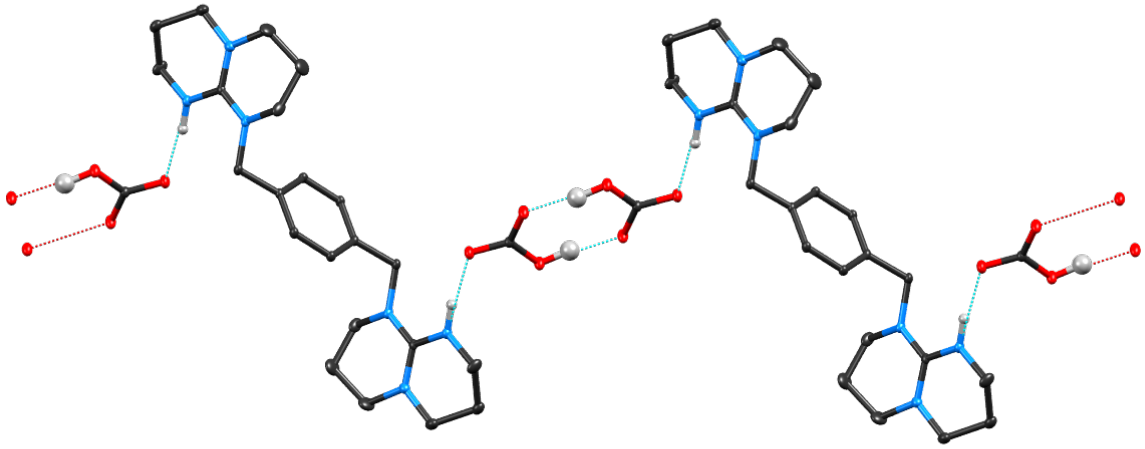

Figure 5.2: Thermal ellipsoid (20%) representation of hydrogen-bonding framework in extended structure **I** of **32*c*.** Hydrogens in cation (except N*H*) omitted for clarity.

Single crystal X-ray diffraction performed on a separate crystalline sample of this product (structure **II**) revealed a different packing of molecular units than observed in the previously described solid-state structure of compound **32*c***. These crystals were obtained through storage of the bicarbonate product **32*c*** in a solution of acetonitrile at -30 °C. The two compounds are chemically identical (see Table **5.3** for comparison bond lengths, and Table **5.4** for calculated geometric parameters of the guanidinium units for **32*c***, structure **II**). However, there is a difference in the arrangement of the hydrogen bonds (Figure **5.3**).

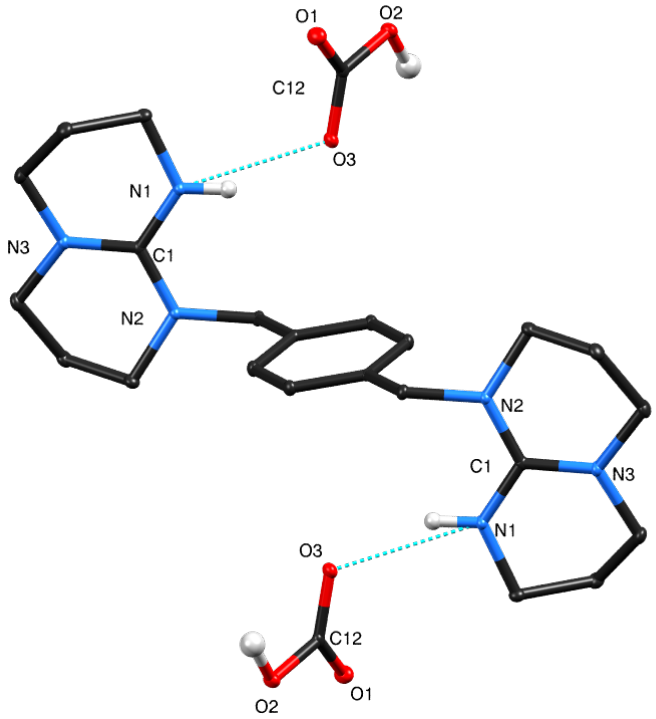

Figure 5.3: Thermal ellipsoid (20%) representation of **32*c***, structure **II**. Hydrogens within cation (except N*H*) omitted for clarity.

Bond	**32*c*:** Structure **II**	**32*c*:** Structure **I**	**Neutral 32**
N**1**—C**1**	1.337(1) Å	1.331(2) Å	1.291(2) Å
N**2**—C**1**	1.345(1) Å	1.343(2) Å	1.387(2) Å
N**3**—C**1**	1.342(1) Å	1.340(2) Å	1.378(2) Å
O**1**—C**12**	1.231(1) Å	1.267(2) Å	--
O**2**—C**12**	1.367(1) Å	1.342(2) Å	--
O**3**—C**12**	1.273(1) Å	1.242(2) Å	--

Table 5.3: Select comparison bond lengths for compound **32*c*** (**I**), **32*c*** (**II**), and neutral **32**

Δ_{CN} / Å	0.008
Δ'_{CN} / Å	0.001
DP_{N2}	0%
DP_{N3}	0.02%
ρ **ratio**	1.00

Table 5.4: Summary of geometric data for the guanidinium components of bicarbonate salt **32*c*** (Structure **II**)

Figure **5.4** shows the extended molecular structure of **32*c***-structure **II**. As in structure **I**, this crystalline sample forms an infinite chain bound together through hydrogen-bonding interactions between two bicarbonate anions. However unlike structure **I** where all three oxygen atoms are each involved in the hydrogen-bonding framework, the polymeric chain of structure **II** involves incorporates only two oxygen atoms in the hydrogen-bonding network, with O**1** representing a terminal O-atom.

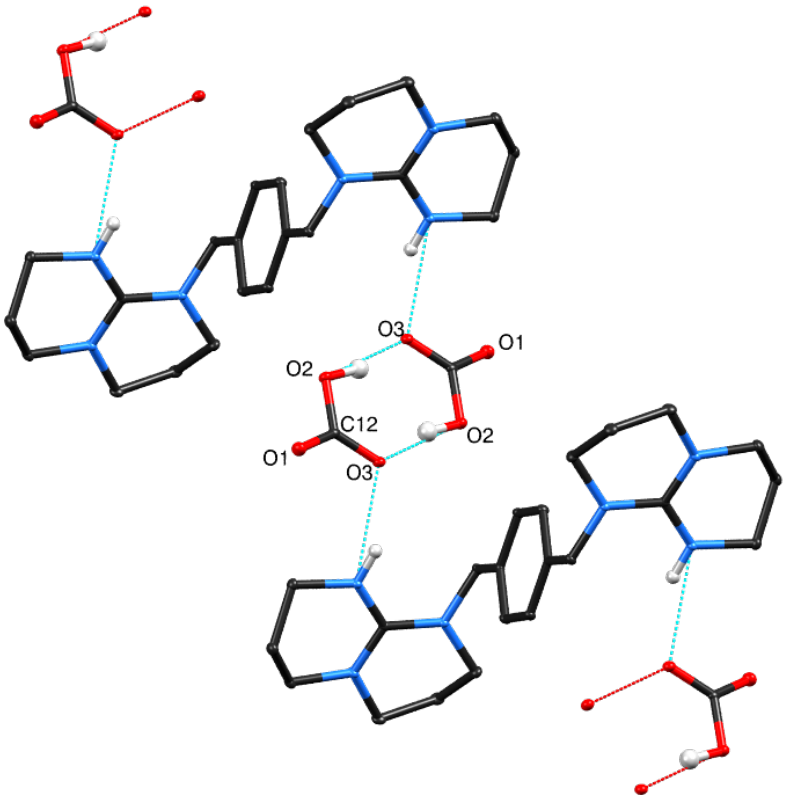

Figure 5.4: Thermal ellipsoid (20%) representation of hydrogen-bonding framework in extended structure in structure **II** of compound **32*c***. Hydrogens within cationic species (except N*H*) omitted for clarity.

Comparison of the C—O bond lengths (Table **5.3**) within the anionic species reveals an interesting difference between the two molecular structures. Within structure **I**, the guanidinium cationic species has hydrogen bonding interactions with the oxygen atom that is involved in the C—O bond with the most double bond character (O**3**—C**12**, 1.242(2) Å). However in structure **II**, the oxygen atom within the double bond (O**1**—C**12**, 1.231(1) Å) is not involved in the hydrogen-bonding framework. The bonding scheme between the $[hppH]^+$ fragment and the bicarbonate anion for each structure is shown pictorially in Figure **5.5**.

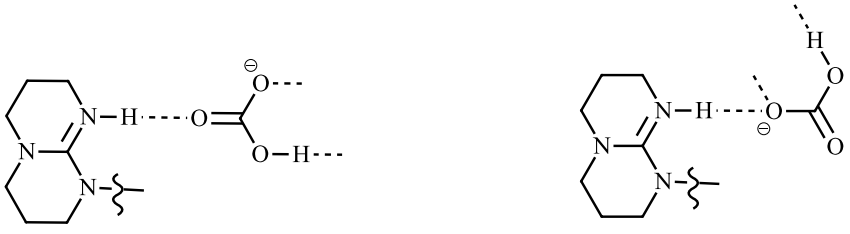

Structure I **Structure II**

Figure 5.5: Hydrogen-bonding in structure **I** and **II** of compound **32*c***

5.1.5 Optimization of Reaction Conditions

Having confirmed that compound **32** is able to effectively capture and activate carbon dioxide when in the presence of a proton source, a series of reactions was performed in order to optimize the reaction conditions for CO_2 capture and subsequent bicarbonate formation. Factors that were taken into consideration were toxicity and cost of the proton source, stoichiometric equivalents of the proton source, and reaction time. Supplementary factors, such as the addition of water (5 mol % H_2O) and carbon dioxide (added at a steady stream for 4 h), were also examined within the reaction trials to assess their impact on bicarbonate formation. This series of optimization reactions is summarized in Table **5.5**. It should be noted that method 1 listed within this table corresponds to synthetic strategy previously described in Chapter 5.1.2.

Each reaction was carried out in a similar fashion (Scheme **5.2**). Under air, a varied stoichiometric amount of a proton source was added to a 3 mL solution of 0.10 g (0.26 mmol.) 1,4-$(CH_2hpp)_2$-C_6H_4 (**32**). The resulting solution was stirred for varied lengths of time, and the volatiles removed by slow evaporation. Recrystallization was attempted through storage of the product in a solution of acetonitrile at -30 °C and/or slow evaporation at room temperature. In method 3 and 5 (Table **5.5**) distilled water (5 mol % H_2O) was added directly to the reaction mixture. In method 5 and 7 (Table **5.5**) CO_2 was added at a steady stream for the duration of the stirring time (4 h).

Multiple solvents were initially investigated in this series of reactions. However, solubility issues of both the neutral precursor and proton sources limited the scope of this variable. Thus, each reaction was performed in acetonitrile. Previous literature has shown that polar, aprotic solvents, such as acetonitrile, promote CO_2 capture.[33,34]

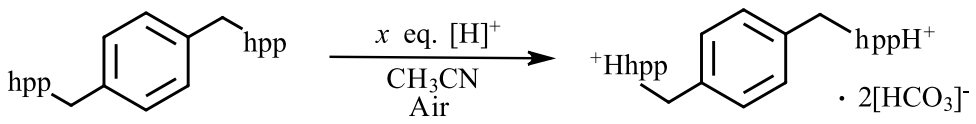

32 **32*c***

Scheme 5.2: General equation describing the series of optimization reactions for the formation of [1,4-$(CH_2hppH)_2$-C_6H_4][HCO_3]$_2$ (**32*c***)

Method	$[H]^+$ Source	Equivalents of $[H]^+$	Stir time	Additional reaction conditions	Outcome of Reaction
1	Triethylamine hydrochloride	0.5 equiv.	1 h	No added conditions	Bicarbonate species **32*c*** formed. Characterized through ^{1}H NMR, ^{13}C NMR and crystallographic analysis.
2	No protonation source	--	24 h	No additional conditions	No reaction. Crystals obtained under air of neutral starting material.
3	No protonation source	--	24 h	Additional H_2O introduced to reaction system	No reaction. Characterized by ^{1}H NMR and ^{13}C NMR analysis.
4	Triethylamine hydrochloride	0.1 equiv.	0.5 h	No added conditions	Bicarbonate species **32*c*** formed. Characterized by ^{1}H NMR, ^{13}C NMR and crystallographic analysis.
5	Triethylamine hydrochloride	0.1 equiv.	4 h	Additional H_2O and CO_2 introduced to the reaction system	Bicarbonate species **32*c*** formed. Characterized by ^{1}H NMR, ^{13}C NMR and crystallographic analysis.
6	Triethylamine hydrochloride	0.2 equiv.	0.5 h	No added conditions	Bicarbonate species **32*c*** formed. Characterized by ^{1}H NMR and ^{13}C NMR analysis.
7	Triethylamine hydrochloride	2 equiv.	4 h	Additional CO_2 introduced to the reaction system	Hydrochloride species **32*c*** formed. Characterized by ^{1}H NMR, and ^{13}C NMR analysis.
8	Benzoic Acid	0.1 equiv.	1 h	No added conditions	Bicarbonate species **32*c*** formed. Characterized by ^{1}H NMR, ^{13}C NMR and crystallographic analysis.
9	Benzoic Acid	1 equiv.	1 h	No added conditions	$[1,4\text{-}(CH_2hppH)_2\text{-}C_6H_4][HCO_3][PhCO_2]$ formed. Characterized by ^{1}H NMR, ^{13}C NMR and crystallographic analysis.

Table 5.5: Optimization reactions for the formation of bicarbonate salt **32*c***

A major focus of these optimization reactions was to determine the minimum amount of acid necessary for this reaction to proceed. Two control reactions (entries 2 and 3, Table **5.5**) were carried out under air in the absence of an external protonation source, each resulting in no reaction. The crystallized product from the reaction described in entry 2 was determined through single crystal X-ray diffraction to be the neutral starting material. From the initial conditions utilized to make bicarbonate salt **32*c*** (entry 1, Table **5.5**), it was shown that both guanidine functionalities within 1,4-$(CH_2hpp)_2$-C_6H_4 (**32**) were spontaneously protonated from the addition of only 0.5 equivalents of triethylamine hydrochloride (a 1:4 ratio of additional $[H]^+$:hpp-unit). As found within previous literature results, the superbasic compound most likely extracted the additional hydrogen atoms from the solvent or adventitious water found within the air.[10] It was found that utilizing sub-stoichiometric amounts as low as 0.1 equivalents of both triethylamine hydrochloride and benzoic acid successfully allowed for the formation of the bicarbonate salt **32*c*** with fully protonated hpp-groups (Table **5.5**, methods 4, 5, 6, 8). These results indicate that although this compound can abstract protons from an ambient source, the reaction system first requires the addition of acid to initiate full protonation. Unfortunately, the reasoning as to why this addition is necessary is not yet fully understood.

The results of this series of reactions also indicate that extended stirring times do not have an effect on the capability of this superbasic compound to capture CO_2. This is consistent with results reported in the literature, which state that when reacted under 1 atm CO_2, the molar CO_2 loading capacity of hppH hits a maximum plateau level after approximately 15 minutes.[35] It should be noted that the removal of the volatiles via slow evaporation occurred over a minimum period of 24 hours and exposure to atmospheric CO_2 continued during this time, so it is difficult to have control over this variable. Due to the capricious nature of crystallization, crystalline product was not obtained for every reaction, and thus the crystallized yield cannot be used as an accurate measure of comparison. Yield of the collected crude product did not vary depending on the conditions, as the reactions successfully resulting in the formation of the bicarbonate species (methods 1, 4, 5, 6 and 8, Table **5.5**) afforded quantitative yield of **32*c***. The incorporation of additional CO_2 or H_2O had no effect on the reactivity of this system (Table **5.5**, methods 3,5, and 7). Thus, the optimal conditions, for the formation of bicarbonate salt **32*c*** was determined to be method 8, which implements the use of 0.1 equivalents of benzoic acid, the least expensive of the experimented acid reagents, and a stirring time of 1 hr, with no additional conditions introduced into the reaction system (Scheme **5.3**).

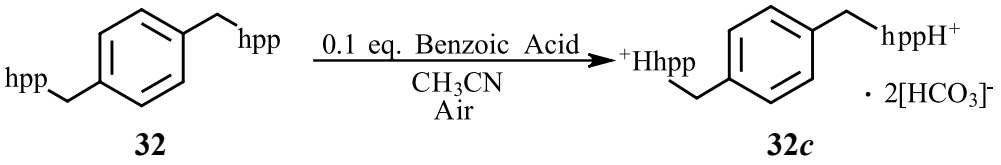

Scheme 5.3: Optimized conditions for formation of bicarbonate salt **32*c***

5.1.6 Spectroscopic Anomalies

A significant limitation to the characterization of these bicarbonate salts in solution that emerged as this project progressed were inconsistencies found in the ^{1}H NMR spectral data. Although the different synthetic methods within the series of optimization reactions each afforded compound **32*c***, and each product was determined by crystallographic analysis to be the same compound, the corresponding ^{1}H NMR chemical shift varied significantly for the cationic species. This data discrepancy will be addressed here through examples of ^{1}H NMR spectra that correspond to the redissolved crystalline samples whose molecular structures had been previously elucidated through single crystal X-ray diffraction. Full ^{1}H NMR spectral data collected for each method of the optimization reactions is listed within the experimental section (Chapter 8).

Figure **5.6** shows an overlay of four ^{1}H NMR spectra: the spectrum of the neutral starting material 1,4-$(CH_2hpp)_2$-C_6H_4 (**32**) shown in red, the corresponding hydrochloride salt **32*b*** shown in blue, the bicarbonate salt **32*c*** produced from a reaction utilizing 0.5 equivalents of triethylamine hydrochloride (Table **5.5**, method 1) in green, and the bicarbonate salt **32*c*** produced from a reaction utilizing 0.1 equivalents of triethylamine hydrochloride (Table **5.5**, method 4) in grey. As there is significant overlap in other regions of the spectrum, the region in which the benzyl-methylene protons (s, 4H, $C_6H_4CH_2$) resonate is expanded to most clearly demonstrate this inconsistency.

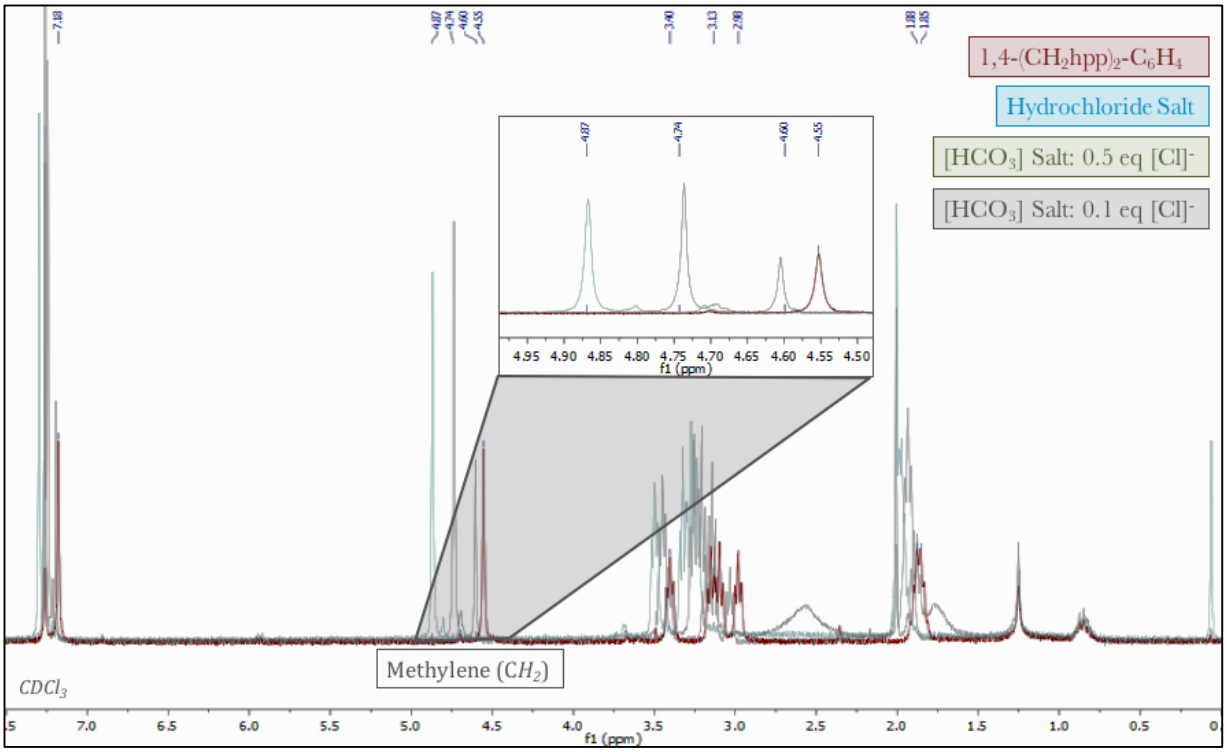

Figure 5.6: Overlay of ^{1}H NMR spectra corresponding to neutral **32**, hydrochloride salt **32*b***, and bicarbonate salt **32*c*** produced through two separate methods.

As discussed in the previous chapter, both the hydrochloride salt and bicarbonate salt methylene proton resonances are shifted downfield in comparison to the neutral product due to deshielding effects of the protonated guanidinium species. However, the protons of the two bicarbonate product (**32*c***) samples resonate at different chemical shifts, (δ_H 4.74 and 4.60 ppm) even though both were found to be structurally indistinguishable. The reason for this discrepancy has not been determined. As there is not large variation within the ^{13}C NMR spectra of these products, it is likely relevant to the extent of hydrogen bonding within the product in solution.

One theory to this inconsistency is described in Scheme **5.4**. Assuming free rotation about the ···CH_2–hppH bond, the N*H* proton of the guanidinium units is either projected away from or pointing towards to the benzyl-methylene protons. This will likely affect the magnetic environment at the CH_2 position, thus changing the chemical shift. Ordinarily this would be a rapid process, resulting in an average within the spectrum. However, the NH···[X] hydrogen bonding between the guanidinium unit and anion will not only vary with the identity of the anionic species ([X] = [Cl], [BPh_4], [HCO_3]), but may generate preferential arrangements in solution. This then could result in differing chemical shifts of the resonating benzyl-methylene protons.

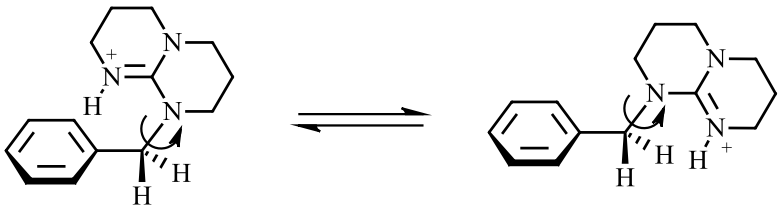

Scheme 5.4: Rotation of the hppH-unit affecting chemical shift of benzyl-methylene protons

5.2 Synthesis and Characterization of [1,3-(CH_2hppH)$_2$-C_6H_4][HCO_3]$_2$ (**31*c***)

5.2.1 Synthesis

Utilizing the optimized reaction conditions developed for the synthesis of the isomeric bicarbonate product **32*c***, 0.1 equivalents of benzoic acid were added to a solution of neutral 1,3-(CH_2hpp)$_2$-C_6H_4 (**31**) in acetonitrile, and stirred under air for one hour (Scheme **5.5**). The removal of the volatiles via slow evaporation at room temperature gave a colorless oil. Recrystallization through storage of the product in a solution of acetonitrile at -30 °C afforded white crystals in 38% isolated yield, though the crystalline product was unsuitable for crystallographic analysis. Product **31*c*** was characterized through ^{1}H NMR and ^{13}C NMR analysis.

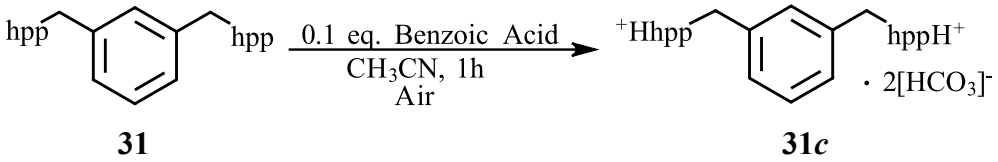

31 **31*c***

Scheme 5.5: Synthesis of [1,3-(CH_2hppH)$_2$-C_6H_4][HCO_3]$_2$ (**31*c***)

5.2.2 Spectroscopic Properties

As found within the data of the previously characterized guanidine salts, the comparison of the ^{1}H NMR spectrum of the product **31*c*** with that of the neutral starting material **31** shows a general downshift of the proton signals. The signal correlating to the benzyl-methylene protons

is found at δ_H 4.60 ppm within the product **31*c***, and at δ_H 4.56 ppm within the starting material. There is also a broad singlet at δ_H 5.19 ppm that can be attributed to the resonance of an exchangeable N*H* proton found within the guanidinium functionality. Unlike the low field signals found in the hydrochloride salt [hppH$_2$][Cl][13], this upfield signal could be attributed to the shielding caused by a more rigid hydrogen bonding network that would be expected with bicarbonate salts. The presence of water is seen within this spectrum (δ_H 2.00 ppm, HOD), as expected with this highly hygroscopic compound. The upfield shift of the *C*N$_3$ resonance at δ_C 151.3 ppm within the ^{13}C NMR spectrum of compound **31*c*** is consistent with the slightly more shielded environment found within the delocalized framework of the protonated hpp-functionalities. The slight downfield shift in the benzyl-methylene carbon (δ_C 51.9 ppm) in comparison to the neutral starting material further suggests successful protonation of both guanidine units. However, there is no resonance within this spectrum that can be assigned to the bicarbonate central carbon.

5.3 Synthesis and Characterization of [Ph(CH$_2$hppH)][HCO$_3$] (29*c*)

5.3.1 Synthesis

Implementing the optimized procedure, 0.1 equivalents of benzoic acid were added to a solution of neutral Ph(CH$_2$hpp) (**29**) in acetonitrile, and stirred under air for one hour (Scheme **5.6**). The removal of the volatiles by slow evaporation at room temperature gave a yellow oil. Recrystallization through storage of the product in a solution of acetonitrile at -30 °C afforded fine yellow crystals that were unsuitable for crystallographic analysis. The oily product **29*c*** was collected in 88% yield, and characterized by ^{1}H NMR and ^{13}C NMR analysis.

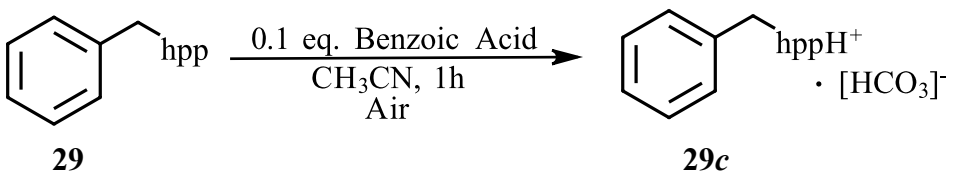

Scheme 5.6: Synthesis of [Ph(CH$_2$hppH)][HCO$_3$] (**29*c***)

5.3.2 Spectroscopic Properties

As seen in the previously characterized bicarbonate salts, the ^{1}H NMR spectrum of the product **29*c*** displays the downfield shift of resonances consistent with the successful protonation of the guanidine functionality. The benzyl-methylene protons of **29*c*** resonate at δ_H 4.63 ppm, compared to δ_H 4.58 ppm in the neutral starting material **29**. Similar shift discrepancies are observed for the NC*H*$_2$ hpp-proton resonances (δ_H 3.41, 3.16 and 3.05 ppm). The introduction of a broad singlet signal at δ_H 2.61 ppm can be attributed to the resonance of an exchangeable N*H* proton, most likely undergoing exchange with protons within water molecules. It should be noted that the spectrum showed low intensity peaks for the $[PhCO_2]^-$ anion present in the sample. Slight changes within the ^{13}C NMR spectrum collected for this product support the formation of compound **29*c***. There is a downfield shift of the benzyl-methylene carbon (δ_C 52.2 ppm) consistent with the results found in the previously characterized bicarbonate salts. Resonances of the methylene carbon atoms (NCH$_2$*C*H$_2$) within the hpp-unit (δ_C 22.2 and 22.1 ppm) are shifted downfield compared to the neutral starting material **29**, further indicating the change in chemical environment associated with the formation of the guanidinium cation. Although the presence of the anionic bicarbonate species cannot be distinctly confirmed, the data shows the formation of only one compound, and supports the successful protonation of the superbase.

5.4 Synthesis and Characterization of [1,3,5-(CH$_2$hppH)$_3$-2,4,6-(Et)$_3$-C$_6$][HCO$_3$]$_3$ (35*c*)

5.4.1 Synthesis

To compensate for the inherent inaccuracies in measuring the low mass of reagent, a slightly greater concentration of benzoic acid was used in the reactions involving the more massive superbasic compounds. Thus, 0.3 equivalents of benzoic acid were added to a solution of neutral 1,3,5-(CH$_2$hpp)$_3$-2,4,6-(Et)$_3$-C$_6$ (**35**) in acetonitrile. The resulting solution was stirred for one hour under air, and subsequent removal of the volatiles through slow evaporation yielded a colorless oil (Scheme **5.7**). Storage of the crude product in solution of acetonitrile at -30 °C

afforded white crystals of **35*c*** in 71% isolated yield. The resulting product was characterized through ^{1}H NMR and ^{13}C NMR analysis.

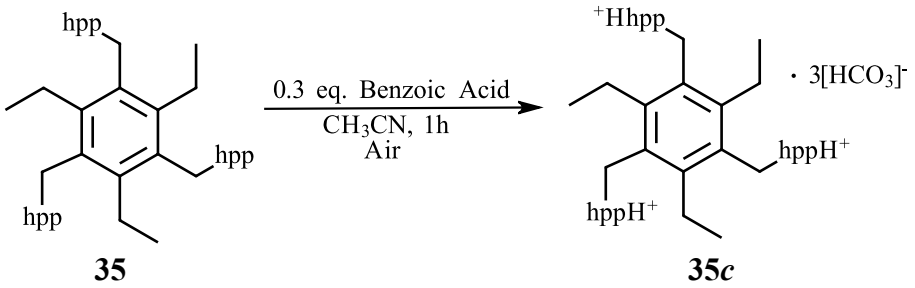

35 **35*c***

Scheme 5.7: Synthesis of [1,3,5-(CH_2hppH)$_3$-2,4,6-(Et)$_3$-C_6][HCO_3]$_3$ (**35*c***)

5.4.2 Spectroscopic Properties

^{1}H NMR and ^{13}C NMR analysis of the product supports the successful synthesis of the bicarbonate salt **35*c***. Comparison of the ^{1}H NMR spectrum of the neutral starting material **35** shows a consistent downfield shift in the proton resonances found within the product. The benzyl-methylene signal within the product is found at δ_H 4.66 ppm, in contrast to δ_H 4.58 ppm in the starting material. Similar downfield shifts are seen in the NC*H*$_2$ hpp-proton resonances of **35*c*** (δ_H 3.45, 3.13, 3.01, 2.73 ppm), offering further evidence for the successful protonation of all three guanidine functionalities. As in the previously discussed guanidinium salts, there is a large water peak found at δ_H 2.00 ppm (HOD), and the absence of an N*H* signal. This can be attributed to rapid proton exchange between the solvent or adventitious water.

The comparison of the ^{13}C NMR spectra of the product and neutral starting material shows discrete changes within the resonating carbon signals that would be expected for the formation of compound **35*c***. As in the corresponding hydrochloride salt **35*b***, there is not an observed downfield shift of the benzyl-methylene carbon resonance (δ_C 48.3 ppm) as found in the previous bicarbonate salts. This could possibly be due the alkyl-substituents within this compound, shielding this carbon from electronic effects of the cationic guanidinium units. Upfield shifts are seen in the hpp-carbon resonances (N*C*H$_2$) found at δ_C 47.8, 46.8 and 37.7 ppm within compound **35*c***. These data are consistent with the shifts observed in the ^{13}C NMR spectrum for the analogous bicarbonate salt [hppH$_2$][HCO_3] characterized within the literature.[9] Despite a highly concentrated sample and long experimental run times, there is no

low-field resonance seen within this spectrum that can be attributed to the carbon within the bicarbonate anionic species.

5.4.3 Solid-State Structure

A low-quality X-ray diffraction data set was collected. The solution indicated the successful formation of the bicarbonate salt **35*c***. The molecular structure of the cation shows the energetic preferential conformation discussed in Chapter 2, with all three hppH functionalities on the same face of the plane defined by the C_6-ring. One bicarbonate anion is also seen, confirming the ability of this guanidine superbase to capture and activate CO_2. However, there is significant disorder within the other anionic species and multiple areas of electron density assigned to the oxygen atoms of water molecules that have prevented elucidation of the full molecular structure of this ionic compound.

5.5 Synthesis and Characterization of $[hppH_2]_2[CO_3]$ (**1*d***)

5.5.1 Synthesis

The optimized reaction conditions were employed to confirm formation of the bicarbonate salt $[hppH_2][HCO_3]$ with sub-stoichiometric proton source under ambient CO_2 from the atmosphere. Thus, 0.1 equivalents of benzoic acid were added to a solution of sublimed hppH (**1**) in acetonitrile, and stirred under air for one hour. The volatiles were removed via slow evaporation, and subsequent storage of the resulting product in a solution of acetonitrile at -30 °C afforded white crystals. However, single crystal X-ray diffraction revealed the structure of this product to be the carbonate salt $[hppH_2]_2[CO_3]$ (**1*d***), in contrast to the expected bicarbonate product (Scheme **5.8**). The crystalline product was isolated in 69% yield. In addition to the collected crystallographic data, this structure was characterized through, elemental analysis, and ^{1}H NMR and ^{13}C NMR spectroscopy.

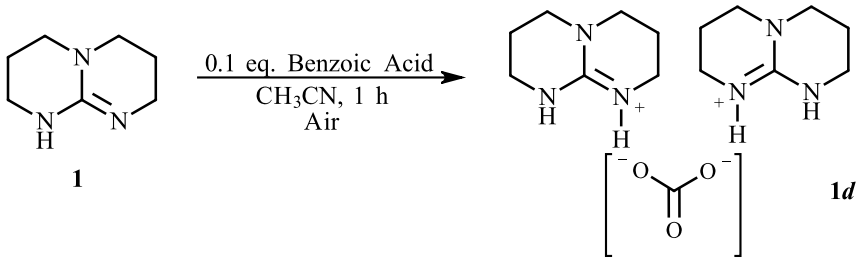

Scheme 5.8: Synthesis of $[hppH_2]_2[CO_3]$ (**1*d***)

5.5.2 Spectroscopic Properties

The ^1H and ^{13}C NMR spectra of compound **1*d*** are consistent with a symmetric structure in solution, displaying only half of the resonances predicted for a structure in which the two rings of the bicyclic framework are inequivalent by maintained localized C—N single and C=N double bonds. This spectral evidence indicates rapid proton exchange between the two nitrogen atoms of each amidine component, or intermolecular exchange between two guanidine units, and is consistent with the literature values of previously characterized $[hppH_2]^+$ salts.[13] Resonances of the methylene protons within the bicyclic framework found at δ_H 3.28, 3.24 and 1.96 ppm within the ^1H NMR spectra of **1*d*** are shifted downfield in comparison to ^1H NMR data collected for neutral hppH (**1**), and are consistent with the induced deshielding upon protonation of the guanidine species.

The ^{13}C NMR spectroscopic data further affirms the formation of the carbonate product **1*d***. The signal found at δ_C 163.2 ppm can be attributed to the resonance of the carbon within the $[CO_3]^{2-}$ anionic species. In comparison to literature values[9] of the analogous bicarbonate salt $[hppH_2][HCO_3]$, this signal is shifted downfield to that found within the bicarbonate species and is consistent with the higher degree of deshielding of the central carbon within the dianionic species.

5.5.3 Solid-State Structure

Single crystal X-ray diffraction of the crystalline product confirmed the synthesis of the monomeric dicationic carbonate salt $[hppH_2]_2[CO_3]$ (**1*d***, Figure **5.7**). This compound crystallizes in the Pbcn space group, and was found to be associated with six molecules of water through hydrogen-bonding interactions (omitted from Figure **5.7** for clarity). There is

hydrogen bonding between both N*H* protons within the guanidinium units and the central carbonate anion. Select bond lengths of the cationic species are listed in Table **5.6**, and calculated geometric parameters of the guanidinium functionalities are listed in Table **5.7**.

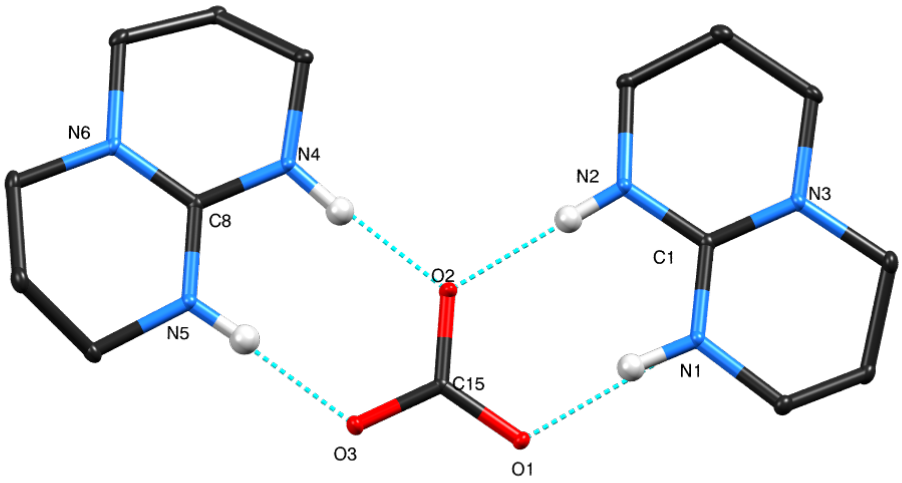

Figure 5.7: Thermal ellipsoid (20%) representation of carbonate salt $[hppH_2]_2[CO_3]$ (**1*d***). Water molecules and hydrogens (except N*H*) omitted for clarity.

Previous studies have reported the molecular structure of the neutral hppH (**1**) species.[36] It was found that this compound exists as a hydrogen-bonded dimer in the solid-state, having disorder in the position of the N*H* atoms between two possible tautomers (Figure **5.8**). This disorder prevents meaningful discussion of carbon-nitrogen bond lengths.[36]

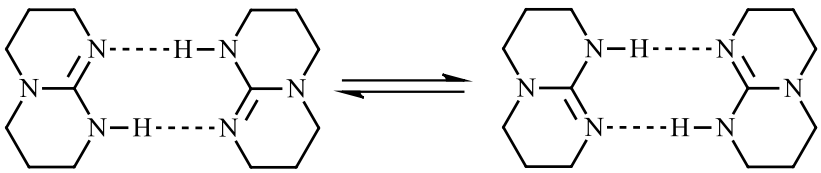

Figure 5.8: Disorder present in the crystal structure of hppH (**1**)[13]

Therefore, the elucidated bond lengths of the guanidine unit from the structural data of 1,4-$(CH_2hpp)_2$-C_6H_4 (**32**) will be used as a measure of the C—N bond distances within the neutral hpp-fragment.

Table 5.6: Select bond lengths in carbonate salt **1*d*** and neutral hpp-derivative (**32**)

Bond	**$[hppH_2]_2[CO_3]$ (1*d*)**	**Neutral 1,4-$(CH_2hpp)_2$-C_6H_4 (32)**
N**1**—C**1**	1.334(2) Å	1.387(2) Å
N**2**—C**1**	1.332(2) Å	1.291(2) Å
N**3**—C**1**	1.339(2) Å	1.378(2) Å
N**4**—C**8**	1.335(2) Å	1.387(2) Å*
N**5**—C**8**	1.332(2) Å	1.291(2) Å*
N**6**—C**8**	1.343(2) Å	1.378(2) Å*

* Guanidine units are equivalent in neutral compound **32**. Bond lengths of N**4**—C**8**, N**5**—C**8**, N**6**—C**8** are the same as N**1**—C**1**, N**2**—C**1**, N**3**—C**1**, respectively.

The geometric parameters calculated from the structural data of compound **1*d*** reflect efficient delocalization within guanidinium functionalities. The low Δ_{CN} values of 0.002 and 0.003 Å shows a very minimal difference between C—N single and C=N double bond lengths as expected in a delocalized system, whereas within the neutral hpp-derivative (**32**) this difference is much more pronounced (Δ_{CN} = 0.096 Å). The small Δ'_{CN} values of 0.006 and 0.010 Å and low DP percentage range (0.11—0.22%) also indicate delocalization throughout the hpp-unit. Finally, the ρ ratios of 1.00 reflect effectively distributed positive charge across the carbon-nitrogen bonds, and almost complete symmetrical bonding within the guanidinium cation.

$\Delta_{CN(1\text{-}3)}$ / Å	0.002	$\Delta_{CN(4\text{-}6)}$ / Å	0.003
$\Delta'_{CN(1\text{-}3)}$ / Å	0.006	$\Delta'_{CN(4\text{-}6)}$ / Å	0.010
DP_{N3}	0.11%	**DP_{N6}**	0.22%
ρ ratio (N**1**-N**3**)	1.00	**ρ ratio** (N**4**-N**6**)	1.00

Table 5.7: Summary of geometric data for guanidinium components of carbonate salt **1*d***

5.6 Synthesis and Characterization of [hppH$_2$][HCO$_3$] (**1*c***)

5.6.1 Synthesis

It was hypothesized that the isolated carbonate salt **1*d*** could act as an intermediate for the formation of the corresponding bicarbonate salt [hppH$_2$][HCO$_3$] (**1*c***). The generation of a bicarbonate from a carbonate species through addition of water and carbon dioxide (Scheme **5.9**) is a well-documented process, and has been employed in previous studies involving guanidinium-carbonate salts.[20]

$$CO_3^{2-} + H_2O + CO_2 \longrightarrow 2\ HCO_3^-$$

Scheme 5.9: Bicarbonate formation from carbonate, water, and CO_2[20]

Utilizing this synthetic strategy, the crystalline carbonate product **1*d*** was dissolved in a solution of acetonitrile containing 5 mol % H_2O. This solution was stirred for one hour, and the volatiles removed via slow evaporation. Storage of the crude product in solution of acetonitrile at -30 °C afforded white crystals in 83% isolated yield, determined by single crystal X-ray diffraction to be the desired bicarbonate salt [hppH$_2$][HCO$_3$] (**1*c***, Scheme **5.10**). Compound **1*c*** was characterized through crystallographic analysis, and ^{1}H NMR and ^{13}C NMR spectroscopy.

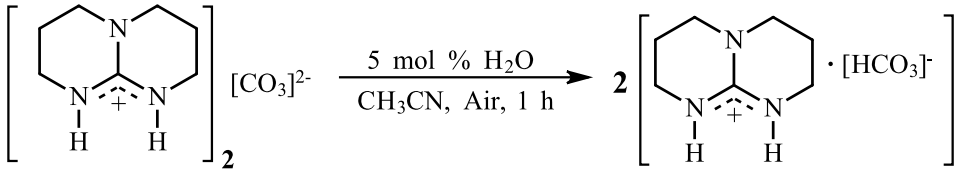

1*d* **1*c***

Scheme 5.10: Formation of bicarbonate salt [hppH$_2$][HCO$_3$] **1*c***

5.6.2 Spectroscopic Properties

^{1}H NMR and ^{13}C NMR analysis support the synthesis of the desired bicarbonate salt **1*c***. As observed in the spectral evidence collected for the carbonate salt **1*d***, the ^{1}H and ^{13}C NMR spectra of this product display half of the resonances predicted for a structure in which the two rings are inequivalent due to maintained localized C—N single and C=N double bonds, indicating a symmetric structure in solution. Resonances of the hppH-methylene protons

within the ^{1}H NMR spectrum (δ_H 3.28 and 1.98 ppm) integrate in a 2:1 ratio, respectively, and are shifted downfield in comparison to the spectrum of the neutral parent species hppH (**1**), which is consistent with the deshielding effects caused by protonation of the guanidine unit. The ^{13}C NMR data supports the formation of the bicarbonate salt **1*c***. The resonance observed at δ_C 162.1 ppm can be attributed to the carbon within the bicarbonate anion. These data are consistent with the literature values of previously characterized [hppH$_2$][HCO$_3$].[12] This resonance is shifted up field in comparison to the CO_3^{2-} resonance found in the spectral evidence of the carbonate salt **1*d***, and is indicative of successful bicarbonate formation.

5.6.3 Solid-State Structure

Single crystal X-ray diffraction confirmed the formation of [hppH$_2$][HCO$_3$] (**1*c***), shown in Figure **5.9**. The compound crystallizes in the $P\bar{1}$ space group, and was found to be associated with one water molecule through hydrogen bonding interactions. As in the discussion of carbonate salt **1*d***, bond lengths of the neutral compound 1,4-(CH$_2$hpp)$_2$-C$_6$H$_4$ (**32**) will be used for comparison. Select bond lengths from compound **32** and bicarbonate salt **1*c*** are listed in Table **5.8**.

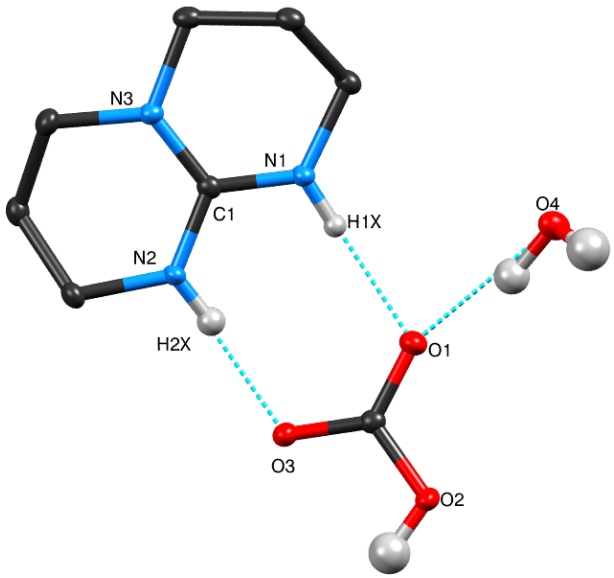

Figure 5.9: Thermal ellipsoid representation (20%) of [hppH$_2$][HCO$_3$]·H$_2$O (**1*c***). Hydrogens within cation (except N*H*) omitted for clarity. Selected bond lengths are reported in Table **5.8**.

Bond	$[hppH_2][HCO_3]\cdot H_2O$ (**1*c***)	Neutral 1,4-$(CH_2hpp)_2$-C_6H_4 (**32**)
N**1**—C**1**	1.334(3) Å	1.291(2) Å
N**2**—C**1**	1.338(4) Å	1.387(2) Å
N**3**—C**1**	1.335(3) Å	1.378(2) Å

Table 5.8: Select bond lengths in bicarbonate salt **1*c*** and neutral hpp-derivative (**32**)

The geometric parameters calculated from the structural data of compound **1*c*** support successful protonation and sufficient delocalization within the guanidinium moieties (Table **5.9**). The low Δ_{CN} value of 0.004 Å shows little discrepancy in the C—N single and C=N double bond lengths, as expected with a delocalized system. This difference is much more pronounced in the neutral hpp-fragment (**32**, Δ_{CN} = 0.096 Å). The negative Δ'_{CN} value of -0.001 indicates that the C1—N3 bond distances are significantly shorter than those observed for typical N—C_{sp2} bonds, suggesting delocalization of the lone-pairs into the CN_3 core of the cation, offsetting the formal positive charge at the protonated nitrogen. This is consistent with calculated Δ'_{CN} values of hppH hydrohalide salts.[13] The relatively low DP percentage (range = 0.11—0.78%) further support effective delocalization within the guanidinium species. The ρ ratio calculated from the structural data of the bicarbonate salt **1*c*** is 1.00, whereas the structure for the neutral hpp-unit of **32** gives ρ = 0.93. This increase reflects the lengthening of the C=N double bond and shortening of the C—N single bond within the CN_3 core of the guanidine.

Δ_{CN} / Å	0.004
Δ'_{CN} / Å	-0.001
DP_{N2}	0.78%
DP_{N3}	0.11%
ρ ratio	1.00

Table 5.9: Summary of geometric data for the guanidinium components of bicarbonate salt **1*c***

The extended molecular structure of this crystal shows a centrosymmetric chain formation connected through a hydrogen-bonding network between the $[hppH_2]^+$ cationic species, the

bicarbonate anions, and water molecules present in the solid-state (Figure **5.10**). As this crystallized compound is the hydrated species ([hppH$_2$][HCO$_3$]·H$_2$O), this framework differs from the corresponding anhydrous salt previously characterized within the literature (Figure **1.5**).[32]

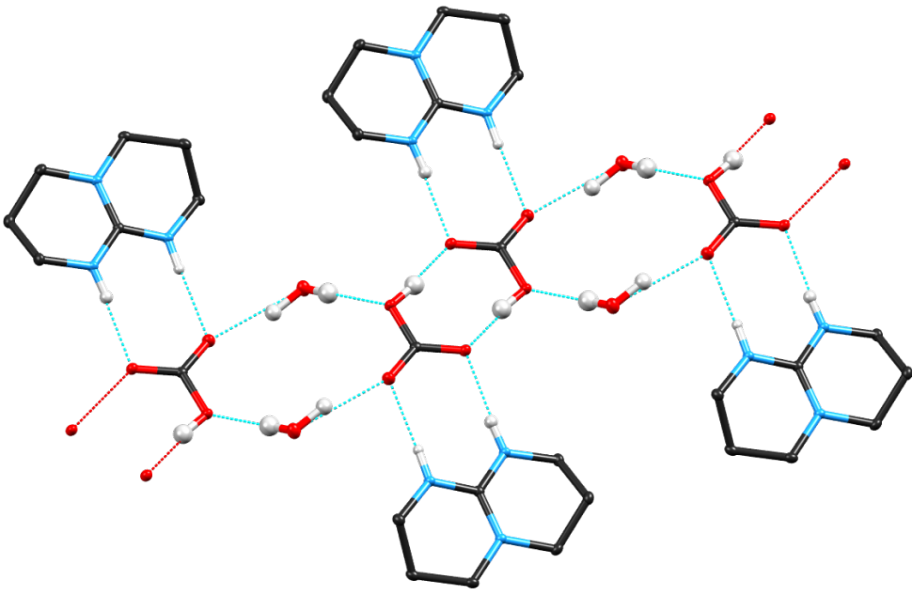

Figure 5.10: Thermal ellipsoid representation (20%) of the extended chain network of [hppH$_2$][HCO$_3$]·H$_2$O (**1*c***). Hydrogens within the cation (except N*H*) omitted for clarity.

5.7 Attempted Synthesis of [1,2-(CH$_2$hppH)$_2$-C$_6$H$_4$][HCO$_3$]$_2$

Previous literature[19,20] has shown that the recrystallization process of these protonated guanidine species under air plays a large role in the formation of the corresponding bicarbonate salt. One postulated theory within the scope of this research was that the recrystallization of a stable hydrochloride salt could give the analogous bicarbonate product, through capture of ambient CO$_2$ and water to form the [HCO$_3$]$^-$ anion, and dissipation of the chloride anion from the reaction system. This hypothesis was tested with the hydrochloride salt [1,2-(CH$_2$hppH)$_2$-C$_6$H$_4$][Cl]$_2$ (**30*b***), in the attempts to synthesize through bicarbonate formation [1,2-(CH$_2$hppH)$_2$-C$_6$H$_4$][HCO$_3$]$_2$ (**30*c***, Scheme **5.11**). The crystalline product of compound **30*b*** was dissolved in acetonitrile, and subsequent storage at -30 °C afforded white crystals.

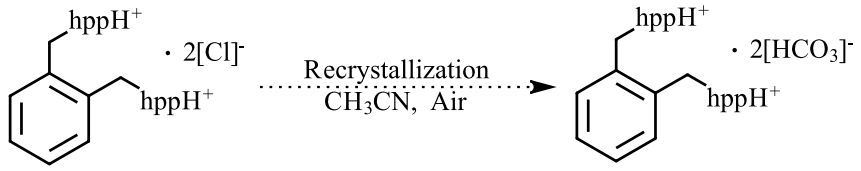

30*b* **30*c***

Scheme 5.11: Synthetic strategy to achieve bicarbonate salt **30*c*** through recrystallization of hydrochloride salt **30*b***

However, through single crystal X-ray diffraction, the structure of this crystalline compound was determined to be $[hppH_2][HCO_3]$ (**1*c***) . This unexpected result can be attributed to the limited solubility of compound **30*b***, which required excessive heat to solvate in acetonitrile, causing degradation of the product and release of the tethered hpp-units. Although the desired compound $[1,2\text{-}(CH_2hppH)_2\text{-}C_6H_4][HCO_3]_2$ (**30*c***) was not achieved through this experiment, the resulting product does affirm that subsequent recrystallization of a hydrochloride salt can produce the corresponding bicarbonate species.

Chapter 6

Functionalization Reactions

6.1 Introduction

Much of the current research exploring activation of carbon dioxide seeks to utilize CO_2 as a C1 building block within organic transformations. Due to the thermodynamic and kinetic stability of carbon dioxide, efficient reductive functionalization of CO_2 requires a system that is able to promote concurrent C—O bond cleavage and C—C and C—H bond formation. Although there has been extensive past work examining the capability of metallic centers from *d*- and *f*-blocks to activate CO_2[38,39], the use of organocatalysts for this process is a recent advancement. One focus within this area of study has been the implementation of various nucleophilic compounds, such as N-heterocyclic carbenes (NHCs)[40], Frustrated Lewis Pairs (FLPs)[41], or guanidines[42], within CO_2 transformation reactions. Bicyclic guanidines, such as hppH, have shown a great deal of promise as effective organocatalysts for the reductive functionalization of CO_2 under mild conditions.

6.1.1 hppH in Alkyl Carbonate and Carbamate Formation

Cantat and coworkers employed hppH (**1**) to promote the insertion of CO_2 into O—H and N—H bonds of alcohols and amines, respectively, to form corresponding alkyl carbonate and carbamate salts.[43] Their methodology involved a two-step reaction, outlined in Scheme **6.1**. First, an hppH-CO_2 adduct was formed through reacting neutral hppH under 1 atm CO_2. Subsequent stoichiometric addition of methanol afforded the carbonate salt [hppH$_2$][MeCO$_3$] (**36**) in quantitative yield. Carbonates **37** and **38** were also prepared from the more acidic benzyl alcohol and the bulkier, isopropanol, respectively. It was found that these carbonate species readily decarboxylate under reduced pressure (Scheme **6.1**).[43]

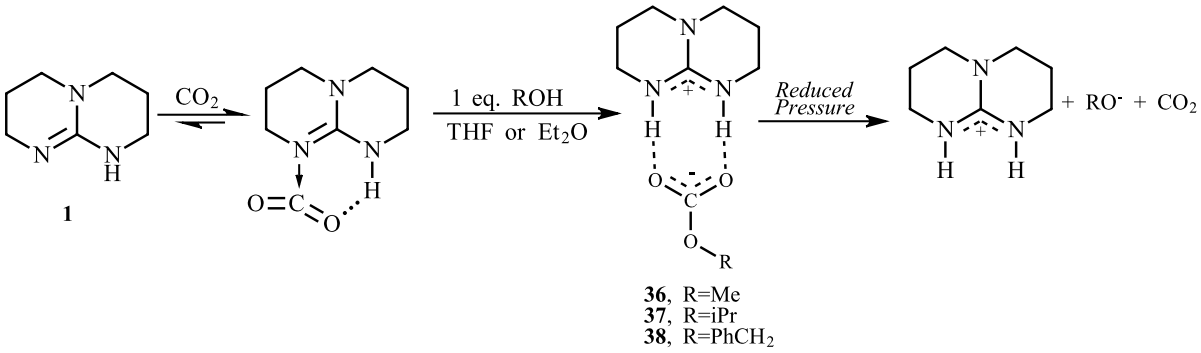

Scheme 6.1: Alkyl carbonate formation through CO_2 reductive functionalization by hppH[43]

This same synthetic strategy was employed in the formation of carbamate salts. Following the formation of the hppH-CO_2 adduct, the addition of one equivalent of morpholine (**39**) afforded carbamate **40** in quantitative yield (Scheme **6.2**).[43]

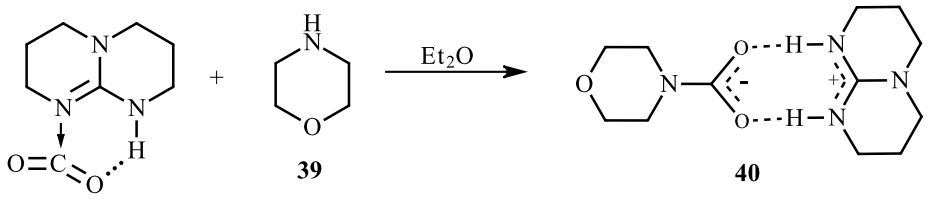

Scheme 6.2: Alkyl carbamate formation through CO_2 reductive functionalization by hppH[43]

6.1.2 hppH in the Methylation of Amines

hppH has also been implemented as a catalyst in the methylation of amines, in the presence of hydroborane reductants.[44] The reaction of diphenylamine (**41**) with 1 atm CO_2 and 4 equiv 9-borabicyclo(3.3.1)nonane (9-BBN), in the presence of 1.0 mol % hppH affords *N*-methyldiphenylamine (**42**) in 59% yield (Scheme **6.3**). As a nitrogenous base, hppH has the ability to significantly enhance the reduction capability of hydroboranes through coordination to the boron vacant site. Although the guanidine was not as effective in catalyzing this transformation as proazaphosphatrane superbases, hppH did prove to be more effective than N-heterocyclic carbenes, in addition to recent developed metal catalysts.[44] The increased reactivity of the guanidine base in comparison to metal catalysts is significant, as the use for organic catalysts as an alternative to metal-based compounds is desirable in order to avoid high costs, harsher conditions and unnecessary toxicity.

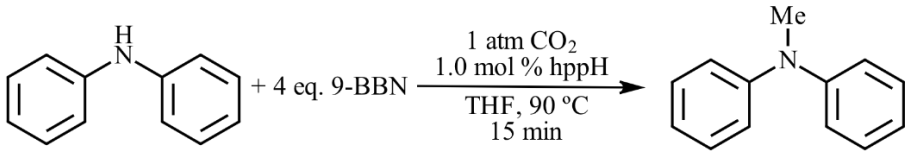

41 **42**

Scheme 6.3: Methylation of amines through use of catalytic hppH[44]

6.1.3 Mechanistic Study of CO_2 Functionalization Using Catalytic hppH

Previous research has briefly examined the mechanistic pathway of the hppH-catalyzed reductive functionalization of CO_2. Li and co-workers published a mechanistic study on the hppH-catalyzed chemical fixation of CO_2 with 2-aminobenzonitrile (**43**) to quinazoline-2,4(1*H*, 3*H*)-dione (**44**, Scheme **6.4**).[45]

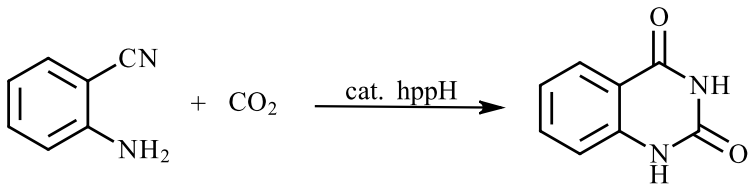

43 **44**

Scheme 6.4: Formation of quinazoline-2,4(1*H*,3*H*,)-dione (**44**) through use of catalytic hppH[45]

DFT calculations have identified two possible mechanistic reaction pathways. The CO_2 activation mechanism involves the formation of the zwitterionic hppH-CO_2 adduct. The second pathway is through a general base mechanism, in which the guanidinium unit primarily plays a catalytic role as a strong base to promote the fixation of CO_2 by the amino group of 2-aminobenzonitrile, without the formation of an hppH-CO_2 adduct intermediate.[45] It was found that the energetically preferred route is through the general base mechanism in a four-stage process: (I) guanidine-assisted fixation of CO_2 by the amino group of 2-aminobenzonitrile (**43**), (II) intramolecular nucleophilic attack from the carbamate to the nitrile group, (III) formation of the isocyanate intermediate, and (IV) intramolecular cyclization and hydrogen migrations, forming the desired product **45** and regenerating hppH. This result is interesting to note, as many other discussed mechanisms of hppH and CO_2 involve the formation of a carbamic intermediate.[11-12,45]

6.2 Synthetic Strategy

6.2.1 Mechanistic Considerations

There has been very little investigation of the mechanism of CO_2 capture and activation utilizing hindered nitrogenous bases. As discussed in chapter 1, Franco and co-workers proposed a mechanism for the formation of the bicarbonate salt [DBUH][HCO_3] (**12**).[11] Their postulate stated that bicarbonate formation occurred through structural changes to the DBU-CO_2 zwitterionic complex during the crystallization process. Mechanistically, this is formed by proton transfer from a water molecule to the zwitterion, followed by nucleophilic attack of the hydroxyl anion on the N-COOH moiety (Scheme **1.2**).

Within this project, it was reasoned that the reactivity leading to bicarbonate formation could be extended to the formation of alkyl carbonates utilizing the hpp-containing superbasic compounds. As shown in Scheme **6.5**, following CO_2 capture by hppH, proton transfer could occur from an alcohol (ROH) to the zwitterionic carbamate complex. Nucleophilic attack by the alkoxide anion on the carbonyl carbon and subsequent proton transfer would afford the corresponding [$hppH_2$][RCO_3] carbonate salt.

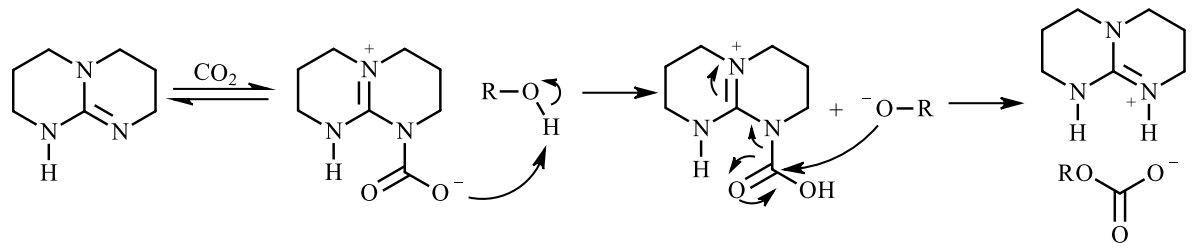

Scheme 6.5: Theoretical generalized mechanism for the formation of carbonate salt [$hppH_2$][RCO_3] through addition of CO_2 and an alcohol to hppH

There are many factors to consider in order to achieve this result from this mechanism. Firstly, the initial proton transfer must occur preferentially from the alcohol present, and not from adventitious water within the system. Thus, alcohols with higher acidity than water were implemented in this series of reactions. Secondly, the resulting alkoxide functionality (RO^-) must have high enough nucleophilicity to react at the carbonyl center. A range of alcohols were tested for this purpose.

6.2.2 Experimental Considerations

Rakamanickam and co-workers[35] explored the tuneability of reactions between equivalent mixtures of different guanidines and alcohols with CO_2 to yield guanidinium alkylcarbonate salts. Their work focused on the varying apparent equilibrium constant (K_{app}) in the reaction between a superbasic guanidine (SB), an alcohol (ROH) and CO_2 to form an ionic species composed of a guanidinium cation (SBH^+) and alkylcarbonate anion (RCO_3^-) (Scheme **6.6**). The reactions were performed in N-methyl-2-pyrrolidone (NMP), a polar aprotic solvent. As pressurized CO_2 was employed within the series of reactions, the partial pressure of CO_2 (P_{CO2}) was assumed to be 1 atm.[35]

$$SB + ROH + CO_2 \rightleftharpoons SBH^+ + RCO_3^- \quad ; \quad K_{app} = \frac{([SBH^+][RCO_3^-])}{(P_{CO2}[SB][ROH])}$$

Scheme 6.6: Equilibrium reaction and apparent equilibrium constant for the formation of alkyl carbonates[35]

In principle, an excess of alcohol can affect the carbonation reaction in two ways. It can increase the concentration of alcohol, resulting in a shift in the equilibrium toward the formation of the alkylcarbonate salt with no change in the equilibrium constant, as explained through Le Chatelier's principle. Additionally, the excess alcohol could stabilize the ion pairs by hydrogen-bonding, resulting in a change in the equilibrium constant that favors the carbonated state. Experimental results were consistent with these principles, finding that K_{app} increased with increasing concentrations of the alcoholic reagent (ROH).[35] Contrastingly, K_{app} decreased when using more dilute samples, containing larger levels of NMP. This result was attributed to the inability of this solvent to form hydrogen bonds, thus destabilizing the alkyl-carbonate in solution. These equilibrium results were taken into consideration in the attempted formation of alkyl-carbonates utilizing the hpp-containing superbases.

6.3 Functionalization Reactions

6.3.1 General Synthesis

From the evidence presented in the literature, a series of reactions implementing the developed hpp-containing compounds was carried out in the attempts to functionalize CO_2 and an

alcohol, forming an alkyl carbonate species. Two neutral hpp-species were implemented in this series of reactions, 1,4-$(CH_2hpp)_2$-C_6H_4 (**32**), and hppH (**1**). Five different alcohols were chosen as functionalization reagents, pictured in Figure **6.1**: methanol (**45**), phenol (**46**), 2,6-dimethylphenol (**47**), 2,6-di-*tert*-butylphenol (**48**), and diphenylmethanol (**49**).

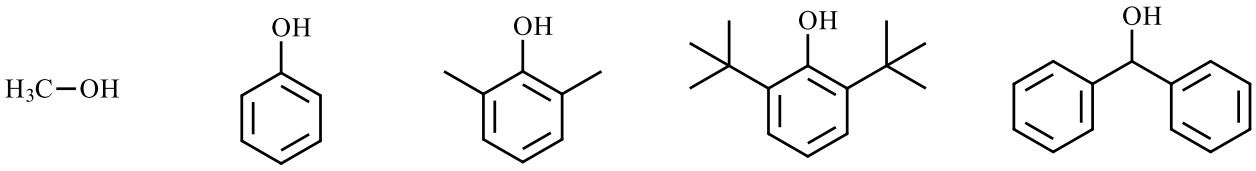

45 **46** **47** **48** **49**

Figure 6.1: Alcohols and phenols implemented as functionalization reagents

As the proposed mechanism requires proton donation from the alcohol to form an alkoxide anion, alcohols more acidic than water were chosen. Table **6.1** lists the pK_a values of each employed alcohol. Furthermore, molecular sieves were implemented in the reaction system in the attempts reduce the amount of adventitious water, unless otherwise stated.

Alcohol	**pK_a**
Water	15.74
Methanol	15.17
Phenol	9.86
2,6-Dimethylphenol	10.66
2,6-di-*tert*-butylphenol	12.16
diphenylmethanol	13.54

Table 6.1: p*K*a values of implemented alcohols in functionalization reactions

Table **6.2** and **6.3** describe the specific conditions for each functionalization reaction involving compound **32** and hppH (**1**), respectively. Each reaction was performed under air, in either neat alcoholic solvent or acetonitrile, as specified. Like NMP, acetonitrile is a polar aprotic solvent. Although Rakamanickam's equilibrium studies[35] indicated that polar aprotic solvents destabilize the alkyl carbonate salts, the insufficient solubility of the implemented reagents limited the scope of useable solvents.

As shown in Tables **6.2** and **6.3**, some of the reactions involve the addition of the external proton source, triethylamine hydrochloride. As the addition of this acid had shown to act as an initiator in bicarbonate formation, it was thought it could have the same effect in the formation of alkyl carbonate species. Triethylamine hydrochloride was chosen as the proton source as the anionic species, Cl^-, is small and volatile, thus less likely to interfere with the desired reaction. The addition of this proton source and the alcohol occurred simultaneously, unless otherwise stated.

6.3.2 Results and Discussion

The products of each reaction were characterized through ^1H NMR and ^{13}C NMR analysis. Single crystal X-ray diffraction was used on reactions that produced suitable crystals, that were obtained through storage of the product in a solution of acetonitrile at -30 °C. Unfortunately using all of the methods described in Tables **6.2** and **6.3**, the corresponding CO_2-functionalized alkyl carbonate salts were not synthesized. The results found are discussed here.

As shown by entries 1-3 in Table **6.2**, attempts at functionalizing methanol (**45**) using excess MeOH in the synthesis of the carbonate salt $[1,4\text{-}(CH_2hppH)_2\text{-}C_6H_4][MeCO_3]_2$ species resulted in the formation of the corresponding methoxide salt $[1,4\text{-}(CH_2hppH)_2\text{-}C_6H_4][MeO]_2$. This was determined by ^1H NMR and ^{13}C NMR spectra, in which peaks at δ_H 3.44 ppm (s, 6H, OC*H*$_3$) and δ_C 50.49 ppm (O*C*H$_3$) can be attributed to the methoxide anion. This carbon signal for the collected product is seen further upfield than the corresponding literature values found for the analogous methylcarbonate salt, $[hppH_2][MeCO_3]$ (δ_C 52.0 ppm, *C*H$_3$)[43], indicating a greater degree of shielding consistent with the formation of a methoxide anion. Furthermore, there is no low-field resonance within the ^{13}C NMR spectrum that can be assigned to the carbonyl carbon found within the anticipated $[MeCO_3]^-$ species. A two-step reaction (Table **6.2**, entry 4) in which the acid was reacted with the superbase for one hour before the addition of methanol led to the isolation of solely the bicarbonate salt **32*c***. Attempts at forming the methyl carbonate species utilizing hppH were equally unsuccessful (Table **6.3**, entries 1-3). Reacting neutral hppH in neat methanol resulted in the cationic species $[hppH_2]^+$, although spectral results gave no information as to the identity of the anion (Table **6.3**, entry 1). The same reaction in the presence of 0.1 equivalents of $[HNEt_3][Cl]$ yielded the

carbonate salt $[hppH_2]_2[CO_3]$ (Table **6.3**, entry 3). It should be noted that subjecting this product to reduced pressure caused decarboxylation (Table **6.3**, entry 2).

Table 6.2: 1,4-$(CH_2hpp)_2$-C_6H_4 (**32**) in functionalization reactions

Entry	Acid	Equivalents $[H]^+$	Alcohol	Equivalents Alcohol	Solvent	Additional Reaction Conditions/Comments	Outcome of Reaction
1	No acid	---	Methanol	Neat MeOH	MeOH	---	Characterized by ^1H NMR and ^{13}C NMR analysis. Methoxide salt [1,4-$(CH_2hppH)_2$-C_6H_4][MeO]$_2$ formed.
2	Triethylamine Hydrochloride	1 equiv.	Methanol	Neat MeOH	MeOH	---	Characterized by ^1H NMR and ^{13}C NMR analysis. Methoxide salt [1,4-$(CH_2hppH)_2$-C_6H_4][MeO]$_2$ formed
3	Triethylamine Hydrochloride	0.1 equiv.	Methanol	10 equiv.	CH_3CN	Molecular sieves used in reaction mixture.	Characterized by ^1H NMR and ^{13}C NMR analysis. Methoxide salt [1,4-$(CH_2hppH)_2$-C_6H_4][MeO]$_2$ formed.
4	Triethylamine Hydrochloride	0.1 equiv.	Methanol	10 equiv.	CH_3CN	Two step reaction. Addition of acid to form isolated bicarbonate salt, then addition of MeOH.	Characterized by ^1H NMR and ^{13}C NMR analysis. Bicarbonate salt [1,4-$(CH_2hppH)_2$-C_6H_4][HCO_3]$_2$ formed.
5	No Acid	---	Phenol	0.5 equiv.	CH_3CN	Molecular sieves used in reaction mixture.	Characterized by ^1H NMR and ^{13}C NMR analysis. Phenoxide salt [1,4-$(CH_2hppH)_2$-C_6H_4][PhO]$_2$ formed
6	Triethylamine Hydrochloride	0.1 equiv.	Phenol	10 equiv.	CH_3CN	Molecular sieves used in reaction mixture.	Characterized by ^1H NMR and ^{13}C NMR analysis. Shows protonated guanidine units and unreacted phenol.
7	Triethylamine Hydrochloride	0.1 equiv.	Phenol	2 equiv.	CH_3CN	Molecular sieves used in reaction mixture. Solvent removed *in vacuo.*	Characterized by ^1H NMR and ^{13}C NMR analysis. No evidence supporting formation of $[PhCO_3]^-$.

8	Triethylamine Hydrochloride	0.1 equiv.	Phenol	2 equiv.	CH_3CN	Molecular sieves used in reaction mixture. Solvent removed via slow evaporation.	Characterized by ^1H NMR and ^{13}C NMR analysis. Single crystal X-ray diffraction on crystals shows formation of $[1,4\text{-}(CH_2hppH)_2\text{-}C_6H_4][HCO_3]_2$
9	No acid	---	2,6-xylenol	10 equiv.	CH_3CN	Molecular sieves used in reaction mixture.	Characterized by ^1H NMR and ^{13}C NMR analysis. $[1,4\text{-}(CH_2hppH)_2\text{-}C_6H_4][(CH_3)_2PhO]_5$.
10	No acid	---	2,6-di-*tert*-butylphenol	10 equiv.	CH_3CN	Molecular sieves used in reaction mixture.	Alcohol oxidized to 3,3',5,5'-tetra-*tert*-butyl-4,4'-diphenoquinone.
11	Triethylamine Hydrochloride	0.1 equiv.	diphenylmethanol	2 equiv.	CH_3CN	Molecular sieves used in reaction mixture.	Characterized by ^1H NMR and ^{13}C NMR analysis. No evidence supporting formation of $[Ph_2CHCO_3]^-$.

Table 6.3: hppH (**1**) in functionalization reactions

Entry	Acid	Equivalents $[H]^+$	Alcohol	Equivalents Alcohol	Solvent	Additional Reaction Conditions/Comments	Outcome of Reaction
1	No Acid	---	Methanol	Neat MeOH	MeOH	Molecular sieves used in reaction mixture.	Characterized by ^{1}H NMR and ^{13}C NMR analysis. $[hppH_2]^+$ formed; no evidence of $[MeCO_3]^-$.
2	Triethylamine Hydrochloride	0.1 equiv.	Methanol	Neat MeOH	MeOH	Molecular sieves used in reaction mixture. Solvent removed *in vacuo*.	Characterized by ^{1}H NMR and ^{13}C NMR analysis. $[hppH_2]^+$ formed; no evidence of $[MeCO_3]^-$.
3	Triethylamine Hydrochloride	0.1 equiv.	Methanol	Neat MeOH	MeOH	Molecular sieves used in reaction mixture. Solvent removed via slow evaporation.	Characterized by ^{1}H NMR and ^{13}C NMR analysis. $[hppH_2]_2[CO_3]$ formed.
4	No Acid	---	Phenol	1 equiv.	CH_3CN	Molecular sieves used in reaction mixture.	Characterized by ^{1}H NMR and ^{13}C NMR analysis. Bicarbonate salt $[hppH_2][HCO_3]$ formed.
5	Triethylamine Hydrochloride	0.1 equiv.	2,6-xylenol	1 equiv.	CH_3CN	Molecular sieves used in reaction mixture.	Characterized by ^{1}H NMR and ^{13}C NMR analysis. $[hppH_2][(CH_3)_2PhO]$ formed.
6	Triethylamine Hydrochloride	0.1 equiv.	2.6-di-*tert*-butylphenol	1 equiv.	CH_3CN	Molecular sieves used in reaction mixture.	Alcohol oxidized to 3,3',5,5'-tetra-*tert*-butyl-4,4'-diphenoquinone.
7	Triethylamine Hydrochloride	0.1 equiv.	diphenylmethanol	1 equiv.	CH_3CN	Molecular sieves used in reaction mixture.	Characterized by ^{1}H NMR and ^{13}C NMR, and crystallographic analysis. Carbonate salt $[hppH_2]_2[CO_3]$ formed.

Phenol (**46**) was implemented as a functionalization reagent for its adequate acidity and good nucleophilicity. However, attempts at synthesizing the carbonate salts [1,4-(CH_2hppH)$_2$-C_6H_4][$PhCO_3$]$_2$ (Table **6.2**, entries 5-8), and [hppH$_2$][$PhCO_3$] (Table **6.3**, entry 4) were unsuccessful. As shown in Table **6.2** (entry 5), the addition of 0.5 equivalents of phenol to compound **32** in the absence of an additional proton source afforded the corresponding phenoxide salt, [1,4-(CH_2hppH)$_2$-C_2H_4][PhO]$_2$. This was determined by ^{1}H NMR spectroscopy, through characteristic peaks found at δ_H 7.10 (t, 4H, *m*-C_6H_5), 6.77 (d, 4H, *o*-C_6H_5), and 6.68 (t, 2H, *p*-C_6H_5) ppm can be attributed to the [PhO]$^-$ anion. These data are consistent with literature values of analogous guanidinium phenoxide derivatives containing the cationic [hppH$_2$]$^+$ species.[46] The absence of a low-field peak corresponding to a carbonate species indicated the unsuccessful functionalization of CO_2. Crystalline product was obtained from a reaction of neutral starting material **32**, 0.1 equivalents [$HNEt_3$][Cl], and two equivalents of phenol (Table **6.2**, entry 8), but was determined through single crystal X-ray diffraction to be the bicarbonate salt **32*c***.

^{1}H NMR spectral data of the powder product collected from the reaction of hppH with phenol (**46**) in the presence of a proton source suggested the presence of a cationic [hppH$_2$]$^+$ (δ_H 3.23 (pseudo-t, 8H, NC*H*$_2$), 1.94 (quint, 4H, NCH_2CH_2) ppm) and deprotonated [PhO]$^-$ anion (δ_H 7.14 (t, 2H, *m*-C_6H_5), 6.80 (d, 2H, *o*-C_6H_5), 6.67 (t, 1H, *p*-C_6H_5) ppm). ^{13}C NMR spectral results also support the presence of these two species, however an additional signal at δ_C 161.1 ppm indicates the presence of a third species. This resonance is further upfield than a signal expected for the carbonate anion [$PhCO_3$]$^-$, and instead is characteristic of a bicarbonate species. Although this was not the target synthetic product, this result does show that the bicarbonate salt [hppH$_2$][HCO_3] (**1*c***) can be formed and isolated without crystallization, which contradicts postulations made within the literature.[20]

The implementation of bulkier alcohols in this series of functionalization reactions also proved to be unsuccessful. Reactions with 2,6-dimethylphenol (**47**) with compound **32** and hppH in the presence of substoichiometric quantities of acid resulted in the corresponding alkoxide products (Table **6.2**, entry 9, and Table **6.3**, entry 5). In the reaction involving guanidine **32**, integration values within the ^{1}H NMR spectra of the product showed the association of five [$(CH_3)_2$PhO]$^-$ anions to each one [1,4-(CH_2hppH)$_2$-C_6H_4]$^{2+}$ cationic species. The use of 2,6-di-*tert*-butylphenol (**48**) with both hpp-derived starting materials resulted in the dimerization and oxidation of the alcohol to form 3,3',5,5'-tetra-*tert*-butyl-4,4'-diphenoquinone (Table **6.2**,

entry 10, and Table **6.3**, entry 6). Finally, implementing the bulk diphenylmethanol (**49**) reagent gave no functionalized carbonate product when in the reaction of compound **32** (Table **6.2**, entry 11), and afforded the carbonate salt $[hppH_2]_2[CO_3]$ (***1d***) in the reaction involving neutral hppH (Table **6.3**, entry 7).

6.3.3 Conclusions

Although the results of this series of reactions do indicate the ability of the hpp-containing superbases to effectively capture and activate carbon dioxide from ambient air, they have not demonstrated to be effective in the functionalization of alcohols to form alkyl carbonates under the reaction conditions examined. This lack of success cannot be attributed to only one factor, as there are a multitude of variables that need to be considered. One inherent issue to this synthetic strategy is the hygroscopic nature of these superbasic guanidines, that causes preferential reaction with water over the alcohol. Within these reactions, it is necessary to perform the reaction under air to be able to sequester carbon dioxide. However, water vapor within the atmosphere is found at approximately 100 times higher concentration than CO_2, so it is very difficult to simultaneously promote the capture of carbon dioxide and prevent the capture of water. This complication could be prevented through implementation of dry air within the reaction conditions, however this was not investigated due to time constraints of this study.

The experimental procedures implemented in the attempted synthesis of these alkyl carbonate species was built upon the diagramed in Scheme **6.5**, though this reaction path may not be accurate. As seen through the synthesis of quinazoline-2,4(1*H*,3*H*,)-dione (**44**, Scheme **6.4**)[45], hppH can act as a synthetic catalyst through a general-base mechanism, as opposed to through a zwitterionic carbamate intermediate. Future mechanistic studies, including experimental and energetic and DFT calculations to understand the distinct reaction pathway will help in achieving the target alkyl carbonates.

Chapter 7

Concluding Remarks

This study has demonstrated the ability of protonated superbasic hppH derivatives to efficiently and effectively capture and activate carbon dioxide from ambient air, to form the corresponding guanidinium-bicarbonate salts. A series of seven neutral poly-hpp compounds was developed for examination, and utilized in this study: Ph(CH_2hpp) (**29)**, 1,2-(CH_2hpp)$_2$-C_6H_4 (**30**), 1,3-(CH_2hpp)$_2$-C_6H_4 (**31**), 1,4-(CH_2hpp)$_2$-C_6H_4 (**32**), 1,3,5-(CH_2hpp)$_3$-C_6H_3 (**33**), 2,4,6-(CH_2hpp)$_3$-mesitylene (**34**), 1,3,5-(CH_2hpp)$_3$-2,4,6-(Et)$_3$-C_6 (**35**).

All isolated bicarbonate products were characterized through ^{1}H NMR and ^{13}C NMR analysis. Elemental analysis, IR spectroscopy, and single crystal X-ray diffraction were also utilized as analysis techniques where applicable. Molecular structures determined from single crystal X-ray diffraction techniques indicate the efficient delocalization of the formal charge within the cationic guanidinium species, and have revealed complex hydrogen-bonded networks of the ionic species involving the anionic, H_2O, and solvent molecules. An optimized procedure for bicarbonate formation was developed, and revealed that substoichiometric concentrations of a proton source activate this class of compounds, leading to fully protonated guanidinium species and CO_2 activation. The optimized procedure employed only 0.1 equivalents of commercially available benzoic acid. This work also demonstrated that protonation of solely hppH allows for capture and activation of carbon dioxide, affording both the corresponding bicarbonate salt [hppH$_2$][HCO_3] (**1*c***), and carbonate salt [hppH$_2$]$_2$[CO_3] (**1*d***).

There were inconsistencies found within the ^{1}H NMR spectra of the chemical shift data corresponding to the cationic species within crystalline bicarbonate species. As each sample was of an equal concentration and each experiment had sufficient run time, the reasons to this are not yet known. Additionally, although crystallographic analysis confirmed the formation of the bicarbonate salt, resonances corresponding to the anionic bicarbonate species do not always

appear within the spectral data. These inconsistencies limit the applications and characterization of these products.

The cationic guanidinium species were analyzed through the synthesis under air of various hydrochloride and tetraphenylborate salts, and were characterized through ^{1}H NMR, ^{13}C NMR and crystallographic analysis. It was found that this class of compounds is able to successfully form these ionic compounds under air without the capture of carbon dioxide. Molecular structures determined through single crystal X-ray diffraction showed effective delocalization within the guanidinium units, as found within the corresponding bicarbonate salts.

A series of reactions was carried out utilizing both 1,4-$(CH_2hpp)_2$-C_6H_4 and hppH, in the attempts of functionalizing an alcohol and atmospheric carbon dioxide to form the corresponding alkyl carbonate salts. Although a large range of reaction conditions was employed, the alkyl carbonate species was not successfully synthesized. The reactions instead afforded the corresponding alkoxide salts, bicarbonate salts, or carbonate salts. The hygroscopic nature of these compounds and preferential reaction with water over the alcohol limits the application of this synthetic method. Time constraints of this project prevented further investigation, though energetic calculations and further experimentation could lead to the successful synthesis of alkyl carbonate products.

Chapter 8

Experimental

8.1 General Considerations

With the exception of the synthesis of neutral hpp-containing compounds (*vide infra*), all manipulations were carried out under air. Tetrahydrofuran (THF), dichloromethane (CH_2Cl_2) and toluene were dried using a PureSolv. System (Innovative Technologies). Methanol (MeOH) was distilled in the presence of sodium metal. All other solvents were dried with molecular sieves for 24 hours prior to use. Triethylammonium tetraphenylborate ($[HNEt_3][BPh_4]$) was synthesized according to literature procedures.[47] hppH was purified by sublimation prior to use. All other reagents were purchased from the Sigma-Aldrich chemical company and used as received, unless stated otherwise. NMR spectra were recorded in either $CDCl_3$ or CD_3CN at 298 K, using a Varian INOVA system at 300 MHz (^1H), 500 MHz (^1H) or 125 MHz (^{13}C), as specified. All ^1H and ^{13}C chemical shifts are referenced internally to residual solvent resonances. Elemental analyses were performed by S. Boyer at London Metropolitan University.

8.2 Crystallography

Crystals were covered in inert oil. Suitable single crystals were selected under a microscope and mounted on an Agilent SuperNova diffractometer fitted with an EOS S2 detector. Data were collected at 120.0(2) K using focused microsource Cu Kα radiation at 1.5418 Å. Intensities were corrected for Lorentz and polarization effects and for absorption using multi-scan methods.[48] Space groups were determined from systematic absences and checked for higher symmetry. All structures were solved using direct methods with SHELXS[49] refined on F^2 using all data by full matrix least-squares procedures with SHELXL-97[50] within WinGX.[51] Non-

hydrogen atoms were refined with anisotropic displacement parameters. Hydrogen atoms were placed in calculated positions or manually assigned from residual electron density where appropriate unless otherwise stated. The functions minimized were $\Sigma w(F2o\text{-}F2c)$, with w = [σ2(F2o) + aP2 + bP]-1, where P = [max(Fo)2 + 2F2c]/3. The isotropic displacement parameters are 1.2 or 1.5 times the isotropic equivalent of their carrier atoms.

All data collection and structure solutions were provided by A/Prof. Martyn P. Coles.

8.3 Neutral hpp-Containing Reagents

All neutral starting hpp-containing reagents were synthesized under dry nitrogen using standard Schlenk-line and cannula techniques, or in a conventional nitrogen-filled glovebox. Sodium hydride (NaH) was obtained as 60% (w/w) dispersion in paraffin oil, and used as purchased. Weight and molar quantities listed correspond to that of solely NaH.

It should be noted that literature values[52] of ^{13}C NMR data characterizing Ph(CH_2hpp) (**29**) show the absence of one N*C*H_2 resonance within the guanidine unit, that has been attributed to overlapping signals, and is consistent with the spectral data of **29** collected in this study. This absence has also been found in the ^{13}C NMR spectra of the neutral hpp-derivatives **31**, **32**, and **33** utilized in this project, and is noted within the experimental data of these compounds.

8.3.1 Ph(CH_2hpp) (29)

One equivalent of NaH (0.069 g, 2.87 mmol.) was added to a solution of hppH (0.40 g, 2.87 mmol.) in THF (25 mL). The resulting suspension was heated to 60 °C and stirred for 2 hours. At room temperature, one equivalent of benzyl bromide (0.34 mL, 2.87 mmol.) was added dropwise to the mixture and stirred for 18 hours. Following the removal of the volatiles *in vacuo.*, the resulting white precipitate was dissolved in toluene (10 mL), filtered through celite, and concentrated. Purification of the product **29** was performed by recrystallization through storage of the solution at -30 °C for 24 hours. Yield 0.341 g, 52%.

^{1}H NMR ($CDCl_3$, 300MHz): δ 7.28 (pseudo-t, 1H, *p*-C_6H_5), 7.25 (pseudo-t, 2H, *m*-C_6H_5), 7.20 (d, *J*= 6 Hz, 2H, *o*-C_6H_5), 4.58 (s, 2H, $C_6H_5CH_2$), 3.39 (t, *J*= 6 Hz, 2H, NCH_2), 3.12 (pseudo-t, 4H, NCH_2), 3.00 (t, *J*= 6 Hz, 2H, NCH_2), 1.87 (pseudo-quint, 4H, NCH_2CH_2).

^{13}C NMR ($CDCl_3$, 125MHz): δ 151.4 (NCN_2), 139.3, 128.2, 127.7, 126.6 (C_6H_5), 51.1 ($C_6H_5CH_2$), 48.6, 44.6, 43.9 (NCH_2*), 23.2, 23.0 (NCH_2CH_2).

*one NCH_2 resonance not observed.

8.3.2 1,2-$(CH_2hpp)_2$-C_6H_4 (30)

One equivalent of NaH (0.069 g, 2.87 mmol.) was added to a solution of hppH (0.40 g, 2.87 mmol.) in THF (25 mL). The resulting suspension was heated to 60 °C and stirred for 2 hours. At room temperature, a solution of α,α'-dibromo-*o*-xylene (0.38 g, 1.44 mmol.) was added dropwise to the mixture and stirred for 18 hours. Following the removal of the volatiles *in vacuo.*, the resulting white precipitate was dissolved in toluene (10 mL), filtered through celite, and concentrated. Purification of the product **30** was performed by recrystallization through storage of the solution at -30 °C. Yield 0.256 g, 47%.

^{1}H NMR ($CDCl_3$, 300MHz): δ 7.22 (d, *J*= 9 Hz, 2H, *o*-C_6H_4), 7.18 (t, *J*= 6 Hz, 2H, *p*-C_6H_4), 4.59 (s, 4H, $C_6H_4CH_2$), 3.39 (t, *J*= 6 Hz, 4H, NCH_2), 3.24 (t, *J*= 6 Hz, 4H, NCH_2), 3.15 (t, *J*= 6 Hz, 4H, NCH_2), 2.95 (t, *J*= 5 Hz, 4H, NCH_2), 1.87 (pseudo-quint, 8H, NCH_2CH_2).

^{13}C NMR ($CDCl_3$, 125MHz): δ 151.3 (NCN_2), 138.0, 127.9, 126.8 (C_6H_4), 48.6 ($C_6H_4CH_2$), 48.5, 46.9, 44.6, 37.9 (NCH_2), 23.0, 22.8 (NCH_2CH_2).

8.3.3 1,3-$(CH_2hpp)_2$-C_6H_4 (31)

One equivalent of NaH (0.069 g, 2.87 mmol.) was added to a solution of hppH (0.40 g, 2.87 mmol.) in THF (25 mL). The resulting suspension was heated to 60 °C and stirred for 2 hours. At room temperature, a solution of α,α'-dibromo-*m*-xylene (0.38 g, 1.44 mmol.) was added dropwise to the mixture and stirred for 18 hours. Following the removal of the volatiles *in vacuo.*, the resulting off-white precipitate was dissolved in toluene (10 mL), filtered through celite, and

concentrated. Purification of the product **31** was performed by recrystallization through storage of the solution at -30 °C for 24 hours. Yield 0.343 g, 63%.

^{1}H NMR ($CDCl_3$, 500MHz): δ 7.20 (t, *J*= 5 Hz, 1H, *m*-C_6H_4), 7.14 (s, 1H, *o*-C_6H_4), 7.09 (d, *J*= 5 Hz, 2H, *p*-C_6H_4), 4.56 (s, 4H, $C_6H_4CH_2$), 3.39 (t, *J*= 5 Hz, 4H, NCH_2), 3.15 (t, *J*= 5 Hz, 4H, NCH_2), 3.10 (t, *J*= 5 Hz, 4H, NCH_2), 2.99 (t, *J*= 5 Hz, 4H, NCH_2), 1.86 (pseudo-quint, 8H, NCH_2CH_2).

^{13}C NMR ($CDCl_3$, 125MHz): δ 151.5 (NCN_2), 139.1, 128.2, 127.0, 126.0 (C_6H_4), 51.2 ($C_6H_4CH_2$), 48.6, 44.6, 43.8 (NCH_2*), 23.2, 22.9 (NCH_2CH_2).

*one NCH_2 resonance not observed

8.3.4 1,4-$(CH_2hpp)_2$-C_6H_4 (32)

One equivalent of NaH (0.069 g, 2.87 mmol.) was added to a solution of hppH (0.40 g, 2.87 mmol.) in THF (25 mL). The resulting suspension was heated to 60 °C and stirred for 2 hours. At room temperature, a solution of α,α'-dibromo-*p*-xylene (0.38 g, 1.44 mmol.) was added dropwise to the mixture and stirred for 18 hours. Following the removal of the volatiles *in vacuo.*, the resulting yellow precipitate was dissolved in toluene (10 mL), filtered through celite, and concentrated. Purification of the product **32** was performed by recrystallization through storage of the solution at -30 °C for 24 hours. Yield 0.461 g, 84%.

^{1}H NMR ($CDCl_3$, 300MHz): δ 7.20 (s, 4H, C_6H_4), 4.56 (s, 4H, $C_6H_4CH_2$), 3.41 (t, *J*= 6 Hz, 4H, NCH_2), 3.16 (t, *J*= 6 Hz, 4H, NCH_2), 3.10 (t, *J*= 6 Hz, 4H, NCH_2), 2.99 (t, *J*= 6 Hz, 4H, NCH_2), 1.86 (pseudo-quint, 8H, NCH_2CH_2).

^{13}C NMR ($CDCl_3$, 125MHz): δ 151.5 (NCN_2), 137.6, 127.7 (C_6H_4), 50.9 ($C_6H_4CH_2$), 48.7, 44.5, 43.9, (NCH_2*), 23.2, 23.0 (NCH_2CH_2).

*one NCH_2 resonance not observed.

8.3.5 1,3,5-$(CH_2hpp)_3$-C_6H_3 (33)

One equivalent of NaH (0.069 g, 2.87 mmol.) was added to a solution of hppH (0.40 g, 2.87 mmol.) in THF (25 mL). The resulting suspension was heated to 60 °C and stirred for 2 hours. At room temperature, a solution of 1,3,5-tris(bromomethyl)benzene (0.34 g, 0.96 mmol.) was added dropwise to the mixture and stirred for 18 hours. Following the removal of the volatiles *in vacuo*, the resulting white-brown precipitate was dissolved in toluene (10 mL), filtered through celite, and concentrated. Purification of the product was performed by recrystallization through storage of the product in a solution of toluene at -30 °C. Yield 0.223 g, 44%.

^{1}H NMR ($CDCl_3$, 500MHz): δ 6.96 (s, 3H, C_6H_3), 4.52 (s, 6H, $C_6H_3CH_2$), 3.37 (t, J= 5 Hz, 6H, NCH_2), 3.14 (t, J= 5 Hz, 6H, NCH_2), 3.09 (t, J= 5 Hz, 6H, NCH_2), 2.96 (t, J= 5 Hz, 6H, NCH_2), 1.84 (pseudo-quint, 12H, NCH_2CH_2).

^{13}C NMR ($CDCl_3$, 125MHz): δ 151.4 (NCN_2), 139.0, 125.4 (C_6H_3), 51.1 ($C_6H_3CH_2$), 48.7, 44.5, 43.8 (NCH_2*), 23.1, 22.9 (NCH_2CH_2).

*one NCH_2 resonance not observed.

8.3.6 2,4,6-$(CH_2hpp)_3$-mesitylene (34)

One equivalent of NaH (0.069 g, 2.87 mmol.) was added to a solution of hppH (0.40 g, 2.87 mmol.) in THF (25 mL). The resulting suspension was heated to 60 °C and stirred for 2 hours. At room temperature, a solution of 2,4,6-tris(bromomethyl)mesitylene (0.38 g, 0.96 mmol.) was added dropwise to the mixture and stirred for 18 hours. Following the removal of the volatiles *in vacuo*, the resulting yellow precipitate was dissolved in toluene (10 mL), filtered through celite, and concentrated. Purification of the product was performed by recrystallization through storage of the solution at -30 °C. Yield 0.377 g, 68%.

^{1}H NMR ($CDCl_3$, 500MHz): δ 4.61 (s, 6H, $C_6H_3CH_2$), 3.45 (t, J= 5 Hz, 6H, NCH_2), 3.16 (t, J= 5 Hz, 6H, NCH_2), 3.04 (t, J= 5 Hz, 6H, NCH_2), 2.72 (t, J= 5 Hz, 6H, NCH_2), 2.23 (s, 9H, $C_6(CH_3)_3$), 1.87 (quint, J= 5 Hz, 6H, CH_2NCH_2), 1.72 (quint, J= 5 Hz, 6H, CH_2NCH_2).

^{13}C NMR ($CDCl_3$, 125MHz): δ 151.6 (N*C*N_2), 138.4, 132.2 (*C*$_6$), 48.5, 48.3 (N*C*H_2), 45.7 (C_6*C*H_2), 43.2, 41.3 (N*C*H_2), 23.0, 22.8 (NCH_2*C*H_2), 16.5 (*C*H_3).

8.3.7 1,3,5-$(CH_2hpp)_3$-2,4,6-$(Et)_3$-C_6 (35)

One equivalent of NaH (0.069 g, 2.87 mmol.) was added to a solution of hppH (0.40 g, 2.87 mmol.) in THF (25 mL). The resulting suspension was heated to 60 °C and stirred for 2 hours. At room temperature, a solution of 1,3,5-tris(bromomethyl)-2,4,6-triethylbenzene (0.42 g, 0.96 mmol.) was added dropwise to the mixture and stirred for 18 hours. Following the removal of the volatiles *in vacuo*, the resulting pale yellow precipitate was dissolved in toluene (10 mL), filtered through celite, and concentrated. Purification of the product was performed by recrystallization through storage of the solution at -30 °C. Yield 0.361 g, 61%.

^{1}H NMR ($CDCl_3$, 500MHz): δ 4.58 (s, 6H, C_6CH_2), 3.45 (t, *J*= 5 Hz, 6H, N*CH*$_2$), 3.13 (t, *J*= 5 Hz, 6H, N*CH*$_2$), 3.01 (t, *J*= 5 Hz, 6H, N*CH*$_2$), 2.73 (t, *J*= 5 Hz, 6H, N*CH*$_2$), 2.68 (pseudo-q, 6H, C*H*$_2$), 1.86 (quint, *J*= 5 Hz, 6H, NCH_2CH_2), 1.69 (quint, *J*= 5 Hz, 6H, NCH_2CH_2), 1.10 (t, *J*= 5 Hz, 9H, C*H*$_3$).

^{13}C NMR ($CDCl_3$, 125MHz): δ 151.3 (N*C*N_2), 145.4, 129.0 (*C*$_6$), 48.6 (C_6*C*H_2), 48.3, 46.9, 41.9, 41.5 (N*C*H_2), 23.1 (NCH_2*C*H_2), 23.0 (*C*H_2CH_3), 22.8 (NCH_2*C*H_2), 16.0 (CH_2*C*H_3).

8.4 Tetraphenylborate Salts

8.4.1 $[1,2\text{-}(CH_2hppH)_2\text{-}C_6H_4][BPh_4]_2$ (30*a*)

Under air, two equivalents of a solution of triethylammonium tetraphenylborate (0.221 g, 0.53 mmol.) in THF (3 mL) was added to a solution of 1,2-$(CH_2hpp)_2$-C_6H_4 (**30**, 0.10 g, 0.26 mmol) in THF (3 mL). The resulting white mixture was stirred for 24 hours. Following the removal of the volatiles *in vacuo*, the resulting white powder was redissolved in acetonitrile (2 mL).

Recrystallization was performed via slow evaporation of the solvent yielding white crystals. Yield 0.249, 94%.

^{1}H NMR (CD_3CN, 300MHz): δ 7.43 (pseudo-d, 2H, *o*-C_6H_4), 7.21 (t, J= 6 Hz, 2H, *p*-C_6H_4), 7.36 (m br, 16H, *o*-C_6H_5), 7.08 (t, J= 6 Hz, 16H, *m*-C_6H_5), 6.93 (t, J= 6 Hz, 8H, *p*-C_6H_5), 4.40 (s, 2H, $C_6H_4CH_2$), 3.37 (pseudo-t, 8H, NCH_2), 3.21 (pseudo-t, 8H, NCH_2), 2.09 (quint, J= 6 Hz, 4H, NCH_2CH_2), 1.94 (quint, J= 6 Hz, 4H, NCH_2CH_2).

^{13}C NMR (CD_3CN, 125MHz): δ 163.8 (q, *i*-C_6H_5), 151.0 (NCN_2), 135.8, 132.0, 128.1, 125.6, 125.2, 121.8 (C_6H_4 and $B(C_6H_5)_4$), 50.2, ($C_6H_4CH_2$), 47.6, 47.1, 47.0, 38.7 (NCH_2), 20.5, 20.2 (NCH_2CH_2).

8.4.2 [1,4-(CH$_2$hppH)$_2$-C$_6$H$_4$][BPh$_4$]$_2$ (32*a*)

Under air, two equivalents of a solution of triethylammonium tetraphenylborate (0.221 g, 0.53 mmol.) in THF (3 mL) was added to a solution of 1,4-$(CH_2hpp)_2$-C_6H_4 (**32**, 0.10 g, 0.26 mmol) in THF (3 mL). The resulting white mixture was stirred for 24 hours. Following the removal of the volatiles *in vacuo.*, the resulting pink powder was redissolved in acetonitrile (2 mL). White crystals were obtained through storage of the solution at -30 °C. Yield 0.103 g, 39%.

Anal. Cacld. for $C_{70}H_{74}B_2N_6$ (*1020.97*): C, 82.34; H, 7.31; N, 8.25. **Found:** C, 80.56; H, 7.46; N, 8.25.

^{1}H NMR (CD_3CN, 300MHz): δ 7.27 (m br, 16H, *o*-C_6H_5), 7.24 (s, 4H, C_6H_4), 6.99 (t, J= 6 Hz, 16H, *m*-C_6H_5), 6.84 (t, J= 6 Hz, 8H, *p*-C_6H_5), 4.44 (s, 4H, $C_6H_4CH_2$), 3.29 (pseudo-t, 8H, NCH_2), 3.19 (pseudo-t, 8H, NCH_2), 1.94 (pseudo-quint, 8H, NCH_2CH_2).

^{13}C NMR (CD_3CN, 125MHz): δ 163.8 (q, *i*-C_6H_5), 151.2 (NCN_2), 135.8, 134.6, 127.2, 125.6, 121.8 (C_6H_4 and $B(C_6H_5)_4$), 52.5, ($C_6H_4CH_2$), 47.6, 47.2, 46.6, 38.5 (NCH_2), 20.4, 20.2 (NCH_2CH_2).

8.4.3 [1,3,5-(CH$_2$hppH)$_3$-C$_6$H$_3$][BPh$_4$]$_3$ (**33*a***)

Under air, three equivalents of a solution of triethylammonium tetraphenylborate (0.237 g, 0.56 mmol.) in THF (3 mL) were added to a solution of 1,3,5-(CH$_2$hpp)$_3$-C$_6$H$_3$ (**33**, 0.10 g, 0.19 mmol.) in THF (3 mL). The resulting white mixture was stirred for 24 hours. The removal of the volatiles *in vacuo.* yielded a white powder. White crystals were obtained through storage of the product in a solution of dichloromethane (2 mL) at -30 °C, but were unsuitable for crystallographic analysis. Yield 0.252 g, 89%.

^{1}H NMR (CD$_3$CN, 500MHz): δ 7.26 (m br, 24H, *o*-C$_6$*H*$_5$), 7.02 (t, *J*= 5 Hz, 24H, *m*-C$_6$*H*$_5$), 6.86 (t, *J*= 10 Hz, 12H, *p*-C$_6$*H*$_5$), 6.42 (s, 3H, C$_6$*H*$_3$), 4.44 (s, 6H, C$_6$H$_3$C*H*$_2$), 3.32 (pseudo-t, 12H, NC*H*$_2$), 3.28 (t, *J*= 5 Hz, 6H, NC*H*$_2$), 3.23 (t, *J*= 5 Hz, 6H, NC*H*$_2$), 1.93 (pseudo-quint, 12H, NCH$_2$C*H*$_2$).

^{13}C NMR (CD$_3$CN, 125MHz): δ 163.8 (q, *i*-*C*$_6$H$_5$), 151.0 (N*C*N$_2$), 136.6, 135.7, 125.6, 124.8, 121.8 (*C*$_6$H$_3$ and B(*C*$_6$H$_5$)$_4$), 52.3 (C$_6$H$_3$*C*H$_2$), 47.7, 47.2, 46.6, 38.6 (N*C*H$_2$), 20.5, 20.3 (NCH$_2$*C*H$_2$).

8.4.4 [1,3,5-(CH$_2$hppH)$_3$-2,4,6-(Et)$_3$-C$_6$][BPh$_4$]$_3$ (**35*a***)

Under air, three equivalents of a solution of triethylammonium tetraphenylborate (0.201 g, 0.48 mmol.) in THF (3 mL) were added to a solution of 1,3,5-(CH$_2$hpp)$_3$-2,4,6-(Et)$_3$-C$_6$ (**35**, 0.10 g, 0.16 mmol.) in THF (3 mL). The resulting white mixture was stirred for 24 hours. The removal of the volatiles *in vacuo.* yielded a white powder. White crystals were obtained through storage of the product in a solution of dichloromethane (2 mL) at -30 °C, but were unsuitable for crystallographic analysis. Yield 0.206 g, 82%.

^{1}H NMR (CD$_3$CN, 500MHz): δ 7.31 (m br, 24H, *o*-C$_6$*H*$_5$), 7.03 (t, *J*= 10 Hz, 24H, *m*-C$_6$*H*$_5$), 6.88 (t, *J*= 15 Hz, 12H, *p*-C$_6$*H*$_5$), 4.39 (s, 6H, C$_6$C*H*$_2$), 3.35 (t, *J*= 5 Hz, 6H, NC*H*$_2$), 3.28 (t, *J*= 5 Hz, 6H, NC*H*$_2$), 3.14 (t, *J*= 5 Hz, 6H, NC*H*$_2$), 2.68 (t, *J*= 5 Hz, 6H, NC*H*$_2$), 2.59 (q, *J*= 5 Hz, 6H, C*H*$_2$), 1.95 (pseudo-quint, 6H, NCH$_2$C*H*$_2$), 1.71 (quint, *J*= 5 Hz, 6H, NCH$_2$C*H*$_2$), 1.17 (t, *J*= 5 Hz, 9H, C*H*$_3$).

^{13}C NMR (CD_3CN, 125MHz): δ 164.4, 164.0, 163.6, 163.2 (C—B), 151.4 (N*C*N_2), 147.4, 128.4 (*C*$_6$), 135.7, 125.6, 121.8 (*C*$_6H_5$), 47.6, 47.0 (N*C*H_2), 45.2 (C_6*C*H_2), 41.4, 38.7 (N*C*H_2), 22.7 (*C*H_2CH_3), 20.8, 20.3 (NCH_2*C*H_2), 14.6 (CH_2*C*H_3).

8.5 Hydrochloride Salts

8.5.1 [Ph(CH$_2$hppH)][Cl] (29*b*)

Under air, one equivalent of a solution of triethylamine hydrochloride (0.060 g, 0.44 mmol.) in acetonitrile (3 mL) was added to a solution of one equivalent of Ph(CH_2hpp) (**29**, 0.10 g, 0.44 mmol.) in acetonitrile (3 mL). The resulting solution was stirred under air for one hour. The removal of the volatiles via slow evaporation at room temperature yielded a colorless oil. White crystals were obtained through storage of the product in a solution of dichloromethane (1.5 mL) at -30 °C, but were unsuitable for crystallographic analysis. Yield 0.101 g, 76%.

^{1}H NMR ($CDCl_3$, 300MHz): δ 9.64 (br s, 1H, N*H*), 7.31 (s, 1H, *p*-C_6H_5), 7.27 (pseudo-t, 2H, *m*-C_6H_5*) 4.93 (s, 2H, $C_6H_5CH_2$), 3.51 (t, J= 6 Hz, 2H, NCH_2), 3.31 (pseudo-t, 6H, NCH_2), 1.98 (pseudo-quint, 4H, NCH_2CH_2).

*o-C_6H_5 not observed due to significant overlap

^{13}C NMR ($CDCl_3$, 125MHz): δ 150.9 (N*C*N_2), 134.9, 128.8, 128.1, 128.0 (*C*$_6H_5$), 53.7 (C_6H_5*C*H_2), 48.3, 47.5, 45.5, 38.6 (N*C*H_2), 21.1, 20.7 (NCH_2*C*H_2).

8.5.2 [1,2-(CH$_2$hppH)$_2$-C$_6$H$_4$][Cl]$_2$ (30*b*)

Under air, one equivalent of a solution of triethylamine hydrochloride (0.036 g, 0.26 mmol.) in acetonitrile (5 mL) was added to a solution of one equivalent of 1,2-$(CH_2hpp)_2$-C_6H_4 (**30**, 0.10 g, 0.26 mmol.) in acetonitrile (5 mL). The resulting solution was stirred under air for one hour. The removal of the volatiles via slow evaporation at room temperature yielded a yellow oil. ^{1}H NMR analysis of the crude product indicated successful protonation of both hpp-

functionalities. The resulting product was dissolved in acetonitrile (2 mL), and subsequent storage of the solution at -30 °C yielded white crystals. Single crystal X-ray diffraction performed on an isolated crystal indicated the successful formation of the desired salt.
Yield 0.058 g, 82% (crystallized yield).

^{1}H NMR ($CDCl_3$, 300MHz): δ 7.32 (pseudo-d, 2H, *o*-C_6H_4), 7.30 (pseudo-t, 2H, *p*-C_6H_4), 4.93 (s, 4H, $C_6H_3CH_2$), 3.36 (t, J= 6 Hz, 4H, NCH_2), 3.25 (t, J= 6 Hz, 4H, NCH_2), 3.21 (pseudo-t, 8H, NCH_2), 1.98 (pseudo-quint, 8H, NCH_2CH_2). **m*-C_6H_4 not observed due to significant overlap

^{13}C NMR spectrum not obtained due to degradation of the product when heated to force into solution

8.5.3 [1,3-$(CH_2hppH)_2$-C_6H_4][Cl]$_2$ (**31*b***)

Under air, one equivalent of a solution of triethylamine hydrochloride (0.036 g, 0.26 mmol.) in acetonitrile (3 mL) was added to a solution of one equivalent of 1,3-$(CH_2hpp)_2$-C_6H_4 (**31**, 0.10 g, 0.26 mmol.) in acetonitrile (3 mL). The resulting solution was stirred under air for one hour. The removal of the volatiles via slow evaporation at room temperature yielded a colorless oil. The resulting product was dissolved in acetonitrile (2 mL), and subsequent storage of the solution at -30 °C afforded white crystals, though they were unsuitable for crystallographic analysis. Yield 0.049 g, 42%.

^{1}H NMR ($CDCl_3$, 300MHz): δ 7.51 (s, 1H, *o*-C_6H_4), 7.26 (pseudo-t, 2H, *p*-C_6H_4), 7.17 (d, J= 9 Hz, 1H, *m*-C_6H_4), 4.83 (s, 4H, $C_6H_4CH_2$), 3.52 (t, J= 6 Hz, 4H, NCH_2), 3.34 (pseudo-t, 8H, NCH_2), 3.24 (t, J= 6 Hz, 4H, NCH_2), 1.98 (pseudo-quint, 8H, NCH_2CH_2).

^{13}C NMR ($CDCl_3$, 125MHz): δ 150.8 (NCN_2), 136.2, 128.6, 128.5, 127.9 (C_6H_4), 53.5 ($C_6H_4CH_2$), 48.3, 47.6, 45.8, 38.9 (NCH_2), 21.2, 21.0 (NCH_2CH_2).

8.5.4 [1,4-(CH_2hppH)$_2$-C_6H_4][Cl]$_2$ (**32*b***)

Under air, one equivalent of a solution of triethylamine hydrochloride (0.036 g, 0.26 mmol.) in acetonitrile (3 mL) was added to a solution of one equivalent of 1,4-(CH_2hpp)$_2$-C_6H_4 (**32**, 0.10 g, 0.26 mmol.) in acetonitrile (3 mL). The resulting solution was stirred under air for one hour. The removal of the volatiles via slow evaporation at room temperature yielded a yellow oil. The resulting product was dissolved in acetonitrile (2 mL), and subsequent removal of the solvent via slow evaporation at room temperature yielded both a yellow oil and yellow crystals. Single crystal X-ray diffraction performed on the resulting crystals indicated the successful formation of the desired salt. Yield 0.051 g, 86% (crystallized yield, calculated using triethylamine hydrochloride as limiting reagent).

^{1}H NMR ($CDCl_3$, 300MHz): δ 7.30 (s, 4H, C_6H_4), 4.87 (s, 4H, $C_6H_4CH_2$), 3.50 (t, J= 6 Hz, 4H, NCH_2), 3.29 (pseudo-t, 12H, NCH_2), 1.97 (pseudo-quint, 8H, NCH_2CH_2).

^{13}C NMR ($CDCl_3$, 125MHz): δ 150.7 (NCN_2), 135.1, 128.5 (C_6H_4), 53.5 ($C_6H_4CH_2$), 48.4, 47.6, 45.7, 39.0 (NCH_2), 21.3, 21.0 (NCH_2CH_2).

8.5.5 [2,4,6-(CH_2hppH)$_3$-mesitylene][Cl]$_3$ (**34*b***)

Under air, three equivalents of a solution of triethylamine hydrochloride (0.072 g, 0.52 mmol.) in acetonitrile (5 mL) were added to a solution of one equivalent of 2,4,6-(CH_2hpp)$_3$-mesitylene (**34**, 0.10 g, 0.17 mmol.) in acetonitrile (5 mL). The resulting solution was stirred under air for one hour. The removal of the volatiles via slow evaporation at room temperature yielded a colorless oil. The resulting product was dissolved into acetonitrile (2 mL). Recrystallization was attempted through both slow evaporation of the solvent at room temperature, and through storage of the solution at -30 °C. No crystalline product was obtained. Yield 0.108 g, 93%.

^{1}H NMR ($CDCl_3$, 500MHz): δ 9.48 (br s, 3H, N*H*), 4.92 (s, 6H, $C_6H_3CH_2$), 3.56 (pseudo-t, 6H, NCH_2), 3.39 (t, J= 5 Hz, 6H, NCH_2), 3.30 (t, J= 5 Hz, 6H, NCH_2), 2.84 (t, J= 5 Hz, 6H, NCH_2), 2.27 (s, 9H, $C_6(CH_3)_3$), 1.92 (pseudo-t, 12H, CH_2NCH_2).

^{13}C NMR ($CDCl_3$, 125MHz): δ 151.3 (NCN_2), 140.2, 130.1 (C_6H_4), 48.3, 47.5 (NCH_2), 45.8 (C_6CH_2), 41.5, 38.7 (NCH_2), 21.4, 20.8 (NCH_2CH_2), 17.0 (CH_3).

8.5.6 [1,3,5-(CH_2hppH)$_3$-2,4,6-(Et)$_3$-C_6][Cl]$_3$ (**35*b***)

Under air, three equivalents of a solution of triethylamine hydrochloride (0.067 g, 0.49 mmol.) in acetonitrile (3 mL) were added to a solution of one equivalent of 1,3,5-(CH_2hpp)$_3$-2,4,6-(Et)$_3$-C_6 (**35**, 0.10 g, 0.16 mmol.) in acetonitrile (3 mL). The resulting solution was stirred under air for one hour. The removal of the volatiles via slow evaporation at room temperature yielded a colorless oil. The resulting product was dissolved into acetonitrile (2 mL). Recrystallization was attempted through both slow evaporation of the solvent at room temperature, and through storage of the solution at -30 °C. No crystalline product was obtained. Yield 0.103 g, 89%.

^{1}H NMR ($CDCl_3$, 300MHz): δ 4.79 (s, 6H, C_6CH_2), 3.55 (t, J= 6 Hz, 6H, NCH_2), 3.37 (t, J= 6 Hz, 6H, NCH_2), 3.27 (t, J= 6 Hz, 6H, NCH_2), 2.87 (t, J= 6 Hz, 6H, NCH_2), 2.50 (pseudo-q, 6H, CH_2), 2.03 (pseudo-quint, 6H, NCH_2CH_2), 1.08 (t, J= 5 Hz, 9H, CH_3).

*NCH_2CH_2 peak not observed due to significant overlap with HOD peak (δ_H 2.00 ppm)

^{13}C NMR ($CDCl_3$, 125MHz): δ 151.2 (NCN_2), 147.0 (C_6*), 48.1 (C_6CH_2), 47.7, 47.0, 42.1, 38.7 (NCH_2), 23.6, 21.5 (NCH_2CH_2), 20.7 (CH_2CH_3), 15.0 (CH_2CH_3).

*one C_6 resonance not observed

8.6 Bicarbonate and Carbonate Salts

8.6.1 [Ph(CH_2hppH)][HCO_3] (**29*c***)

In solution, 0.1 equivalents of benzoic acid (0.005 g, 0.044 mmol) in a solution of acetonitrile (2 mL) was added dropwise to a solution of Ph(CH_2hpp) (**29**, 0.10 g, 0.44 mmol) in acetonitrile (3 mL). The solution was stirred for one hour, and the volatiles were removed via slow evaporation at room temperature, yielding a yellow oil. Fine yellow crystals were obtained through storage of the product in a solution of acetonitrile (2 mL) at -30 °C, but were unsuitable for crystallographic analysis. Yield 0.11 g, 88%.

^{1}H NMR ($CDCl_3$, 300MHz): δ 7.29 (pseudo-t, 1H, *p*-C_6H_5), 7.25 (pseudo-t, 2H, *m*-C_6H_5), 7.21 (d, *J*= 6 Hz, 2H, *o*-C_6H_5), 4.63 (s, 2H, $C_6H_5CH_2$), 3.41 (t, *J*= 6 Hz, 2H, NCH_2), 3.16 (pseudo-t, 4H, NCH_2), 3.05 (t, *J*= 6 Hz, 2H, NCH_2), 1.89 (pseudo-quint, 4H, NCH_2CH_2).

^{13}C NMR ($CDCl_3$, 125MHz): δ 151.5 (NCN_2), 129.4, 128.5, 127.9, 127.2 (C_6H_5), 52.2 ($C_6H_5CH_2$), 48.5, 48.1, 44.9, 41.5 (NCH_2), 22.2, 22.1 (NCH_2CH_2).

* HCO_3 resonance not observed

8.6.2 [1,3-$(CH_2hppH)_2$-C_6H_4][HCO_3]$_2$ (31*c*)

Under air, 0.1 equivalents of benzoic acid (0.003 g, 0.026 mmol.) in a solution of acetonitrile (2 mL) was added dropwise to a solution of 1,3-$(CH_2hpp)_2$-C_6H_4 (**31**, 0.10 g, 0.26 mmol.) in acetonitrile (3 mL). The solution was then stirred for one hour, and the volatiles were removed via slow evaporation at room temperature, yielding a colorless oil. White crystals were obtained through storage of the product in a solution of acetonitrile (2 mL) at -30 °C, but were unsuitable for crystallographic analysis. Yield 0.056 g, 38%.

^{1}H NMR ($CDCl_3$, 500MHz): δ 7.22 (t, *J*= 10 Hz, 1H, *m*-C_6H_4), 7.16 (s, 1H, *o*-C_6H_4), 7.11 (d, *J*= 10 Hz, 2H, *p*-C_6H_5), 5.19 (br s, 2H, N*H*), 4.60 (s, 4H, $C_6H_5CH_2$), 3.40 (t, *J*= 5 Hz, 4H, NCH_2), 3.18 (t, *J*= 5 Hz, 4H, NCH_2), 3.13 (t, *J*= 5 Hz, 4H, NCH_2), 3.03 (t, *J*= 5 Hz, 4H, NCH_2), 1.88 (pseudo-quint, 8H, NCH_2CH_2).

^{13}C NMR ($CDCl_3$, 125MHz): δ 151.3 (NCN_2), 138.2, 129.3, 128.4, 127.4, 127.3, 126.5 (C_6H_4), 51.9 ($C_6H_4CH_2$), 48.6, 48.2, 44.9, 42.1 (NCH_2), 22.4, 22.3 (NCH_2CH_2).

* HCO_3 resonance not observed

8.6.3 [1,3,5-$(CH_2hppH)_3$-2,4,6-$(Et)_3$-C_6][HCO_3]$_3$ (35*c*)

Under air, 0.3 equivalents of benzoic acid (0.006 g, 0.05 mmol.) in a solution of acetonitrile (2 mL) was added dropwise to a solution of 1,3,5-$(CH_2hpp)_3$-2,4,6-$(Et)_3$-C_6 (**35**, 0.10 g, 0.16 mmol.) in acetonitrile (3 mL). The solution was then stirred for one hour, and the volatiles were removed via slow evaporation at room temperature, yielding a colorless oil. White crystals of

35*c* were obtained through storage of the product in a solution of acetonitrile (2 mL) at -30 °C, but were unsuitable for full crystallographic analysis. Yield 0.092 g, 71%.

^{1}H NMR ($CDCl_3$, 300MHz): δ 4.66 (s, 6H, C_6CH_2), 3.48 (t, J= 6 Hz, 6H, NCH_2), 3.17 (t, J= 6 Hz, 6H, NCH_2), 3.06 (t, J= 6 Hz, 6H, NCH_2), 2.76 (t, J= 6 Hz, 6H, NCH_2), 2.68 (pseudo-q, 6H, CH_2), 1,89 (pseudo-quint, 6H, NCH_2CH_2), 1.76 (pseudo-quint, 6H, NCH_2CH_2), 1.12 (t, J= 9 Hz, 9H, CH_3).

^{13}C NMR ($CDCl_3$, 125MHz): δ 151.0 (NCN_2), 146.6 (C_6*), 48.3 (C_6CH_2), 47.8, 46.8, 42.0, 37.7 (NCH_2), 23.6 (NCH_2CH_2), 21.8 (CH_2CH_3), 20.7 (NCH_2CH_2), 15.3 (CH_2CH_3).

*one C_6 resonance and HCO_3 resonance not observed

8.6.4 [1,4-(CH$_2$hppH)$_2$-C$_6$H$_4$][HCO$_3$]$_2$ (32*c*)

The bicarbonate salt [1,4-$(CH_2hpp)_2$-C_6H_4][HCO_3]$_2$ (**32*c***) was produced through a variety of methods in the attempts to optimize the reaction conditions. These conditions are outlined in Table **8.1**, and include the reagent identity, reagent quantity, reaction time, and supplementary conditions for each reaction. As the ^{1}H NMR spectral evidence collected for each reaction method varied, the ^{1}H NMR spectral data for each method is listed below. ^{13}C NMR remained consistent among the reactions producing the bicarbonate product **32*c*** (methods 1, 4, 5, 6 and 8). Reaction conditions in method 7 resulted in the formation of hydrochloride salt **32*b***, and spectral data is not listed below. Reaction conditions in method 9 resulted in the formation of [1,4-$(CH_2hppH)_2$-C_6H_4][HCO_3][$PhCO_2$]. ^{13}C NMR values for this compounds is also listed below.

Each reaction was performed under air. In solution, a quantity of protonation source ($[H]^+$ source) in a solution of acetonitrile (2 mL) was added dropwise to a solution of 1,4-$(CH_2hpp)_2$-C_6H_4 (**32**, 0.10 g, 0.26 mmol.) in acetonitrile (3 mL). The solution was then stirred for variable amounts of time, and the volatiles were removed via slow evaporation at room temperature, leaving a yellow oil product. Recrystallization attempts were performed through storage of the product in a solution of acetonitrile (2 mL) at -30 °C and slow evaporation of the solvent at room temperature.

Table 8.1: Reaction conditions in the optimization of **32*c*** synthesis

Method	$[H]^+$ Source	Equivalents of $[H]^+$	$[H]^+$ quantity	Stirring time (h)	Additional reaction conditions
Method One	Triethylamine hydrochloride	0.5 equiv.	0.018 g, 0.13 mmol	0.5 h	No additional conditions
Method Two	No protonation source	n/a	n/a	24 h	No additional conditions
Method Three	No protonation source	n/a	n/a	24 h	Additional H_2O introduced to the reaction system‡
Method Four	Triethylamine hydrochloride	0.1 equiv.	0.004 g, 0.026 mmol.	0.5 h	No additional conditions
Method Five	Triethylamine hydrochloride	0.1 equiv.	0.004 g, 0.026 mmol.	4 h	Additional H_2O and CO_2† introduced to the reaction system
Method Six	Triethylamine hydrochloride	0.2 equiv.	0.007 g, 0.053 mmol.	0.5 h	No additional conditions
Method Seven	Triethylamine hydrochloride	2 equiv.	0.072 g, 0.53 mmol.	4 h	Additional CO_2† introduced to the reaction system
Method Eight	Benzoic Acid	0.1 equiv.	0.003 g, 0.026 mmol.	1 h	No additional conditions
Method Nine	Benzoic Acid	1 equiv.	0.032 g, 0.26 mmol.	1 h	No additional conditions

† CO_2 bubbled continuously for duration of stirring
‡ 5 mol % distilled H_2O added to reaction

^{13}C NMR ($CDCl_3$, 125MHz): δ 151.4 (N*C*N), 136.4, 128.1 (*C*$_6H_4$), 52.0 (C_6H_4*C*H_2), 48.5, 48.1, 45.0, 41.6 (N*C*H_2), 22.2, 21.9 (NCH_2*C*H_2).

*H*C*O$_3$ resonance not observed.

Method One

^{1}H NMR ($CDCl_3$, 300MHz): δ 7.24 (s, 4H, C_6*H*$_4$), 4.74 (s, 4H, C_6H_4C*H*$_2$), 3.45 (t, *J*= 6 Hz, 4H, NC*H*$_2$), 3.23 (pseudo-t, 8H, NC*H*$_2$), 3.14 (t, *J*= 6 Hz, 4H, NC*H*$_2$), 1.94 (pseudo-quint, 8H, NCH_2C*H*$_2$).

Method Two

^{1}H NMR ($CDCl_3$, 300MHz): δ 7.29 (s, 4H, C_6*H*$_4$), 4.59 (s, 4H, C_6H_4C*H*$_2$), 3.39 (t, *J*= 6 Hz, 4H, NC*H*$_2$), 3.14 (pseudo-t, 8H, NC*H*$_2$), 3.02 (t, *J*= 6 Hz, 4H, NC*H*$_2$), 1.89 (pseudo-quint, 8H, NCH_2C*H*$_2$).

Method Three

^{1}H NMR ($CDCl_3$, 300MHz): δ 7.19 (s, 4H, C_6H_4), 4.58 (s, 4H, $C_6H_4CH_2$), 3.40 (t, *J*= 6 Hz, 4H, NCH_2), 3.15 (pseudo-t, 8H, NCH_2), 3.03 (t, *J*= 6 Hz, 4H, NCH_2), 1.88 (pseudo-quint, 8H, NCH_2CH_2).

Method Four

^{1}H NMR ($CDCl_3$, 300MHz): δ 7.20 (s, 4H, C_6H_4), 4.63 (s, 4H, $C_6H_4CH_2$), 3.45 (t, *J*= 3 Hz, 4H, NCH_2), 3.17 (pseudo-t, 8H, NCH_2), 3.05 (t, *J*= 6 Hz, 4H, NCH_2), 1.89 (pseudo-quint, 8H, NCH_2CH_2).

Method Five

^{1}H NMR ($CDCl_3$, 300MHz): δ 7.21 (s, 4H, C_6H_4), 4.63 (s, 4H, $C_6H_4CH_2$), 3.42 (t, *J*= 6 Hz, 4H, NCH_2), 3.17 (pseudo-t, 8H, NCH_2), 3.07 (t, *J*= 6 Hz, 4H, NCH_2), 1.89 (pseudo-quint, 8H, NCH_2CH_2).

Method Six

^{1}H NMR ($CDCl_3$, 300MHz): δ 7.24 (s, 4H, C_6H_4), 4.73 (s, 4H, $C_6H_4CH_2$), 3.46 (t, *J*= 6 Hz, 4H, NCH_2), 3.23 (pseudo-t, 8H, NCH_2), 3.13 (t, *J*= 6 Hz, 4H, NCH_2), 1.93 (pseudo-quint, 8H, NCH_2CH_2).

Method Eight

^{1}H NMR ($CDCl_3$, 300MHz): δ 7.18 (s, 4H, C_6H_4), 4.57 (s, 4H, $C_6H_4CH_2$), 3.39 (t, *J*= 6 Hz, 4H, NCH_2), 3.13 (pseudo-t, 8H, NCH_2), 3.01 (t, *J*= 6 Hz, 4H, NCH_2), 1.87 (pseudo-quint, 8H, NCH_2CH_2).

Method Nine : $[1,4\text{-}(CH_2hppH)_2\text{-}C_6H_4][HCO_3][PhCO_2]$

^{1}H NMR ($CDCl_3$, 300MHz): δ 8.01 (d, *J*= 6 Hz, 2H, *o*-C_6H_5), 7.28 (t, *J*= 6 Hz, 2H, *m*-C_6H_5), 7.23 (s, 4H, C_6H_4), 4.82 (s, 4H, $C_6H_4CH_2$), 3.51 (t, *J*= 6 Hz, 4H, NCH_2), 3.27 (t, *J*= 6 Hz, 4H, NCH_2), 3.20 (t, *J*= 6 Hz, 4H, NCH_2), 3.12 (t, *J*= 6 Hz, 4H, NCH_2), 1.88 (pseudo-quint, 8H, NCH_2CH_2).

* *p*-C_6H_5 resonance not observed due to overlap.

^{13}C NMR ($CDCl_3$, 125MHz): δ 172.2 (CO_2), 151.2, 139.3, 129.9, 129.0, 128.4, 127.3 (C_6H_4 and C_6H_5), 52.7 ($C_6H_4CH_2$), 48.5, 47.7, 45.3 (NCH_2*), 21.5, 21.3 (NCH_2CH_2).

*HCO_3 resonance and one NCH_2 resonance not observed.

8.6.5 $[hppH_2]_2[CO_3]$ (**1*d***)

Under air, 0.1 equivalents of benzoic acid (0.009 g, 0.072 mmol.) in acetonitrile (2 mL) was added dropwise to a solution of sublimed hppH (**1**, 0.10 g, 0.72 mmol.) in acetonitrile (3 mL). The resulting colorless solution was stirred for one hour, and the volatiles removed via slow evaporation at room temperature. White crystals of **1*d*** were obtained through storage of the crude product in a solution of acetonitrile (2 mL). Yield 0.084 g, 69%.

Anal. Cacld. for $C_{15}H_{40}N_6O_9$ (*448.51*): C, 40.17; H, 8.99; N, 18.74. **Found:** C, 42.48; H, 8.81; N, 18.62.

^{1}H NMR ($CDCl_3$, 500MHz): δ 3.28 (t, *J*= 5 Hz, 8H, NCH_2), 3.24 (t, *J*= 5 Hz, 8H, NCH_2), 1.96 (quint, *J*= 5 Hz, 8H, NCH_2CH_2).

^{13}C NMR ($CDCl_3$, 125MHz): δ 163.2 (HCO_3), 151.4 (NCN_3), 46.9, 37.6 (NCH_2), 20.9 (NCH_2CH_2).

8.6.6 $[hppH_2][HCO_3]$ (**1*c***)

Under air, 161 μL of distilled water (5 mol %, 0.009 mmol.) was added to a solution of previously synthesized $[hppH_2]_2[CO_3]$ (**1*d***, 25 mg, 0.18 mmol.) in acetonitrile (3 mL). The resulting colorless solution was stirred under air for 1 h, and the volatiles removed via slow evaporation at room temperature. White crystals were obtained through storage of the crude product in a solution of acetonitrile (2 mL) at -30 °C. Yield 0.029 g, 83%.

^{1}H NMR ($CDCl_3$, 300MHz): δ 3.28 (pseudo-t, 8H, NCH_2), 1.98 (quint, *J*= 6 Hz, 4H, NCH_2CH_2).

^{13}C NMR ($CDCl_3$, 125MHz): δ 162.1 (HCO_3), 151.3 (NCN_3), 46.9, 37.6 (NCH_2), 20.9 (NCH_2CH_2).

References

[1] Bates, E.; Mayton, R.; Ntai, I.; Davis, J., *J. Am. Chem. Soc.,* **2002**, *124*, 926.

[2] Liu, Q.; Wu, L.; Jackstell, R.; Beller, M., *Nat. Commun.,* **2015**, *6*, 5933.

[3] Rochelle, G., *Science,* **2009**, *325*, 1652.

[4] Dai, S.; Li, H.; Wang, C.; Luo, H.; Jiang, D., *Angew. Chem. Int. Ed.,* **2010**, *122*, 6114.

[5] Dupont, J.; de Souza, R.; Suarez, P., *Chem. Rev.,* **2002**, *102*, 3667.

[6] Bates, E.; Mayton, R.; Ntai, I.; Davis, J., *J. Am. Chem. Soc.,* **2002**, *124*, 926.

[7] Gurau, G.; Rodriguez, H.; Kelley, P.; Janiczek, P.; Kalb, R.; Rogers, R., *Angew. Chem. Int. Ed.,* **2011**, *123*, 12230.

[8] Wang, C.; Luo, X.; Guo, Y.; Ding, F.; Zhao, H.; Cui, G.; Li, H., *Angew. Chem. Int. Ed.,* **2014**, *53*, 7053.

[9] Villers, C., Dognon, J.; Pollet, R.; Thuéry, P.; Ephritikhine, M., *Agnew. Chem. Int. Ed.,* **2010**, *49*, 3465.

[10] González, E.; Pereira, F.; Agostini, D.; Santo, R.; deAzevedo, E.; Bonagama, T.; Job, A., *Green Chem.,* **2011**, *13*, 2146.

[11] Franco, D., Pérez, E.; Santos, R.; Gambardella, M.; de Macedo, L.; Rodrigues-Filho, U.; Launay, J., *J. Am. Chem. Soc.,* **2004**, *69*, 8005.

[12] González, E.; Pereira, F., deAzevedo, E.; Silva, E.; Bonagamba, T.; Agostíni, D.; Magalhães, A.; Job, A., *Tetrahedron,* **2008**, *64*, 10097.

[13] Coles, M. P.; Khalaf, M.; Oakley, S.; Hitchcock, P., *CrystEngComm,* **2008**, *10*, 1653.

[14] Wang, C.; Luo, H.; Luo, X.; Dai, S., *Green Chem.,* **2010**, *12*, 2019.

[15] He, L.; Zhang, S., *Aust. J. Chem.,* **2014**, *67*, 980.

[16] Coles, M. P.; Aragón-Sáez, P.; Oakley, S.; Hitchcock, P.; Davidson, M.; Maksić, Z.; Vianello, R.; Leito, I.; Kaljurand, I.; Apperley, D., *J. Am. Chem. Soc.,* **2009**, *131*, 16858.

[17] Sakakura, T.; Choi, J.; Saito, Y.; Masuda, T.; Sako, T.; Oriyama, T., *J. Org. Chem.,* **1999**, *64*, 4506.

[18] Coles, M. P., *Dalton Trans*, **2006**, 985.

[19] Cotton, F.; Murillo, C.; Wang, X.; Wilkinson, C., *Inorg. Chem.,* **2006**, *45*, 5493.

[20] Seipp, C.; Williams, N.; Kidder, M.; Custelcean, R., *Angew. Chem. Int. Ed.,* **2017**, *55*, 1024.

[21] Custelcean, R.; Williams, N.; Seipp, C., *Angew. Chem. Int. Ed.,* **2015**, *54*, 10525.

[22] Custelcean, R.; Williams, N.; Seipp, A.; Ivanov, A.; Bryantsev, V., *Chem. Eur. J.,* **2016**, *22*, 1997.

[23] Schwamm, R., Unpublished results.

[24] Bailey, P.; Pace, S.; *Coord. Chem. Rev.,* **2001**, *214*, 91.

[25] Aeilts, S.; Coles, M.; Jordan, R.; Swenson, D.; Young, V., *Organometallics*, **1998**, *17*, 3265

[26] Raczyńska, E.; Cyrański, M.; Gutowski, M.; Rak, J.; Gal, J.; Maria, P.; Darowska, M.; Duczmal, K., *J. Phys. Org. Chem.,* **2003**, *16*, 91.

[27] Häfelinger, G.; Kuske, H., *The Chemistry of Amidines and Imidates*, Wiley, Cichester, **1991**.

[28] Coles, M. P.; Hitchcock, P., *Organometallics,* **2003**, *22*, 5201.

[29] Khalaf, M.; Coles, M. P.; Hitchcock, P, *Dalton Trans.,* **2008**, 4288.

[30] Maksić, Z.; Kovačević, B., *J. Chem. Soc., Perkin Trans. 2,* **1999**, 2623.

[31] Raab, V.; Gauchenova, E.; Merkoulov, A; Harms, K.; Sundermeyer, J.; Kovačević, B.; Maksić, Z., *J . Org. Chem.,* **2003**, *8*, 8790.

[32] Himmel, H.; Wild, U.; Roquette, P.; Kaifer, E.; Mautz, J.; Hübner, O.; Wadepohl, H., *Eur. J. Inorg. Chem.,* **2008**, 1248.

[33] Huang, W.; Mi, Y.; Li, Y.; Zheng, D., *Ind. Eng. Chem. Res.,* **2015**, *54*, 3430.

[34] Kortunov., P.; Baugh, L.; Calabro, D.; Siskin, M.; Kamakoti, P.; Li, Q.; Peiffer, D., CA 2810519, **2012**.

[35] Rajamanickam, R.; Kim, H.; Park, J., *Sci. Rep.*, **2015**, *5*, 10688

[36] Oakley, S.; Soria, D.; Coles, M.; Hitchcock, P., *Dalton Trans.,* **2004**, 537.

[37] Coles, M. P.; Lee, S.; Oakley, S.; Estiu, G.; Hitchcock, P., *Org. Biomol. Chem.,* **2007**, *5*, 3909.

[38] Fernandez-Alvarez, F.; Aitani, A.; Oro, L., *Catal. Sci. Tech.*, **2014**, *4*, 611.

[39] Walther, D.; Ruben, M.; Rau, S., *Coord. Chem. Rev.,* **1999**, *182*, 67.

[40] Kayaki, Y.; Yamamoto, M.; Ikariya, T., *Angew. Chem. Int. Ed.,* **2009**, *48*, 4194.

[41] Cantat, T.; von Wolff, N.; Villiers, C.; Thuéry, P.; Lefèvre, G.; Ephritikhine, M., *Eur. J. Org. Chem.,* **2016**, *2017*, 676.

[42] Belli Dell'Amico, D.; Calderazzo, F.; Labella, L.; Marchetti, F.; Pampaloni, G., *Chem. Rev.,* **2003**, *103*, 3857.

[43] Cantat, T.; Das Neves Gomes, C.; Jacquet, O.; Villiers, C.; Thuéry, P.; Ephritikhine, M., *Angew. Chem. Int. Ed.,* **2012**, *51*, 187.

[44] Cantat, T.; Pouessel, J.; Blondiaux, E., *Angew. Chem. Int. Ed.,* **2014**, *53*, 12186.

[45] Li, W.; Yang, N.; Lyu, Y., *Org. Chem. Front.,* **2016**, *3*, 823.

[46] Brzezinkski, B.; Ng, S.; Naumov, P.; Chantrapromma, S.; Shanmuga Sundara Raj, S.; Fun, H.; Ibrahim, A.; Woiciechowski, G., *J. Mol. Struct.,* **2001**, *562*, 185.

[47] Casely, I. J.; Ziller, J. W.; Fang, M.; Furche, F.; Evans, W. J., *J. Am. Chem. Soc.,* **2011**, *133*, 5244.

[48] Blessing, R., *Acta Cryst.,* **1995**, *A51*, 33.

[49] Sheldrick, G., *Acta Cryst.,* **2008**, *A64*, 112.

[50] SHELXL-97 Sheldrick, G., University of Gottingen, Germany, **1997**.

[51] Farrugia, L., *J. Appl. Cryst.,* **1999**, *32*, 837.

[52] Landais, Y.; Cramail, H.; Alsarraf, J.; Ait Ammar, Y.; Rober, F.; Cloutet, E., *Macromolecules,* **2012**, *45*, 2249.

Appendix

Appendix A: Crystal Data and Structure Refinement

Appendix A1: Crystal data and structure refinement for $[1,2\text{-}(CH_2hppH)_2\text{-}C_6H_4][BPh_4]_2$ (compound ***30a***)

Appendix A2: Crystal data and structure refinement for $[1,2\text{-}(CH_2hppH)_2\text{-}C_6H_4][Cl]_2$ (compound ***30b***)

Appendix A3: Crystal data and structure refinement for $1,4\text{-}(CH_2hpp)_2\text{-}C_6H_4$ (compound **32**) crystallized under air

Appendix A4: Crystal data and structure refinement for $[1,4\text{-}(CH_2hppH)_2\text{-}C_6H_4][BPh_4]_2$ (compound ***32a***)

Appendix A5: Crystal data and structure refinement for $[1,4\text{-}(CH_2hppH)_2\text{-}C_6H_4][Cl]_2$ (compound ***32b***)

Appendix A6: Crystal data and structure refinement for $[1,4\text{-}(CH_2hppH)_2\text{-}C_6H_4][HCO_3]_2$ (compound ***32c***- Structure **I**)

Appendix A7: Crystal data and structure refinement for $[1,4\text{-}(CH_2hppH)_2\text{-}C_6H_4][HCO_3]_2$ (compound ***32c***- Structure **II**)

Appendix A8: Crystal data and structure refinement for $[hppH_2][HCO_3]$ (compound ***1c***)

Appendix A9: Crystal data and structure refinement for $[hppH_2]_2[CO_3]$ (compound ***1d***)

Appendix B: Select Bond Angles of Molecular Structures

Appendix B1: Select bond angles for $[hppH_2][HCO_3]$ (***1c***)

Appendix B2: Select bond angles for $[1,4\text{-}(CH_2hppH)_2\text{-}C_6H_4][HCO_3]_2$ (***32c***-Structure **I**)

Appendix B3: Select bond angles for $[1,4\text{-}(CH_2hppH)_2\text{-}C_6H_4][HCO_3]_2$ (***32c***-Structure **II**)

Appendix B4: Select bond angles for $[1,4\text{-}(CH_2hppH)_2\text{-}C_6H_4][Cl]_2$ (***32b***)

Appendix B5: Select bond angles for $[1,4\text{-}(CH_2hppH)_2\text{-}C_6H_4][BPh_4]_2$ (***32a***)

Appendix B6: Select bond angles for $[1,2\text{-}(CH_2hppH)_2\text{-}C_6H_4][BPh_4]_2$ (***30a***)

Appendix B7: Select bond angles for $[1,2\text{-}(CH_2hppH)_2\text{-}C_6H_4][Cl]_2$ (***30b***)

Appendix B8: Select bond angles for $[hppH_2]_2[CO_3]$ (***1d***)

Appendix A1: Crystal data and structure refinement for [1,2-(CH_2hppH)$_2$-C_6H_4][BPh_4]$_2$ (**30*a***)

Empirical formula	$C_{72}H_{79}B_2N_7O$
Formula weight	1080.04
Temperature	120.01(10) K
Crystal system	Monoclinic
Space group	$P\,2_1/c$ (No.14)
Unit cell dimensions	a = 17.95494(18) Å, α = 90°. b = 14.72534(14) Å, β = 95.8621(8)°. c = 22.5684(2) Å, γ = 90°.
Volume	5935.72(10) Å^3
Z	4
Density (calculated)	1.209 g/cm^3
Absorption coefficient	0.547 mm^{-1}
F(000)	2312.0
Crystal size	0.31 x 0.23 x 0.12 mm^3
Radiation	Cu Kα ((λ = 1.54184)
Theta range for data collection	8.8658 to 143.567°
Index ranges	-22 ≤ h ≤ 22, -18 ≤ k ≤ 18, -27 ≤ l ≤ 27
Reflections collected	48265
Independent reflections	11561 [R_{int} = 0.0255, R_{sigma} = 0.037]
Data/restraints/parameters	11561/30/785
Goodness-of-fit on F^2	0.987
Final R indexes [I>2σ (I)]	R_1 = 0.035, wR_2 = 0.094
Final R indexes [all data]	R_1 = 0.041, wR_2 = 0.097
Largest diff. peak and hole	0.25 and -0.21 e.Å^{-3}

Appendix A2: Crystal data and structure refinement for [1,2-(CH_2hppH)$_2$-C_6H_4][Cl]$_2$ (***30b***)

Empirical formula	$C_{22}H_{44}Cl_2N_6O_5$
Formula weight	543.53
Temperature	120.01(10) K
Crystal system	Triclinic
Space group	$P\bar{1}$ (No.2)
Unit cell dimensions	a =9.2349(2) Å, α = 70.556(3)°. b = 11.1753(4) Å, β = 89.505(2)°. c = 14.1538(4) Å, γ = 89.891(2)°.
Volume	1377.35(7) Å^3
Z	2
Density (calculated)	1.311 g/cm^3
Absorption coefficient	2.474 mm^{-1}
F(000)	584.0
Crystal size	0.1598 x 0.1427 x 0.0831 mm^3
Radiation	Cu Kα (λ = 1.54184)
Theta range for data collection	9.5774 to 143.6696°
Index ranges	$-13 \leq h \leq 13$, $-11 \leq k \leq 11$, $-17 \leq l \leq 17$
Reflections collected	13759
Independent reflections	5373 [R_{int} = 0.0414, R_{sigma} = 0.0494]
Data/restraints/parameters	5373/18/388
Goodness-of-fit on F^2	1.247
Final R indexes [I>2σ (I)]	R_1 = 0.055, wR_2 = 0.163
Final R indexes [all data]	R_1 = 0.061, wR_2 = 0.166
Largest diff. peak and hole	0.85 and -0.67 e.Å^{-3}

Appendix A3: Crystal data and structure refinement for neutral 1,4-$(CH_2hpp)_2$-C_6H_4 (**32**) crystallized under air

Empirical formula	$C_{22}H_{32}N_6$
Formula weight	380.53
Temperature	291.24(10) K
Crystal system	Monoclinic
Space group	$P\,2_1/n$ (alternative setting $P\,2_1/c$)
Unit cell dimensions	a = 4.94711(14) Å, $\alpha = 90°$. b = 14.7142(4) Å, $\beta = 92.182(2)°$. c = 13.4335(4) Å, $\gamma = 90°$.
Volume	977.15(5) $Å^3$
Z	2
Density (calculated)	1.293 g/cm^3
Absorption coefficient	0.621 mm^{-1}
F(000)	412.0
Crystal size	0.1952 x 0.1521 x 0.152 mm^3
Radiation	Cu Kα ((λ = 1.54184)
Theta range for data collection	8.917 to 143.1156°
Index ranges	$-5 \leq h \leq 6$, $-16 \leq k \leq 17$, $-16 \leq l \leq 16$
Reflections collected	3422
Independent reflections	1848 [$R_{int} = 0.013$, $R_{sigma} = 0.024$]
Data/restraints/parameters	1848/0/156
Goodness-of-fit on F^2	0.976
Final R indexes [I>2σ (I)]	$R_1 = 0.040$, $wR_2 = 0.104$
Final R indexes [all data]	$R_1 = 0.044$, $wR_2 = 0.107$
Largest diff. peak and hole	0.28 and -0.23 $e.Å^{-3}$

Appendix A4: Crystal data and structure refinement for [1,4-(CH_2hppH)$_2$-C_6H_4][BPh_4]$_2$ (**32*a***)

Empirical formula	$C_{70}H_{74}B_2N_6$
Formula weight	1020.97
Temperature	120.01(10) K
Crystal system	Triclinic
Space group	*P* (No.2)
Unit cell dimensions	a = 9.3605(6) Å, α = 85.944°. b = 10.1911(7) Å, β = 82.334(6)°. c = 15.1351(11) Å, γ = 72.887(6)°.
Volume	1366.78(16) Å^3
Z	1
Density (calculated)	1.24 g/cm^3
Absorption coefficient	0.546 mm^{-1}
F(000)	546.0
Crystal size	0.2421 x 0.1701 x 0.10904mm^3
Radiation	Cu Kα ((λ = 1.54184)
Theta range for data collection	9.0846 to 143.9198°
Index ranges	-10 ≤ h ≤ 11, -12 ≤ k ≤ 12, -18 ≤ l ≤ 18
Reflections collected	7546
Independent reflections	5107 [R_{int} = 0.02, R_{sigma} = 0.0367]
Data/restraints/parameters	5107/0/356
Goodness-of-fit on F^2	1.045
Final R indexes [I>2σ (I)]	R_1 = 0.0408, wR_2 = 0.1001
Final R indexes [all data]	R_1 = 0.0468, wR_2 = 0.1054
Largest diff. peak and hole	0.23 and -0.19 e.Å^{-3}

Appendix A5: Crystal data and structure refinement for [1,4-(CH_2hppH)$_2$-C_6H_4][Cl]$_2$ (***32b***)

Empirical formula	$C_{22}H_{38}Cl_2N_6O_2$
Formula weight	489.48
Temperature	120.0(1) K
Crystal system	monoclinic
Space group	*P* $2_1/n$ (alternative setting *P* $2_1/c$)
Unit cell dimensions	a = 10.0526(7) Å, α = 90°. b = 10.4820(8) Å, β = 89.659(7)°. c = 11.7341(10) Å, γ = 90°.
Volume	1236.42(16) Å^3
Z	2
Density (calculated)	1.315 g/cm^3
Absorption coefficient	2.609 mm^{-1}
F(000)	588.0
Crystal size	0.13 x 0.10 x 0.09 mm^3
Radiation	Cu Kα (λ = 1.54184)
Theta range for data collection	7.5342 to 146.422°
Index ranges	-12 ≤ h ≤ 11, -12 ≤ k ≤ 8, -11 ≤ l ≤ 14
Reflections collected	8586
Independent reflections	2433 [R_{int} = 0.062, R_{sigma} = 0.061]
Data/restraints/parameters	2433/0/157
Goodness-of-fit on F^2	1.060
Final R indexes [I>2σ (I)]	R_1 = 0.068, wR_2 = 0.186
Final R indexes [all data]	R_1 = 0.076, wR_2 = 0.193
Largest diff. peak and hole	0.74 and -0.25 e.Å^{-3}

Appendix A6: Crystal data and structure refinement for [1,4-(CH_2hppH)$_2$-C_6H_4][HCO_3]$_2$ (**32*c***-Structure **I**)

Empirical formula	$C_{28}H_{42}N_8O_6$
Formula weight	586.70
Temperature	120.01(10) K
Crystal system	Monoclinic
Space group	$P\,2_1/c$ (No.14)
Unit cell dimensions	a = 8.2572(2) Å, α = 90°. b = 11.7410(3) Å, β = 104.460(2)°. c = 15.6647(4) Å, γ = 90°.
Volume	1470.55(6) Å^3
Z	2
Density (calculated)	1.325 g/cm^3
Absorption coefficient	0.783 mm^{-1}
F(000)	628.0
Crystal size	0.50 x 0.10 x 0.08 mm^3
Radiation	Cu Kα (λ = 1.54184)
Theta range for data collection	9.5258 to 143.7282°
Index ranges	-10 ≤ h ≤ 9, -19 ≤ k ≤ 19, -7 ≤ l ≤ 8
Reflections collected	3768
Independent reflections	2868 [R_{int} = 0.0277, R_{sigma} = 0.0422]
Data/restraints/parameters	2686/0/199
Goodness-of-fit on F^2	1.025
Final R indexes [I>2σ (I)]	R_1 = 0.047, wR_2 = 0.126
Final R indexes [all data]	R_1 = 0.053, wR_2 = 0.131
Largest diff. peak and hole	0.34 and -0.26 e.Å^{-3}

Appendix A7: Crystal data and structure refinement for [1,4-(CH_2hppH)$_2$-C_6H_4][HCO_3]$_2$ (***32c*-Structure II**)

Empirical formula	$C_{28}H_{42}N_8O_6$
Formula weight	586.69
Temperature	120.01(10) K
Crystal system	Monoclinic
Space group	$P\,2_1/n$ (alternative setting $P\,2_1/c$)
Unit cell dimensions	a = 9.39899(18) Å, $\alpha = 90°$. b = 10.66487(19) Å, $\beta = 97.9240(17)°$. c = 14.2617(2) Å, $\gamma = 90°$.
Volume	1415.93(4) Å^3
Z	2
Density (calculated)	1.376 g/cm^3
Absorption coefficient	0.813 mm^{-1}
F(000)	628.0
Crystal size	0.18 x 0.15 x 0.11 mm^3
Radiation	Cu Kα (λ = 1.54184)
Theta range for data collection	8.2906 to 143.4358°
Index ranges	$-11 \le h \le 11$, $-13 \le k \le 13$, $-17 \le l \le 17$
Reflections collected	7183
Independent reflections	2755 [R_{int} = 0.017, R_{sigma} = 0.026]
Data/restraints/parameters	2755/0/199
Goodness-of-fit on F^2	1.021
Final R indexes [I>2σ (I)]	R_1 = 0.032, wR_2 = 0.080
Final R indexes [all data]	R_1 = 0.035, wR_2 = 0.082
Largest diff. peak and hole	0.21 and -0.20 e.Å^{-3}

Appendix A8: Crystal data and structure refinement for $[hppH_2][HCO_3]\cdot H_2O$ (**1*c***)

Empirical formula	$C_8H_{17}N_3O_4$
Formula weight	219.24
Temperature	120.01(10) K
Crystal system	Triclinic
Space group	$P\bar{1}$ (No.2)
Unit cell dimensions	a = 7.1845(6) Å, α = 65.836(9)°. b = 8.6781(7) Å, β = 73.984(8)°. c = 9.6864(10) Å, γ = 78.131(7)°.
Volume	526.45(8) Å^3
Z	2
Density (calculated)	1.383 g/cm^3
Absorption coefficient	0.937 mm^{-1}
F(000)	236.0
Crystal size	0.16 x 0.09 x 0.06 mm^3
Radiation	Cu Kα (λ = 1.54184)
Theta range for data collection	10.2522 to 143.4202°
Index ranges	$-8 \leq h \leq 8$, $-10 \leq k \leq 10$, $-11 \leq l \leq 11$
Reflections collected	3366
Independent reflections	2002 [R_{int} = 0.016, R_{sigma} = 0.027]
Data/restraints/parameters	2002/0/156
Goodness-of-fit on F^2	1.312
Final R indexes [I>2σ (I)]	R_1 = 0.052, wR_2 = 0.162
Final R indexes [all data]	R_1 = 0.054, wR_2 = 0.163
Largest diff. peak and hole	0.28 and -0.28 e.Å^{-3}

Appendix A9: Crystal data and structure refinement for $[hppH_2]_2[CO_3]\cdot 6H_2O$ (**1*d***)

Empirical formula	$C_{15}H_{40}N_6O_9$
Formula weight	448.53
Temperature	120.01(10) K
Crystal system	Orthohombic
Space group	*Pbcn*
Unit cell dimensions	a = 20.0916(2) Å, $\alpha = 90°$. b = 13.06564(16) Å, $\beta = 90°$. c = 17.1940(2) Å, $\gamma = 90°$.
Volume	4513.60(10) $Å^3$
Z	8
Density (calculated)	1.32 g/cm^3
Absorption coefficient	0.912 mm^{-1}
F(000)	1952
Crystal size	0.1508 x 0.1308 x 0.0877 mm^3
Radiation	Cu Kα (λ = 1.54184)
Theta range for data collection	4.775 to 71.721°
Index ranges	$-24 \leq h \leq 23$, $-16 \leq k \leq 15$, $-20 \leq l \leq 20$
Reflections collected	5110
Independent reflections	4297 [$R_{int} = 0.0400$, $R_{sigma} = 0.0348$]
Data/restraints/parameters	4297/18/335
Goodness-of-fit on F^2	1.009
Final R indexes [I>2σ (I)]	$R_1 = 0.0348$, $wR_2 = 0.0928$
Final R indexes [all data]	$R_1 = 0.04$, $wR_2 = 0.0971$
Largest diff. peak and hole	0.311 and -0.204 $e.Å^{-3}$

Appendix B1: Selected bond angles of [hppH$_2$][HCO$_3$]·H$_2$O (**1*c***)

Bond	**Angle (°)**
H(**1X**)– N(**1**)–C(**1**)	116(2)
H(**1X**)– N(**1**)–C(**2**)	122(2)
C(**1**)– N(**1**)–C(**2**)	122.4(2)
H(**2X**)– N(**2**)–C(**1**)	120(2)
H(**2X**)– N(**2**)–C(**7**)	117(2)
C(**1**)– N(**2**)–C(**7**)	122.3(2)
C(**1**)– N(**3**)–C(**4**)	121.8(2)
C(**1**)– N(**3**)–C(**5**)	122.3(2)
C(**4**)– N(**3**)–C(**5**)	115.8(2)

Appendix B2: Selected bond angles of [1,4-(CH$_2$hppH)$_2$-C$_6$H$_4$][HCO$_3$]$_2$ (**32*c***-Structure **I**)

Bond	**Angle (°)**
H(**1X**)– N(**1**)–C(**1**)	122(1)
H(**1X**)– N(**1**)–C(**7**)	115(1)
C(**1**)– N(**1**)–C(**7**)	122.13(15)
C(**1**)– N(**2**)–C(**8**)	124.98(13)
C(**1**)– N(**2**)–C(**2**)	120.21(14)
C(**8**)– N(**2**)–C(**2**)	113.96(13)
C(**1**)– N(**3**)–C(**4**)	123.92(16)
C(**1**)– N(**3**)–C(**5**)	122.54(15)
C(**4**)– N(**3**)–C(**5**)	113.51(16)

Appendix B3: Selected bond angles of [1,4-(CH_2hppH)$_2$-C_6H_4][HCO_3]$_2$ (**32*c***-Structure **II**)

Bond	Angle (°)
H(**1X**)– N(**1**)–C(**1**)	121(1)
H(**1X**)– N(**1**)–C(**7**)	117(1)
C(**1**)– N(**1**)–C(**7**)	122.56(9)
C(**1**)– N(**2**)–C(**8**)	121.68(9)
C(**1**)– N(**2**)–C(**2**)	120.23(9)
C(**8**)– N(**2**)–C(**2**)	118.09(9)
C(**1**)– N(**3**)–C(**4**)	122.23(9)
C(**1**)– N(**3**)–C(**5**)	123.59(9)
C(**4**)– N(**3**)–C(**5**)	114.14(9)

Appendix B4: Selected bond angles of [1,4-(CH_2hppH)$_2$-C_6H_4][Cl]$_2$ (***32b***)

Bond	Angle (°)
H(**1X**)– N(**1**)–C(**1**)	125(2)
H(**1X**)– N(**1**)–C(**7**)	112(2)
C(**1**)– N(**1**)–C(**7**)	122.9(3)
C(**1**)– N(**2**)–C(**8**)	123.4(3)
C(**1**)– N(**2**)–C(**2**)	121.7(3)
C(**8**)– N(**2**)–C(**2**)	114.9(3)
C(**1**)– N(**3**)–C(**4**)	122.8(3)
C(**1**)– N(**3**)–C(**5**)	121.8(3)
C(**4**)– N(**3**)–C(**5**)	115.1(3)

Appendix B5: Selected bond angles of [1,4-(CH_2hppH)$_2$-C_6H_4][BPh_4]$_2$ (**32*a***)

Bond	**Angle (°)**
H(**1X**)– N(**1**)–C(**1**)	118(1)
H(**1X**)– N(**1**)–C(**7**)	117(1)
C(**1**)– N(**1**)–C(**7**)	121.7(1)
C(**1**)– N(**2**)–C(**8**)	121.5(1)
C(**1**)– N(**2**)–C(**2**)	121.7(1)
C(**8**)– N(**2**)–C(**2**)	116.6(1)
C(**1**)– N(**3**)–C(**4**)	122.7(1)
C(**1**)– N(**3**)–C(**5**)	121.9(1)
C(**4**)– N(**3**)–C(**5**)	115.5(1)

Appendix B6: Selected bond angles of [1,2-(CH_2hppH)$_2$-C_6H_4][BPh_4]$_2$ (**30*a***)

Bond	**Angle (°)**
H(**1X**)– N(**1**)–C(**1**)	120(1)
H(**1X**)– N(**1**)–C(**7**)	119(1)
C(**1**)– N(**1**)–C(**7**)	120.7(1)
C(**1**)– N(**2**)–C(**8**)	121.3(1)
C(**1**)– N(**2**)–C(**2**)	119.1(1)
C(**8**)– N(**2**)–C(**2**)	119.2(1)
C(**1**)– N(**3**)–C(**4**)	123.1(1)
C(**1**)– N(**3**)–C(**5**)	122.9(1)
C(**4**)– N(**3**)–C(**5**)	114.0(1)

Appendix B7: Selected bond angles of $[1,2\text{-}(CH_2hppH)_2\text{-}C_6H_4][Cl]_2$ (***30b***)

Bond	**Angle (°)**
H(**1X**)– N(**1**)–C(**1**)	120(3)
H(**1X**)– N(**1**)–C(**7**)	116(3)
C(**1**)– N(**1**)–C(**7**)	123.1(2)
C(**1**)– N(**2**)–C(**8**)	120.8(2)
C(**1**)– N(**2**)–C(**2**)	121.8(2)
C(**8**)– N(**2**)–C(**2**)	116.4(2)
C(**1**)– N(**3**)–C(**4**)	122.1(2)
C(**1**)– N(**3**)–C(**5**)	122.1(2)
C(**4**)– N(**3**)–C(**5**)	115.5(2)
H(**1X**)– N(**4**)–C(**9**)	118(3)
H(**1X**)– N(**4**)–C(**15**)	118(3)
C(**9**)– N(**4**)–C(**15**)	124.2(3)
C(**9**)– N(**5**)–C(**16**)	121.3(2)
C(**9**)– N(**5**)–C(**10**)	121.6(3)
C(**16**)– N(**5**)–C(**10**)	116.7(3)
C(**9**)– N(**6**)–C(**13**)	121.1(2)
C(**9**)– N(**6**)–C(**12**)	122.4(3)
C(**13**)– N(**6**)–C(**12**)	116.1(3)

Appendix B8: Selected bond angles of $[hppH_2]_2[CO_3]\cdot 6H_2O$ (**1*d***)

Bond	**Angle (°)**
H(**1N**)– N(**1**)–C(**1**)	119(1)
H(**1N**)– N(**1**)–C(**2**)	118(1)
C(**1**)– N(**1**)–C(**2**)	122.2(1)
H(**5N**)– N(**5**)–C(**8**)	120(1)
H(**5N**)– N(**5**)–C(**14**)	118(1)
C(**8**)– N(**5**)–C(**14**)	121.8(1)
C(**1**)– N(**3**)–C(**4**)	122.4(1)
C(**1**)– N(**3**)–C(**5**)	122.3(1)
C(**4**)– N(**3**)–C(**5**)	115.2(1)
H(**2N**)– N(**2**)–C(**1**)	115(1)
H(**2N**)– N(**2**)–C(**7**)	123(1)
C(**1**)– N(**2**)–C(**7**)	121.6(1)
C(**8**)– N(**6**)–C(**11**)	121.8(1)
C(**8**)– N(**6**)–C(**12**)	122.1(1)
C(**11**)– N(**6**)–C(**12**)	115.9(1)
H(**4N**)– N(**4**)–C(**8**)	115(1)
H(**4N**)– N(**4**)–C(**9**)	123(1)
C(**8**)– N(**4**)–C(**9**)	122.0(1)

Appendix C

^{1}H NMR and ^{13}C NMR Spectra of Notable Compounds

Appendix C1: ^{1}H NMR and ^{13}C NMR spectra of neutral 1,4-$(CH_2hpp)_2$-C_6H_4 (**32**)

Appendix C2: ^{1}H NMR and ^{13}C NMR sepctra of bicarbonate salt [1,4-$(CH_2hppH)_2$-C_6H_4][HCO_3]$_2$ (**32*c***)

Appendix C3: ^{1}H NMR and ^{13}C NMR spectra of carbonate salt [$hppH_2$]$_2$[CO_3] (**1*d***)

Appendix C4: ^{1}H NMR and ^{13}C NMR spectra of bicarbonate salt [$hppH_2$][HCO_3] (**1*c***)

Appendix C1a: ^{1}H NMR spectrum of compound **32**

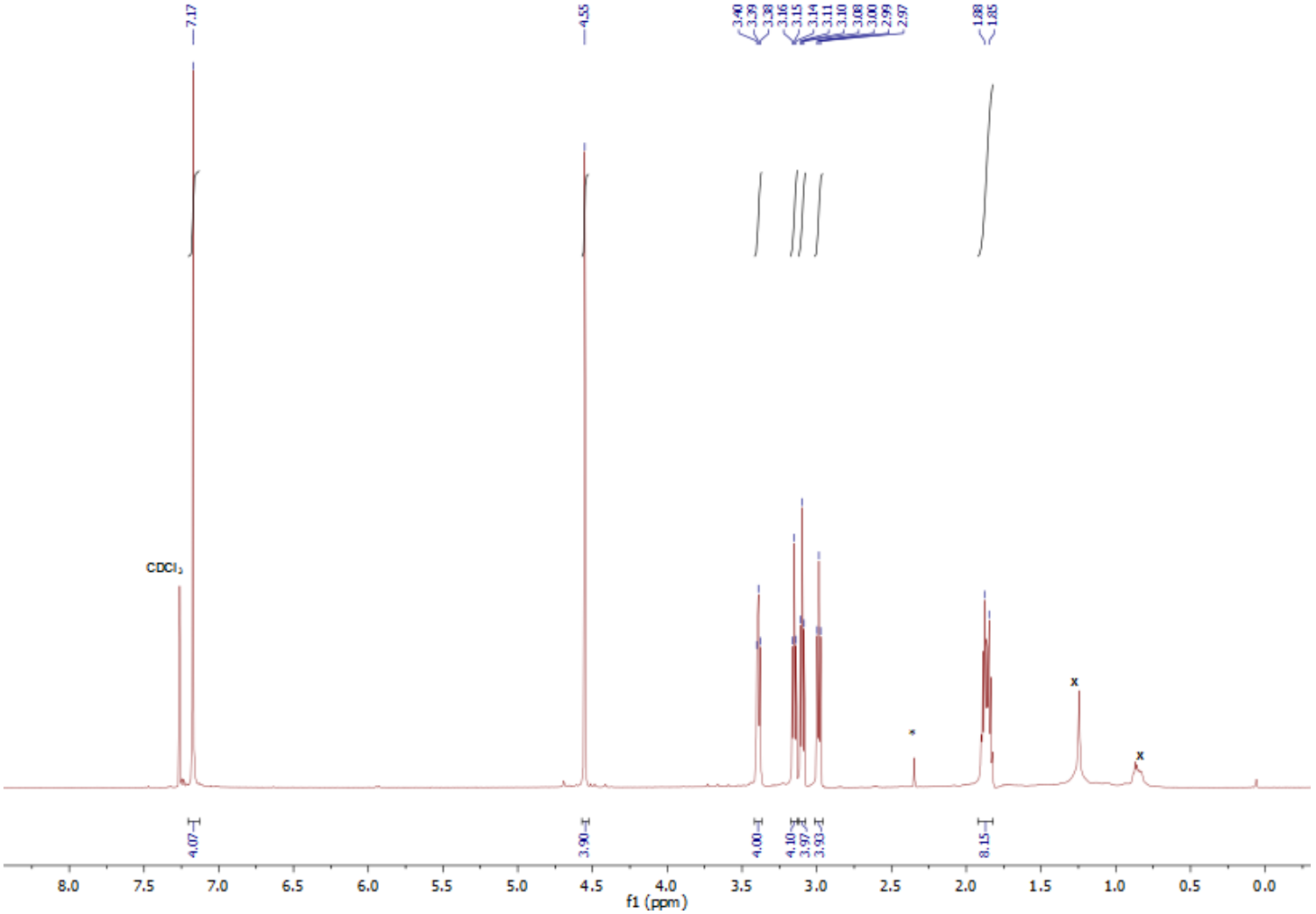

x= H-grease impurity

*= toluene

Appendix C1b: ^{13}C NMR spectrum of compound **32**

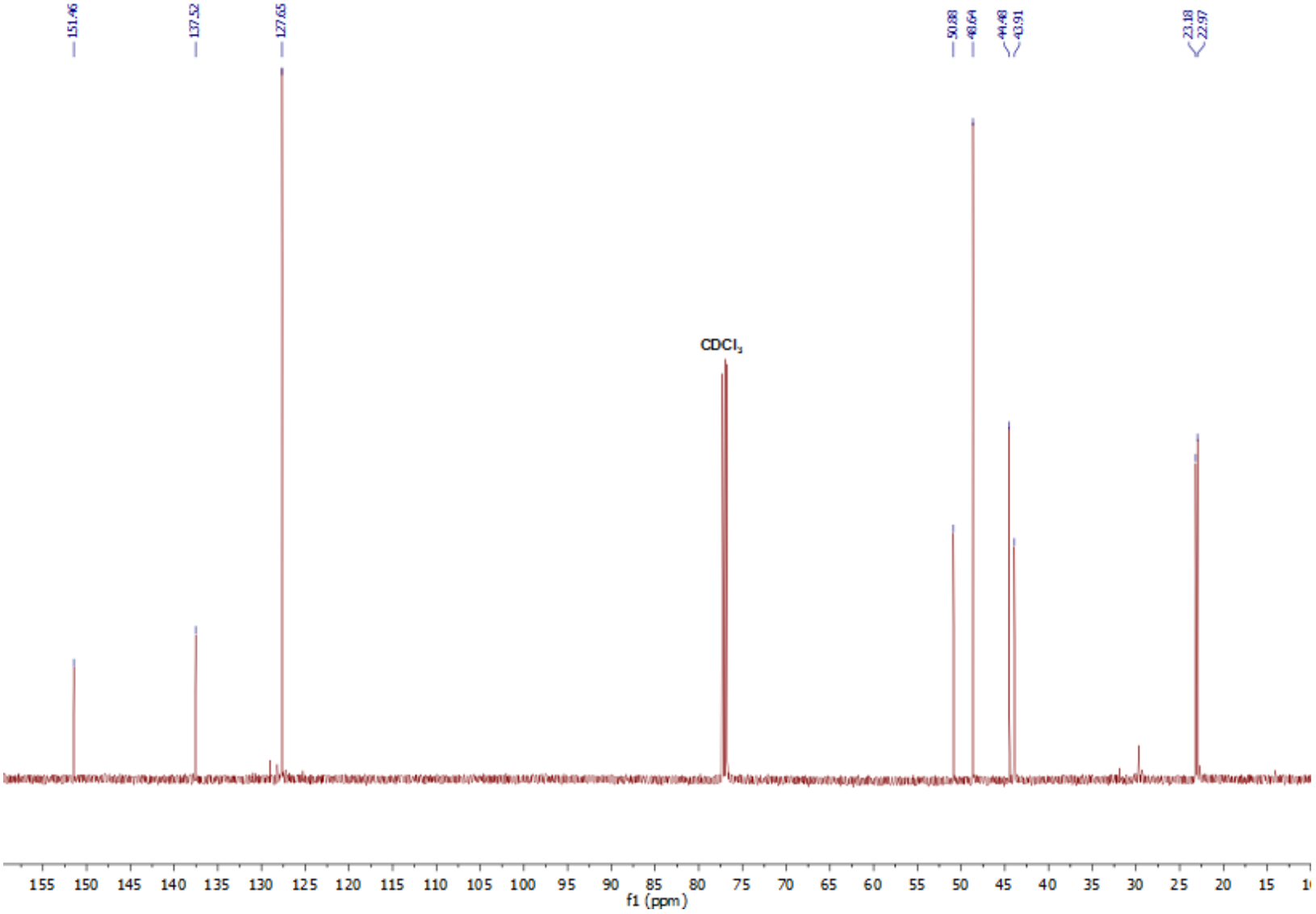

Appendix C2a: ^{1}H NMR spectrum of compound **32*c***

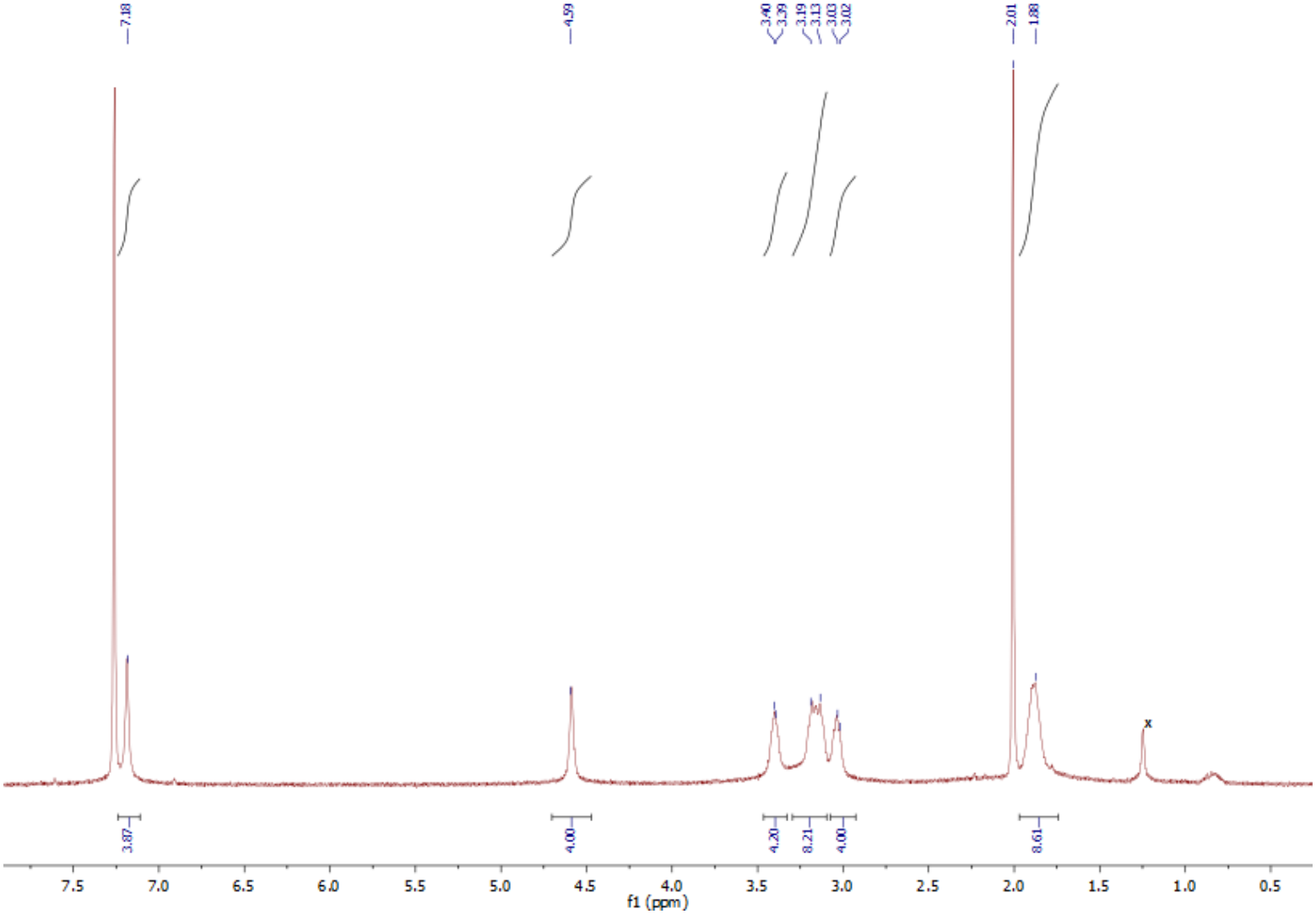

x = H-grease impurity

Appendix C2b: ^{13}C NMR spectrum of compound ***32c***

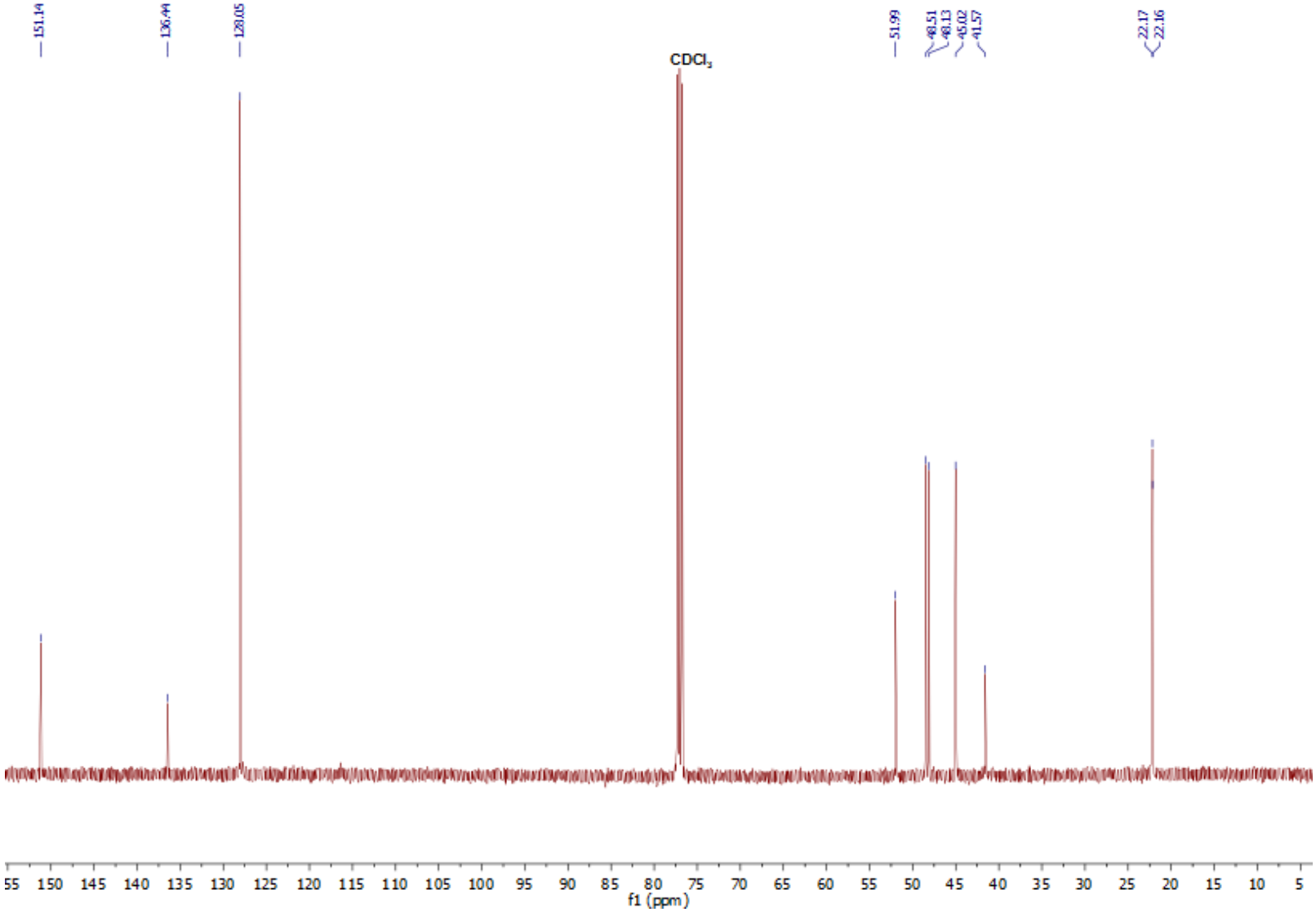

Appendix C3a: ^{1}H NMR spectrum of compound **1*d***

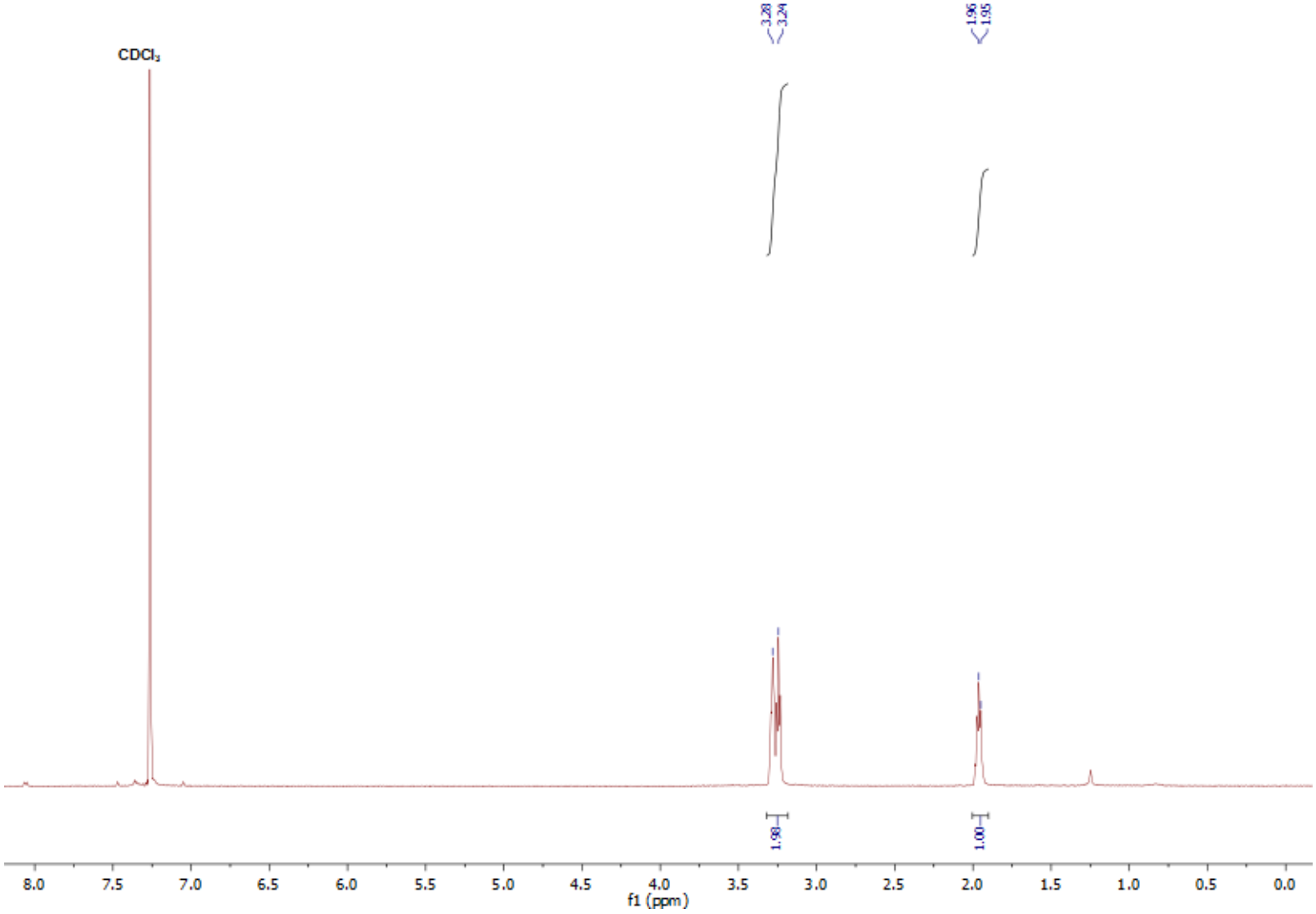

Appendix C3b: ^{13}C NMR spectrum of compound **1*d***

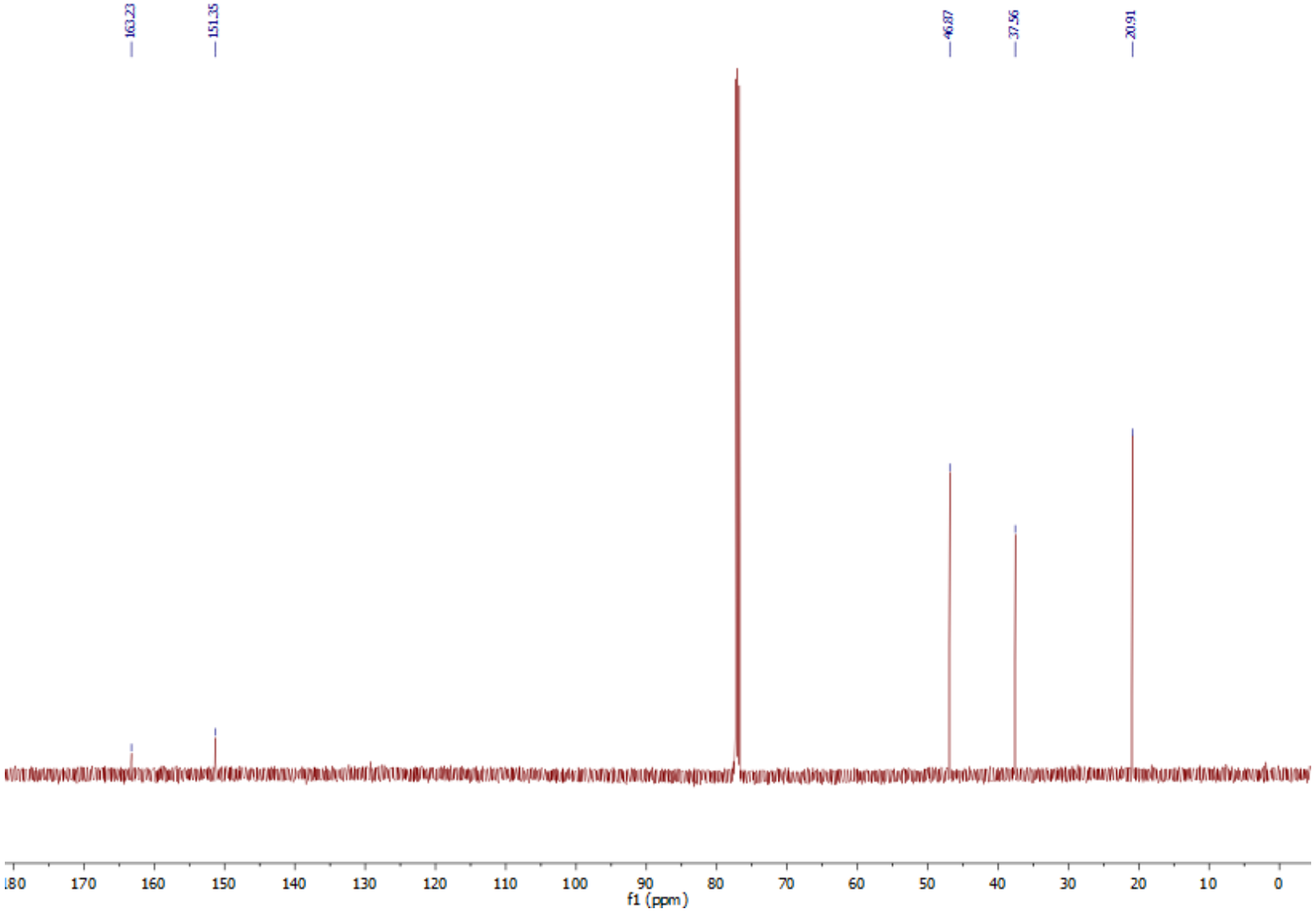

Appendix C4a: [1]H NMR spectrum of compound **1*c***

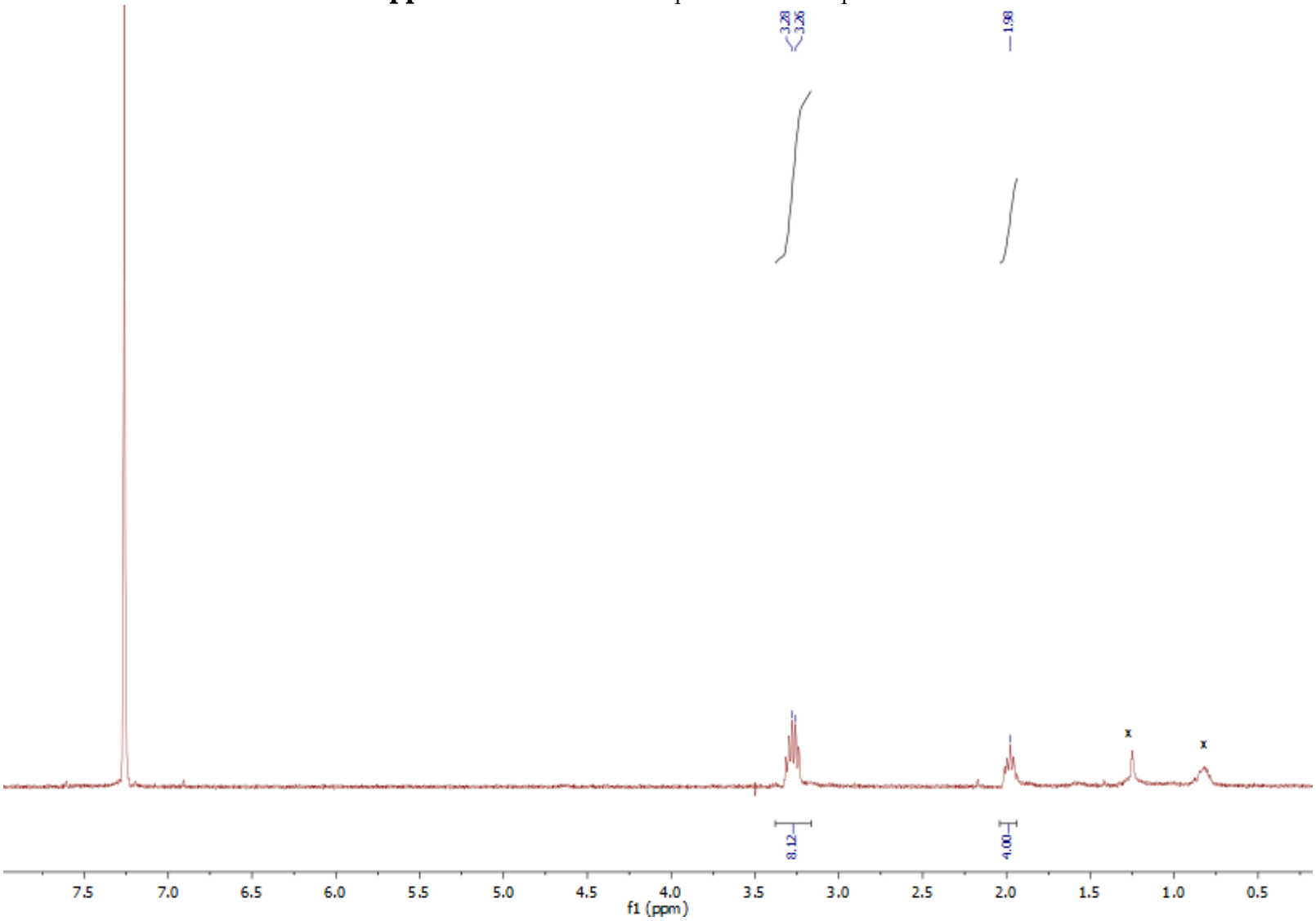

x = H-grease impurity

Appendix C4b: ^{13}C NMR spectrum of compound **1*c***